PB80-181274

Photochemical Study of NOx Removal from Stack Gases

North Carolina Univ. at Chapel Hill

Prepared for

Industrial Environmental Research Lab.
Research Triangle Park, NC

Mar 80

U.S. Department of Commerce
National Technical Information Service
NTIS

PB80-181274

United States
Environmental Protection
Agency

Industrial Environmental Research
Laboratory
Research Triangle Park NC 27711

EPA-600/7-80-038
March 1980

EPA

Photochemical Study of NO_x Removal from Stack Gases

Interagency Energy/Environment R&D Program Report

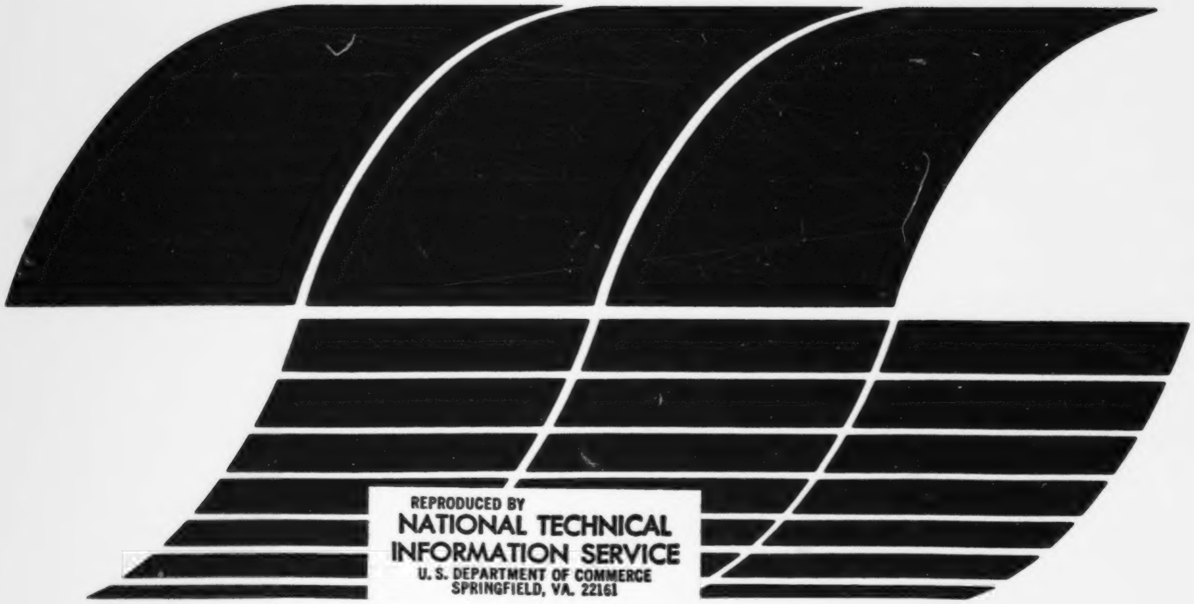

REPRODUCED BY
NATIONAL TECHNICAL
INFORMATION SERVICE
U. S. DEPARTMENT OF COMMERCE
SPRINGFIELD, VA. 22161

RESEARCH REPORTING SERIES

Research reports of the Office of Research and Development, U.S. Environmental Protection Agency, have been grouped into nine series. These nine broad categories were established to facilitate further development and application of environmental technology. Elimination of traditional grouping was consciously planned to foster technology transfer and a maximum interface in related fields. The nine series are:

1. Environmental Health Effects Research
2. Environmental Protection Technology
3. Ecological Research
4. Environmental Monitoring
5. Socioeconomic Environmental Studies
6. Scientific and Technical Assessment Reports (STAR)
7. Interagency Energy-Environment Research and Development
8. "Special" Reports
9. Miscellaneous Reports

This report has been assigned to the INTERAGENCY ENERGY-ENVIRONMENT RESEARCH AND DEVELOPMENT series. Reports in this series result from the effort funded under the 17-agency Federal Energy/Environment Research and Development Program. These studies relate to EPA's mission to protect the public health and welfare from adverse effects of pollutants associated with energy systems. The goal of the Program is to assure the rapid development of domestic energy supplies in an environmentally-compatible manner by providing the necessary environmental data and control technology. Investigations include analyses of the transport of energy-related pollutants and their health and ecological effects; assessments of, and development of, control technologies for energy systems; and integrated assessments of a wide range of energy-related environmental issues.

EPA REVIEW NOTICE

This report has been reviewed by the participating Federal Agencies, and approved for publication. Approval does not signify that the contents necessarily reflect the views and policies of the Government, nor does mention of trade names or commercial products constitute endorsement or recommendation for use.

This document is available to the public through the National Technical Information Service, Springfield, Virginia 22161.

TECHNICAL REPORT DATA
(Please read Instructions on the reverse before completing)

1. REPORT NO. EPA-600/7-80-038

2.

3. RECIPIENT'S ACCESSION NO. PB80-181274

4. TITLE AND SUBTITLE
Photochemical Study of NOx Removal from Stack Gases

5. REPORT DATE March 1980

6. PERFORMING ORGANIZATION CODE

7. AUTHOR(S)
John R. Richards and Donald L. Fox

8. PERFORMING ORGANIZATION REPORT NO.

9. PERFORMING ORGANIZATION NAME AND ADDRESS
University of North Carolina
School of Public Health
Chapel Hill, North Carolina 27514

10. PROGRAM ELEMENT NO. INE623

11. CONTRACT/GRANT NO. Grant No. R804740

12. SPONSORING AGENCY NAME AND ADDRESS
EPA, Office of Research and Development
Industrial Environmental Research Laboratory
Research Triangle Park, NC 27711

13. TYPE OF REPORT AND PERIOD COVERED Final; 1/77 - 3/79

14. SPONSORING AGENCY CODE EPA/600/13

15. SUPPLEMENTARY NOTES IERL-RTP project officer is Joseph A. McSorley, Mail Drop 63, 919/541-2745.

16. ABSTRACT The report gives results of an evaluation of the technical feasibility of a photochemical pretreatment system for NOx control at coal-fired boilers. The approach utilizes reaction mechanisms similar to those responsible for photochemical oxidant incidents. The reactions are initiated under controlled conditions while the pollutants are at high concentration and while the reaction products can be removed. Results indicate that, under time- and light-limited conditions, it is possible to quench the photochemical reactions at the NO2 peak and prior to the formation of ozone, aerosols, and other secondary products. Energy and hydrocarbon requirements were estimated in a series of 159 experimental runs. The optimal operating conditions were identified as a NOx/C3H6 stoichiometric ratio of 1 and an NO2 photolysis rate of 1 to 1.5 reciprocal minutes (equivalent to 3 to 5% station power). These conditions allowed for an 83% oxidation of NO with an exit concentration of NO less than 100 ppm. Variation of the energy input levels or the propylene injection rates resulted in NO oxidation efficiencies of 10 to 99%. Photochemical oxidation of NO was insensitive to SO2 concentration and CO2 concentration. The photochemical system appears compatible with conditions resulting from combustion modifications to suppress NOx generation.

17. KEY WORDS AND DOCUMENT ANALYSIS

a. DESCRIPTORS		b. IDENTIFIERS/OPEN ENDED TERMS	c. COSATI Field/Group
Pollution	Combustion	Pollution Control	13B
Photochemical Reactions		Stationary Sources	07E
Oxidation	Boilers		07B,07C 13A
Flue Gases	Propylene		21B
Nitrogen Oxides			
Coal			21D

18. DISTRIBUTION STATEMENT
Release to Public

19. SECURITY CLASS *(This Report)* Unclassified

20. SECURITY CLASS *(This page)* Unclassified

21. NO. OF PAGES

22. PRICE

EPA Form 2220-1 (9-73)

EPA-600/7-80-038

March 1980

Photochemical Study of NO_x Removal from Stack Gases

by

John R. Richards and Donald L. Fox

University of North Carolina
School of Public Health
Chapel Hill, North Carolina 27514

Grant No. R804740
Program Element No. INE623

EPA Project Officer: Joseph A. McSorley

Industrial Environmental Research Laboratory
Office of Environmental Engineering and Technology
Research Triangle Park, NC 27711

Prepared for

U.S. ENVIRONMENTAL PROTECTION AGENCY
Office of Research and Development
Washington, DC 20460

ABSTRACT

The technical feasibility of a photochemical pretreatment system for NO_x control at coal-fired boilers was evaluated. This approach utilizes reaction mechanism similar to those responsible for photochemical oxidant incidents. The reactions are initiated under controlled conditions while the pollutants are at high concentration and while the reaction products can be removed. Results indicated that under time limited and light limited conditions, it is possible to quench the photochemical reactions at the NO_2 peak and prior to the formation of ozone, aerosols, and other secondary products.

Energy and hydrocarbon requirements were estimated in a series of 159 experimental runs. The optimal operating conditions were identified as a NO_x/C_3H_6 stoichiometric ratio of 1 and an NO_2 photolysis rate of 1 to 1.5 reciprocal minutes which is equivalent to approximately 3 to 5% station power. These conditions allowed for an 83% oxidation of NO with an exit concentration of NO less than 100 ppm. Variation of the energy input levels or the propylene injection rates resulted in NO oxidation efficiencies of 10 to 99%. Photochemical oxidation of NO was insensitive to SO_2 concentration and CO_2 concentration. Conversion was enhanced at low initial NO_x levels, high temperatures, and high CO concentrations. Oxygen concentrations above 2% were necessary. The photochemical system appears compatible with conditions resulting from combustion modifications to suppress NO_x generation.

Reactor products consisted primarily of NO_2, formaldehyde, acetaldehyde, and acetic acid all of which should be removed in the downstream flue gas desulfurization system. Mass spectrometer analyses indicated the presence of a large number of organic compounds; nevertheless, all of these were present in only trace quantities. A major fraction of the injected propylene was also emitted. It was concluded that propylene is not sufficiently reactive for the photochemical system. Other hydrocarbons are recommended for further study.

Capital and annualized cost estimates have been prepared for a model coal-fired power plant of 500 MW generating capacity. Depending on the extent of NO oxidation desired, the capital costs vary from $37/KW to $50/KW. These estimates include the photochemical reactor with mercury lamps, and the propylene storage and distribution system. The annualized costs estimates range from 3.8 to 5.6 mills/kWh. The upper value corresponds to Δ500 ppm NO while the lower value is for Δ200 ppm NO.

The cost estimates are considered high due to the poor reactivity of propylene and the low efficiency of presently available lamps. Further bench scale testing could conceivably yield a photochemical system requiring only 1/2 the annualized cost of the present system. Even with the present limitations, the costs for the photochemical system are competitive with other control techniques involving NO gas phase oxidation followed by NO_2 absorption. Costs for alternative approaches such as selective noncatalytic reduction, however, are substantially lower. It is concluded that the photochemical system will not be commercially competitive unless serious operational problems limit the alternative techniques or unless the photochemical system can be refined to reduce cost.

This report was submitted in fulfillment of Grant No. R804740 by the Department of Environmental Sciences and Engineering of the University of North Carolina. The study was performed under the sponsorship of the Industrial Environmental Research Laboratory of the U.S. Environmental Protection Agency. This report covers the period of December 27, 1976, to December 27, 1978, and work was completed as of February 28, 1979.

ACKNOWLEDGMENTS

This report was prepared for the Industrial Environmental Research Laboratory of the U.S. Environmental Protection Agency. The EPA Project Officer was Mr. Joseph McSorley. UNC appreciates the direction and assistance provided by Mr. McSorley.

The authors gratefully acknowledge the assistance of Mr. Frank Malcolm in the fabrication of the reactor assembly and the gas blending equipment. X-ray fluorescence analyses and liquid chromotography tests of the Millipore filter samples were performed by the U.S.E.P.A. Environmental Research Laboratory. The GC mass spectrometer tests were done under contract at Research Triangle Institute by Dr. E. Pellizzari.

The principal investigator was Dr. Donald L. Fox. The co-principal investigator and principal author of the report was Mr. John Richards. Consulting support was provided by Dr. Harvey Jeffries, Dr. E. Stahel, and Dr. Parker Reist.

CONTENTS

Page

Abstract ii
Acknowledgments iv
Figures vii
Tables x

1. Introduction 1
2. Summary and Conclusions 4
3. Recommendations 8
4. Background 9
    NO_x Control Techniques 9
    Photochemical NO_x Control Techniques 26
5. Experimental 43
    General Design Objectives 43
    Reactor Design and Performance 45
    Actinometry 55
    Reactant and Product Measurement 58
    Gas Handling Apparatus 62
    Experimental Design 66
    Test Procedure 67
6. Results and Discussion 71
    Spectral Effects 71
    Hydrocarbon Requirements 79

Page

Variables Influencing NO Oxidation 91

Reaction Products 102

Cost Estimates 117

References 126

Appendices

FIGURES

Number Page

1. Trends in the emissions of NO_x from stationary sources 10

2. Possible formation mechanism for fuel NO_x 14

3. Effect of excess air on NO_2 emissions 16

4. Effect of secondary air addition on NO_x emissions 17

5. Classification of NO_x flue gas treatment processes 20

6. Effect of temperature on NO_x removal in the selective noncatalytic reduction process 23

7. Photochemical system conceptual design 29

8. Absorption coefficients of flue gas components 33

9. Power requirements as a function of net product quantum yield 35

10a. Photostationary state reactions 37

10b. Simplified olefin/NO_x photochemical reactions 37

10c Simplified aldehyde photochemical reactions 37

11. Typical pollutant concentration-time profile for photochemical reactions in batch reactor 40

12a. View of quartz reactor on support rod 46

12b. View of outer CSTR 46

13. Mercury doped xenon arc output spectra 47

14. Light distribution in quartz reactor 49

15. NO_2 photolysis rate as a function of lamp current 51

16. Initial inlet configuration 54

Number Page

16b. Reactor inlet configuration 54

17. Gas analyzers for NO_x, SO_2, and condensation nuclei 59

18. Gas analyzers for hydrocarbons 59

19. Influence of NO_2 on pulsed fluorescent SO_2 readings 61

20. Side view of reactor and spectrometer 63

21. Front view of blending box 63

22. Gas flow system 65

23. Influence of middle ultraviolet light on NO oxidation 73

24. Typical comparative spectra; during and after experimental run 75

25. Influence of NO_x on absorption spectra 76

26. Influence of SO_2 on NO oxidation 78

27. NO oxidation, influence of initial propylene concentration and light intensity. Low initial NO_x concentration. 81

28. NO oxidation, influence of initial propylene concentration and light intensity. High initial NO_x concentration. 82

29. NO oxidation, influence of initial propylene concentration and light intensity. Low initial NO_x concentration. 83

30. NO oxidation, influence of initial propylene concentration and light intensity. High initial NO_x concentration. 84

31. Comparason of propylene and ethylene 86

32. Unreacted propylene concentration at various inlet NO_x levels and light intensities 88

33. NO oxidation and propylene consumption as a function of NO_2 photolysis rate 89

34. Effect of oxygen content on NO oxidation 92

35. Effect of CO concentration on NO oxidation 96

36. Effect of initial NO_x concentration on NO oxidation 99

Number Page

37. Effect of CO_2 concentration on NO oxidation 101
38. Influence of temperature on NO oxidation 103
39. Nitrate deposits 107
40. Sulfate deposits 110
41. Typical gas chromatograph output 111
42. Aldehyde/propylene decay in sampling bags 115

TABLES

Number Page

1 Typical Flue Gas Composition of Coal-Fired Boilers............ 11

2 Effect of Combustion Modification Techniques on the Emission of Polycyclic Organic Matter.............................. 21

3 Photochemical Reactor Design Assumptions...................... 30

4 Effluent Gas Composition Assumptions.......................... 30

5 Energy Delivery in Model System.............................. 34

6 Comparison of Experimental System and Full Scale Systems....... 44

7 Tracer Results.. 53

8 Experimental Design... 68

9 Influence of Oxygen Content on Propylene Consumption........... 94

10a Nitrogen Material Balance, $[NO_x]_o$ $\sim$600 PPM.................... 105

10b Nitrogen Material Balances, $[NO_x]_o$ $\approx$1200 PPM (v/v)............ 105

11 Nitrate Aerosol Quantities Compared with NO Oxidation.......... 108

12 Sulfur Material Balance....................................... 108

13 X-Ray Fluorescent Sulfur Measurement Expressed as ΔPPM SO_2..... 112

14a Carbon Material Balances, $[NO_x]_o$ $\sim$600 PPM (v/v)............... 112

14b Carbon Material Balances, $[NO_x]_o$ $\sim$1200 PPM (v/v).............. 112

15 Carbon Balance Corrections for Aldehydes...................... 114

16 Relationship Between Aldehyde Formation and NO Oxidation....... 116

17 Major Organic Compounds Determined in GC/MS Tests, PPM (v/v)... 118

Number Page

18. Capital Cost Estimates 122

19. Annualized Cost Estimates 123

20. Comparison of Costs for Flue Gas Treatment Processes 124

B-1. Experimental Data, Influence of Middle UV Filter on NO Oxidation 136

B-2. Experimental Data, Influence of Sulfur Dioxide on NO Oxidation 138

B-3. Experimental Data, Influence of Propylene Concentration and UV Light Intensity on NO Oxidation 141

B-4. Experimental Data, Comparison of Ethylene and Propylene .. 166

B-5. Experimental Data, Influence of Oxygen Content on NO Oxidation 168

B-6. Experimental Data, Influence of CO on NO Oxidation 170

B-7. Experimental Data, Influence of Initial NO_x Concentration on NO Oxidation 171

B-8. Experimental Data, Influence of CO_2 Concentration on NO Oxidation 173

B-9. Experimental Data, Influence of Gas Temperature on NO Oxidation 174

CHAPTER 1

INTRODUCTION

GENERAL

Both utility and industrial boilers are major sources of anthropogenic nitrogen oxide emissions, contributing over 40% of total yearly emissions in the United States. These primary nitrogen oxides (NO_x) emissions react chemically with hydrocarbons in the ambient air through a set of partially understood photochemical reaction mechanisms. Consequences of these reactions include elevated ozone levels and potentially toxic secondary pollutants. Previous photochemical oxidant control strategies directed only at hydrocarbon reduction may be set aside in favor of more balanced NO_x and hydrocarbon control. In fact, there is growing awareness that elevated photochemical oxidant levels in some non-urban areas are sensitive primarily to NO_x concentration.

Strict NO_x control will be required in order to reduce the impact of photochemically generated secondary pollutants such as ozone. Coal-fired boilers will receive a disproportionate share of the control burden since centralized stationary sources are administratively easier to regulate than motor vehicles and since the shift in national energy policy toward greater reliance on domestic coal supplies will result in increased NO_x emissions from this source category.

Unfortunately, combustion modifications which substantially reduce NO_x generation in oil- and gas-fired boilers are not nearly as successful when applied to coal-fired boilers. Such techniques are limited to 30 to 50% NO_x reduction and sometimes result in reduced boiler performance. It is probable that combustion modification alone will not be adequate. There is a need for "add-on" control technology which supplements combustion modifications so that much greater NO_x reductions can be achieved.

A photochemical process is a possible solution. This approach takes advantage of chemical reactions analogous to those culpable ambient reactions leading to photochemical oxidants. The reactions are initiated while the pollutants are still highly concentrated within the flue gas. In this manner, control is maintained over the reaction conditions and collection of reaction products is possible.

There are a number of advantages inherent in photochemical control of NO_x from coal-fired boilers. Since the photochemical system is operated downstream of the boiler, there is no adverse impact on the boiler energy efficiency or on boiler maintenance costs. The stoichiometric requirements of hydrocarbons are much lower than equivalent requirements for ozone or other dark phase oxidizing agents. As a concentration dependent approach, energy requirements are limited to that increment necessary to maintain compliance with applicable standards. By using NO_x outlet concentration monitor feedback control of lamp power, it is possible to follow rapid fluctuations in boiler NO_x emissions, thereby insuring continuous compliance and avoiding expensive over-control. Under light-limited and time-limited conditions, it is possible to selectively oxidize NO to NO_2 and then quench the reactions before most of the undesirable secondary products form.

PURPOSE

The purpose of this study is to evaluate the technical and economic feasibility of photochemical pretreatment for NO_x control. It is a bench scale analysis emphasizing those basic chemical reaction mechanism parameters which influence costs and performance. It is recognized that a certain amount of engineering development is also necessary with respect to lamp optimization and reaction product collection. These subjects are necessarily reserved for later work on a pilot scale.

Specifically, the study is designed to evaluate the efficiency of the reaction mechanisms in the high concentration pollutant gas mixtures characteristic of coal-fired boilers. Relationships between nitric oxide oxidation and energy consumption under various physical conditions are obtained in order to define the limits of the control technique. Molar ratios of SO_2, NO and hydrocarbons are varied to consider the effect of initial concentrations on the type and extent of the secondary chemical reactions. Major reaction products are identified.

APPROACH

A flow reactor system was designed to simulate stack conditions and to allow rapid turnaround for maximum experimental runs. Simulated flue gas was blended externally and then irradiated inside a quartz reactor using a high pressure xenon arc. This UV lamp was a compromise choice having moderate energy output in the 2400-3000 and 3000-4000 Å spectral bands of interest, and also having reasonable temperature stability. Light intensity in the 3000-4000 Å spectral band was routinely measured using NO_2 photolysis. The outer chamber was used as a mounting frame, light shield and heater for the inner reactor. In this manner, the walls of the quartz reactor could be maintained slightly above the internal gas temperature to minimize wall deposition of aerosols. The outer chamber was constantly purged with N_2 to reduce the possibility of O_2 leakage.

Gas analyzers operating off a common outlet manifold with a short residence time were used to measure reactant and product concentrations on a continuous basis. Millipore filter samples were taken for subsequent analysis of possible aerosols. After dark phase steady state conditions matched planned conditions, the xenon arc was turned on. The reactor was allowed to achieve steady state conditions at which time all appropriate data was recorded. The difference between dark and light phase steady state conditions was used as a measure of NO oxidation at the various run conditions.

CHAPTER 2

SUMMARY AND CONCLUSIONS

This study was performed to determine the technical and economical feasibility of a photochemical technique for the oxidation of NO. This approach takes advantage of chemical reactions similar to those responsible for ambient photochemical smog incidents. The reactions are initiated while the pollutants are still highly concentrated within the flue gas and while the reaction products can be safely collected. With carefully controlled light limited and time limited conditions, it is possible to maintain good control on the extent of NO oxidation and the reaction products. Photochemical pretreatment for NO oxidation was proposed as a near term solution for the need for supplemental NO_x control technology for coal-fired boilers.

The experimental program has been designed to address five specific questions concerning photochemical system operating characteristics and cost. One of the principal issues is the total energy requirement. The present analyses are necessarily restricted to the commercially available, low efficiency, laboratory-scale, ultraviolet lamps. Energy requirements using these lamps were anticipated to be high. A second issue concerns the possible need for injected hydrocarbons to sustain the photochemically initiated free radical chain reactions. Propylene has been arbitrarily chosen for study since it is a readily available hydrocarbon of low cost. The fraction of hydrocarbon consumed is the third issue of importance since the hydrocarbon is itself a criteria pollutant. A number of chemical and physical conditions could conceivably influence the extent of NO oxidation and the study of these variables constitutes the fourth major work area. The quantities and chemical characteristics of reaction products are the remaining issues addressed in the experimental program.

A continuous stirred tank reactor was designed to simulate coal-fired power plant stack conditions and to allow rapid turnaround for maximum experimental runs. Simulated flue gas was blended externally and then irradiated inside a quartz reactor using a high pressure mercury-doped xenon arc. Light intensity in the 3000 to 4000 Å spectral band was routinely measured using NO_2 photolysis. Gas analyzers operating off a common outlet manifold with a short residence time were used to measure reactant and product concentrations on a continuous basis. Millipore filter samples were taken for subsequent analysis of possible aerosols.

Strong spectral effects were identified. Ultraviolet light in the middle ultraviolet spectrum of 2400 to 3000 Å appeared to be particularly effective in NO oxidation. It was determined that SO_2 was not responsible for this phenomenon, despite the fact that it was the strongest middle UV absorber in the system. NO conversion actually improved as the SO_2 concentration decreased. The enhancing effect was probably due to the photolysis of aldehydes, nitrous acid and hydrogen peroxide; however, definitive conclusions could not be reached on the basis of available data.

The effect of UV light intensity and propylene concentration were tested in a large series of tests. NO oxidation in the absence of UV light was essentially zero in all runs tested. There was measurable NO oxidation in the absence of hydrocarbon; however, the efficiency of conversion was limited to approximately 10% of the inlet NO_x. A series of NO conversion isopleths were defined for the various levels of the two principal variables. The relationships were characterized by distinct light sensitive zones, hydrocarbon sensitive zones and a ridge between the two in which both variables were important. Generally, it appeared necessary to use propylene at a stoichiometric ratio of 1 to 2, depending on the light intensity. The required light energies appeared to be equivalent to 3 to 5% of station power for tests done with inlet NO_x concentrations of 600 ppm (v/v). System performance at higher NO_x levels of 1200 ppm (v/v) was considerably poorer than those at the low concentrations.

A comparison of system performance using propylene and ethylene indicated that the reactivity of the hydrocarbon is an important limitation on the amount of NO oxidized. Except at high concentrations, the NO conversion was substantially higher with propylene. This work was consistent with results of the SO_2 sensitivity tests which indicated that competition for hydroxy radicals suppresses system performance.

A major problem involved in the use of the photochemical system with propylene appears to be the fraction of injected hydrocarbon which is not consumed in the reactor. In the experimental runs, over 50% of the material was released without reacting.

Due to the favorable cost, it is assumed that combustion modifications will be used to the maximum extent possible before the use of a flue gas treatment system will be considered. Therefore, it is important that the system be compatible with the conditions resulting from such modifications. Tests with various excess air levels confirms that the photochemical systems performs adequately down to oxygen concentrations of 2 to 3%. Also, the efficiency of the reaction mechanisms appears to increase at lower initial NO_x concentrations. It is proposed that the latter phenomenon is due to the consumption of hydroxy radicals by NO_2, nitrous acid, and nitric acid, which would otherwise react with propylene in radical branching reactions. Since combustion modifications could conceivably lead to increased carbon monoxide concentrations, a small test series was performed to test the influence on the system. As expected, the hydroxy radical reaction with CO leading to a hydroperoxy radical appears to enhance conversion of NO. Carbon dioxide at concentrations of up to 20% did not have any measurable influence on the system.

Aerosols were not generated in measurable quantities in any of the runs. Condensation nuclei counter readings were consistently at background levels. X-ray fluorescence tests of the Millipore filter samples indicated that less than 1% of the sulfur was present as aerosol. Minor quantities of deposited nitrate and sulfate material were occasionally visible on the inner surfaces of the reactor and in the effluent lines.

Generally, the sulfur material balance could account for 97 to 99% of the input quantities. Unaccountable nitrogen quantities reached 15% of input values for the very reactive conditions, presumable because the system had proceeded beyond the NO_2 peak and substantial quantities of nitric acid and organic nitrate compounds had begun to form. Between

25 and 50% of the input carbon could not be accounted for as propylene. The principal reaction products included formaldehyde and acetaldehyde. Mass spectrometer analyses of a selected group of runs suggest that an extremely large group of organic coumpounds can form at trace levels. The major compounds identified in the GC-mass spectrometer tests included acetic acid and acetaldehyde. Other compounds present in the range of 1 to 2 ppm included nitromethane, methylformate, methylnitrate, butyl formate, toluene, and acetophenone.

Capital and annualized costs were estimated for a model plant. Results indicate that capital costs could be in the range of $37 to $50 per kW, and that the annualized costs would be 3.8 to 5.6 mills/kWh. The range in values reflects the variation in cost as a function of the desired NO conversion efficiency. These costs are lower than for some costs of comparable systems. Catalytic reductions systems and NH_3 injection systems, however, have reported costs approximately ½ those for the photochemical system. It is concluded that the photochemical system based on propylene will be used only if the alternative processes cannot be adapted for coal-fired boilers, or if there are operational problems with such systems when used in full-scale systems.

The principal conclusion of the study is that photochemical control techniques, as presently conceived, are not competitive. Additional bench-scale study of different hydrocarbons and improved lamps, however, could conceivably yield a system considerably better than the alternative flue gas denitrification systems.

CHAPTER 3

RECOMMENDATIONS

1. It is recommended that the present experimental system be utilized to evaluate the system performance with acetone and formaldehyde. Both compounds participate in primary photochemical processes and should, therefore, be less susceptible to the reactivity problem identified with propylene.

2. Further studies should also be done to test system efficiency at lower initial NO_x levels. The experimental tests in this project suggested improved NO oxidation efficiency at lower NO_x concentrations. The 600 ppm level used in most of the present work is higher than would be expected for coal-fired boilers modified for reduced NO_x generation. Accordingly, the cost estimates could be high.

3. The analytical capability of the system should be improved so that better nitrogen balances could be prepared. The response of the chemiluminescent analyzer to nitrous acid and to nitric acid should be determined.

4. The performance of the photochemical system at temperatures of 700 to 800°F should be analyzed to determine if the irradiation could be one downstream from a hot side electrostatic precipitator.

5. A kinetic simulation model should be used as an aid to understanding the reaction system.

CHAPTER 4

BACKGROUND

NO_x CONTROL TECHNIQUES

The photochemical process for NO_x control is being developed in anticipation of a need for control of coal-fired utility boiler emissions. In this section, the growing importance of coal-fired boiler NO_x emissions is discussed. NO_x formation mechanisms in the combustion process are briefly addressed to indicate the potential benefits of modified operating conditions for NO_x suppression. It is concluded that such "combustion modification techniques" are economical and effective; however, these may not be adequate to achieve the very stringent NO_x emission levels being considered by EPA. Accordingly, some type of supplemental control technology may be necessary. Competitive add-on techniques are briefly described so that the photochemical process studied in this project can be critically evaluated.

Coal-Fired Boilers as Sources of Nitrogen Oxides

Constantly growing energy demands, coupled with the shift toward greater national dependence on available coal supplies, will result in a major increase in NO_x emissions from coal-fired boilers in the next 20 years (Acurex, 1977). As shown in Figure 1, the NO_x emissions from stationary sources (point and area) have increased from 3.9 Tg/Yr in 1950 to a present rate of 12 Tg/Yr and will probably reach 17 Tg/Yr by 1990. Coal-fired boilers are responsible for approximately 30% of these emissions, and thus, represent the largest source category (Salvesen *et al*., 1978).

The typical flue gas composition of coal-fired boilers is provided in Table 1. This is based on 3.5% sulfur, 16% ash coal, 10,500 Btu/Lb. and an excess air rate of approximately 25%. Note that there is a wide

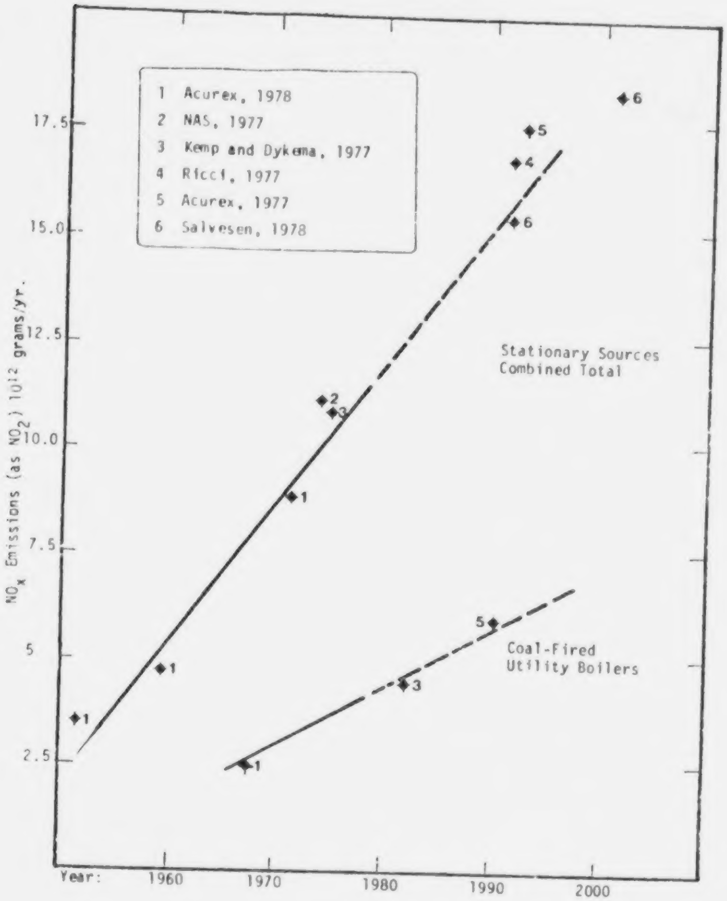

Figure 1. Trends in the emissions of NO_x from stationary sources.

TABLE 1. TYPICAL FLUE GAS COMPOSITION OF COAL-FIRED BOILERS

Contaminants	
NO_x	
Horizontally Opposed Firing[a]	400- 900 ppm
Tangential Firing[a]	300- 600 ppm
Front Wall[a]	400- 850 ppm
Cyclone[a]	500-1200 ppm
SO_2	1000-3000 ppm
SO_3	5- 30 ppm
HC	1- 100 ppm
CO	10- 50 ppm
Major Components	
N_2	74%
O_2	4%
CO_2	13%
H_2O	9%

[a] Reference - Acurex, 1978.

variation in the initial NO_x levels for common firing modes. Tangential units presently comprise 35% of the utility boiler population and will represent a greater share in the future due, partially, to the favorable NO_x emission rates. Cyclone boilers represent only 10-30% of present coal-fired generating capacity but are responsible for over 19-22% of the NO_x emissions from this source category (Ctvrtnecek and Rusek, 1977). These boilers connot achieve the required 0.7 lBs./MMbtu NO_x emission rate[a] due to the high heat release rates characteristic of the cyclone boilers. Because of this problem very few cyclone boilers have been ordered since 1974 (Batayko, 1979) despite the slight energy efficiency advantage over other types of boilers, and the ability to burn high ash-low fusion temperature coals.

The NO_x control requirements will probably be set as low as possible considering available technology due to the increasing concern over NO_x participation in oxidant formation and the health implications of NO_2. EPA has informally stated control technology goals of 200 ppm (v/v) in 1980 and 100 ppm (v/v) in 1985 for pulverized coal-fired boilers (McCutchen, 1977).

Control will be achieved by use of combustion modification techniques, add-on control processes or a combination of the two. To date, most of the research has been devoted to the development of combustion control due to low inherent costs (Ricci, 1977). There is growing realization, however, that such techniques are limited with respect to NO_x reduction in coal-fired boilers and can have some adverse impact on boiler performance when applied zealously.

Combusion Modifications for Control of Nitrogen Oxides

There are two general formation mechanisms leading to the generation of NO_x during the combustion of coal. "Thermal" NO_x results from the high temperature fixation of molecular nitrogen. "Fuel" NO_x results from the oxidation of organically bound nitrogen. The relative importance of each mechanism cannot be determined with presently available information (Armento, 1975); however, it is believed that fuel NO_x comprises 50 to 100% of the total NO_x (Dykema, 1978). Nitric oxide (NO) is the predominant species in each case, with less than 5 to 10% nitrogen dioxide (NO_2). While NO_2 is the thermodynamically favored form at stack temperatures, the formation mechanisms are quenched before significant conversion of NO can occur in the boiler.

---

[a] Standard of Performance for New Sources (NSPS), a regulation promulgated by the U.S. Environmental Protection Agency.

Fuel nitrogen oxidation is a complex physiochemical process governed primarily by the local conditions surrounding the initial combustion zone (Acurex, 1977). As shown in Figure 2, the nitrogen in the coal is partitioned into a vapor fraction and a char fraction upon injection into the boiler. A portion of the volatile fraction is oxidized to NO, some of which escapes the fuel rich reducing conditions of the burner flame (Heap et al., 1976). The nitrogen compounds remaining on the char particle are oxidized at a slower rate. The NO formed on the particle surface must penetrate the boundary layer before it is reduced to N_2. The NO_x yield of this set of simultaneous oxidation mechanisms is fortuitously only 10 to 40% with the lowest yields at the higher fuel nitrogen levels (Faucett et al., 1977).

Thermal NO_x results from a partially understood set of free radical reactions operative throughout the high temperature zone of the boiler. During the early combustion stage, a super equilibrium level of free radicals leads to the rapid formation of NO in a process which is sometimes termed "prompt" NO_x. In the later stages of fuel oxidation, a slower equilibrium moderated set of reactions represented by the Zeldovich mechanism (Reactions 1 to 3).

$$N_2 + O \rightleftarrows NO + N \qquad (1, a \,\&\, b)$$

$$M + O_2 \rightleftarrows M + 2O \qquad (2, a \,\&\, b)$$

$$N + O_2 \rightleftarrows NO + O \qquad (3, a \,\&\, b)$$

These reactions have a strong temperature dependence due to the high activation energy of reaction 1. The role of oxygen in a free radical transfer step explains the strong effect of available oxygen on the extent of thermal NO_x formation.

A number of combustion modification techniques have been developed in order to interfere with the fuel and thermal NO_x formation processes.

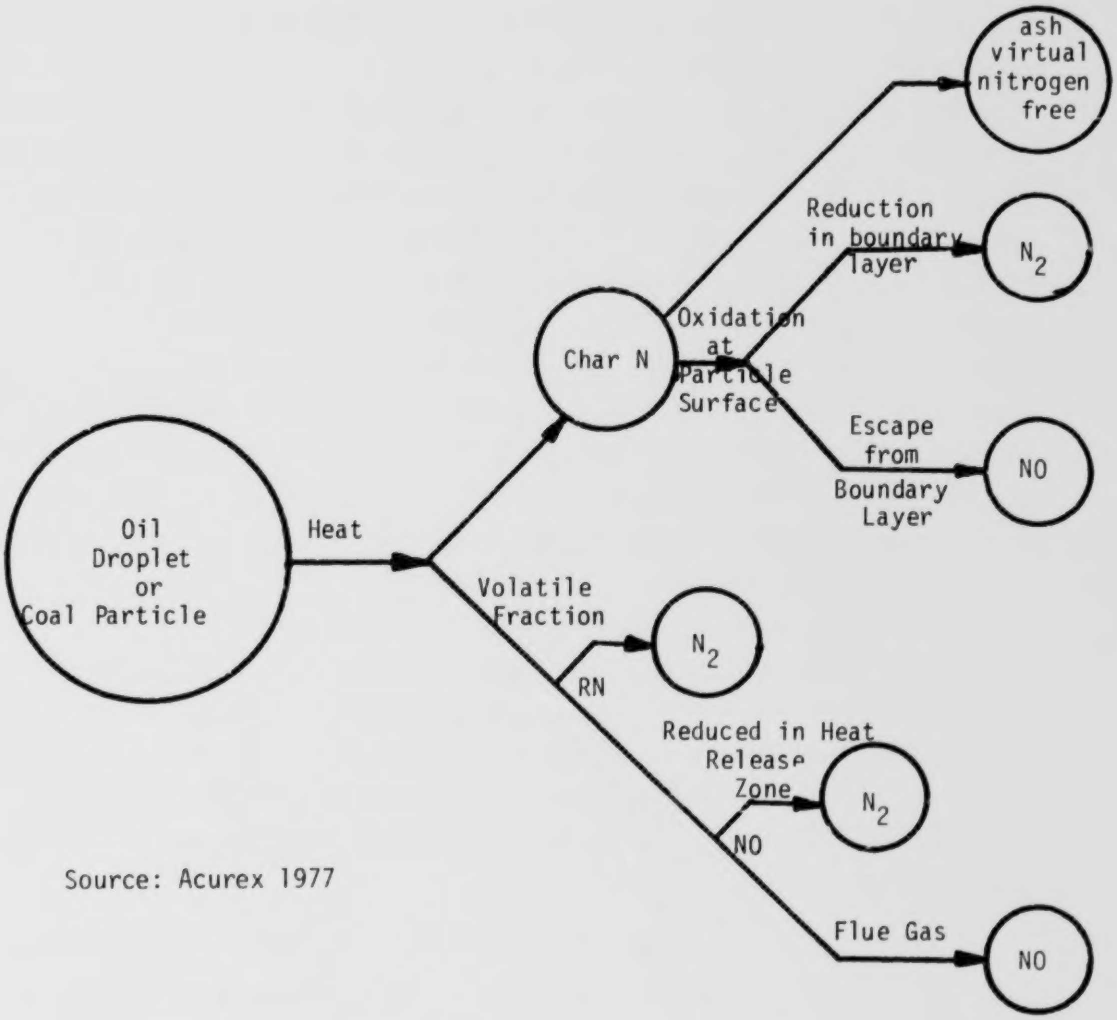

ash virtual nitrogen free
Reduction in boundary layer
N_2
Oxidation at Particle Surface
Char N
Escape from Boundary Layer
NO
Oil Droplet or Coal Particle
Heat
Volatile Fraction
N_2
RN
Reduced in Heat Release Zone
N_2
NO
Flue Gas
NO

Source: Acurex 1977

Figure 2. Possible formation mechanism for fuel NO_x.

These include: (1) low excess air, (2) off-stoichiometric combustion, (3) reduced air preheat, and (4) advanced burner design. Flue gas recirculation, a technique proven useful for gas- and oil-fired systems is not considered acceptable for coal-fired boilers (Armento, 1975) due possibly to the importance of fuel nitrogen oxidation and the insensitivity of fuel nitrogen to temperature reduction schemes.

The most successful techniques appear to be low excess air combustion and off-stoichiometric combustion (Armento, 1975; Selker, 1975). The positive effect of these two approaches is partially because the restricted oxygen level in the high temperature fuel oxidation zone inhibits both fuel and thermal NO_x formation (Armento, 1975).

Low excess air combustion is sometimes considered just good operating practice which should be used at all boilers regardless of NO_x reduction requirements. When the excess air is maintained in the 15 to 25% range, the flue gas volume is minimized and sensible heat loss is minimized. Boiler energy efficiency can be improved more than 1% in this manner. At lower levels of excess air, localized reducing conditions can lead to increased slagging. The potential benefit of low excess air is illustrated in Figure 3. Generally, the effectiveness of low excess air alone is limited to a maximum 20% NO_x reduction (Acurex, 1978).

Off-stoichiometric combustion may be accomplished in several ways depending on whether the boiler is new or is an existing unit which requires retrofit. For the latter case, selected burners can be operated with air only so that others can be operated fuel rich. This minimizes thermal and fuel NO_x formation mechanisms in the high temperature zones. With biased firing in this manner, boiler derating is necessary. For a new boiler, the same result can be accomplished without derating penalties by including a set of overfire air ports. The potential NO_x reduction available by means of off-stoichiometric combustion is limited to less than 40% (Acurex, 1978) as shown in Figure 4. New unit design equipped with overfire air ports show typical NO_x reductions of about 50% (Lachapelle, 1979).

A third approach for NO_x suppression which appears useful is the use of advanced burners. Pilot-scale tests have suggested that 200 ppm levels are achievable with low NO_x burner designs. Demonstration of this equipment on full-scale boilers is in progress (Lachapelle, 1979).

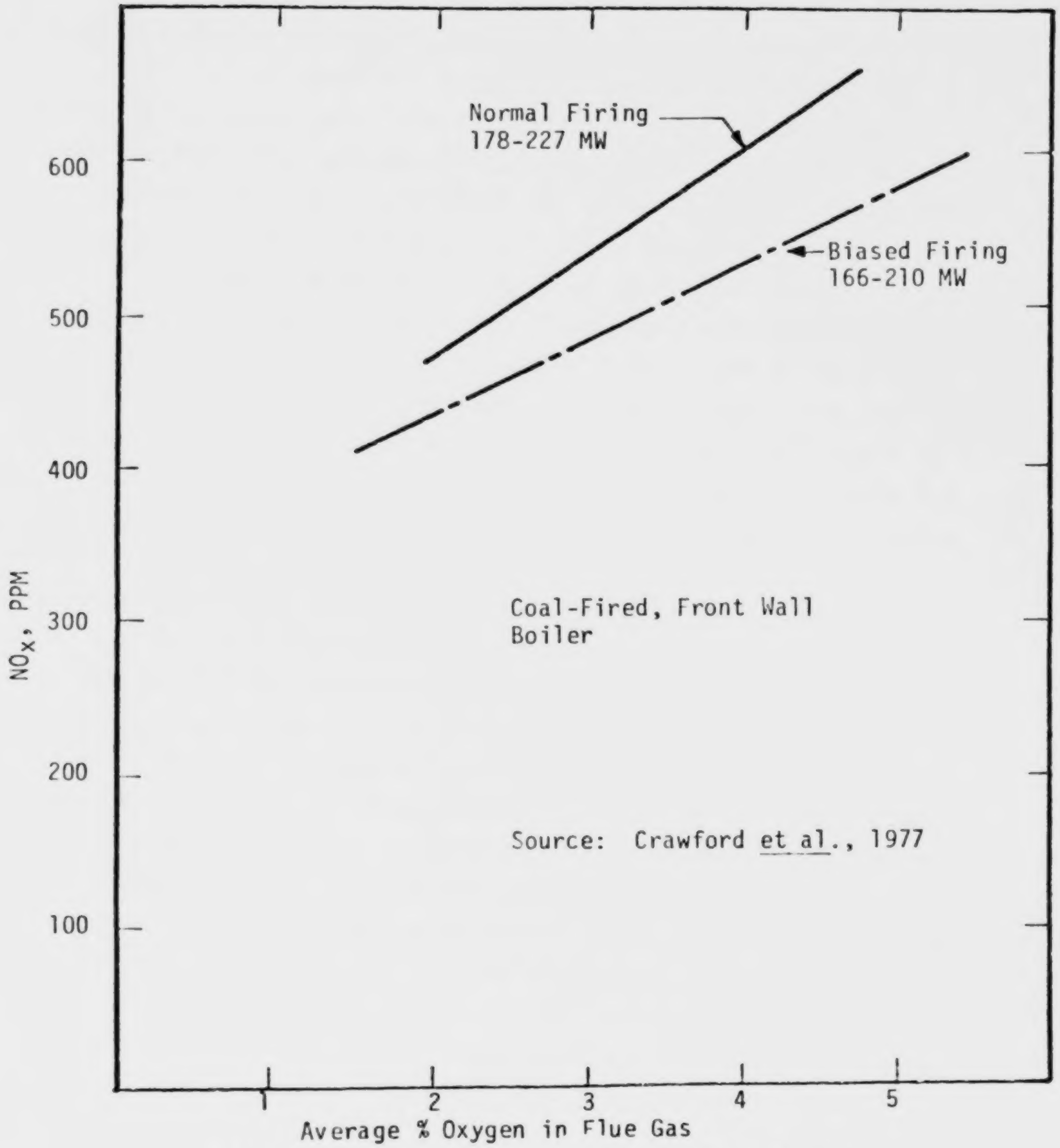

Figure 3. Effect of excess air on NO_2 emissions

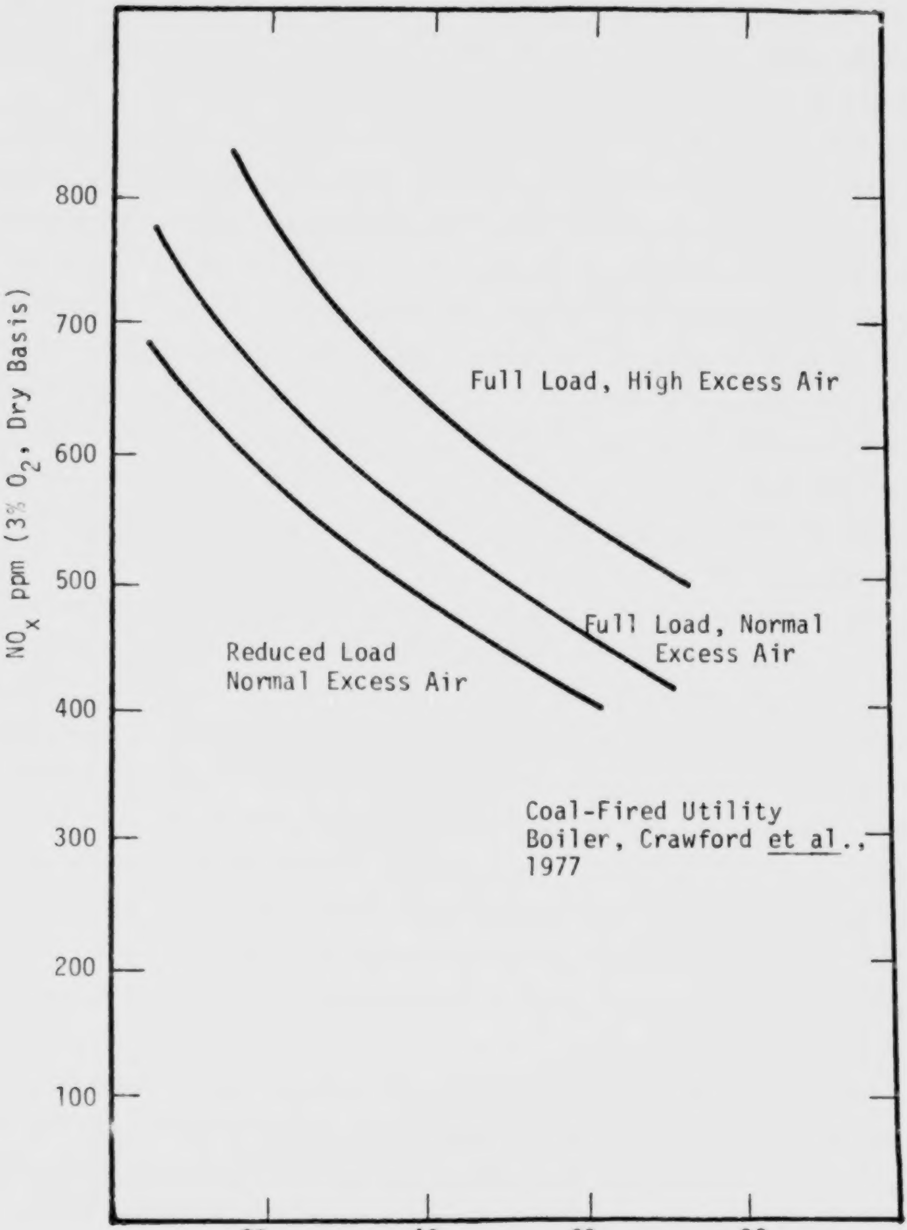

Figure 4. Effect of secondary air addition on NO_x emissions.

A number of other combustion modifications have been tested and found less desirable than low excess air, off-stoichiometric combustion, and advanced burner designs. These techniques include: flue gas recirculation, reduced air preheat, load reduction, and use of low nitrogen coal. All except the last involve energy penalties. These approaches generally provide much less than 20% NO_x reduction and probably will not be used substantially in the near future.

A coal-fired boiler utilizing the low excess air firing and/or off-stoichiometric combustion will probably have flue gases with 2 to 3% oxygen and 300 to 500 ppm (v/v) NO_x. The predominant chemical composition of the NO_x will continue to be NO. It is probable that all new boilers and most existing units less than 10 to 20 years old will include advanced combustion control techniques due to the inherent low cost. The use of low excess air involves no significant capital cost and provides a slight benefit in energy efficiency. The use of off-stoichiometric combustion does require additional burner ports and other equipment; however, retrofit capital costs remain at a very modest $1 to $2/kW (Mason et al., 1977).

There are several practical limitations to the use of combustion modification techniques due simply to the fact that boiler equipment was designed to operate under oxidizing conditions. As excess air and burner conditions are increasingly optimized for low NO_x boilers, operational problems appear. One of the most common of these is the reduction of ash fusion temperature near the base of the boiler which can lead to increased slagging (Crawford et al, 1977). Other potential problems include generation of carbon monoxide and high carbon carryover. The latter condition is important primarily because it represents a loss of boiler energy efficiency. An optimized level on NO_x control can minimize these side effects.

Potential aggravation of polycyclic organic matter concentration (POM) is an important disadvantage of combustion modifications. In one study done by Thompson and McElroy (1976), the use of staged combustion and flue gas recirculation resulted in a 40% increase in boiler POM emissions. It is apparent in Table 2 that some of the individual hydrocarbons such as pyrene and methyl anthracene exhibited dramatic increases when these combustion modifications were used. Considerably more experimental evidence is necessary to document the relationship between POM generation and NO_x combustion controls.

Flue Gas Treatment for Nitrogen Oxides Control

While the need for flue gas denitrication cannot be conclusively demonstrated at this time, there is substantial research interest due to the possible limitations of combustion modifications (Faucett et al., 1977; and Corbett et al., 1978). The potential market for these processes is indicated by the fact that there are over 40 candidates being intensively studied by equipment manufacturers, utilities and interested research organizations.

The flue gas treatment techniques can be categorized into four major groups as shown in Figure 5. The approximate number of processes in each category is indicated on the chart; however, there are undoubtedly a few processes still in the bench scale stage which have not been publicly disclosed.

The dry processes enjoy several competitive advantages over the wet techniques since dry systems are inherently less complex and do not generate a waste liquor stream. Dry processes have received most of the early research attention. Disadvantages of dry NO_x control include low NO_x control efficiency, sensitivity to flyash poisoning of catalyst, $(NH_4)_2SO_4$ and NH_4HSO_4 fouling of heat exchangers, and high additive cost. The wet processes are capable of higher NO_x removal efficiencies and can be used for simultaneous NO_x and SO_2 control. These processes generally yield an undesirable waste stream.

Selective Noncatalytic Reduction

This process is an intuitively attractive approach to NO_x control. Reduction of NO_x to N_2 occurs by means of a set of free radical chain reactions resulting from the injection of NH_3 and/or H_2 in the superheater region of the boiler. There are, in fact, two competing mechanisms represented by the overall reactions shown below (Faucett et al., 1977):

$$4\ NH_{3(g)} + 4\ NO_{(g)} + O_{2(g)} \rightarrow 4\ N_{2(g)} + 6\ H_2O_{(g)} \qquad (4)$$

$$4\ NH_{3(g)} + 5\ O_{2(g)} + \quad \rightarrow 4\ NO_{(g)} + 6\ H_2O_{(g)} \qquad (5)$$

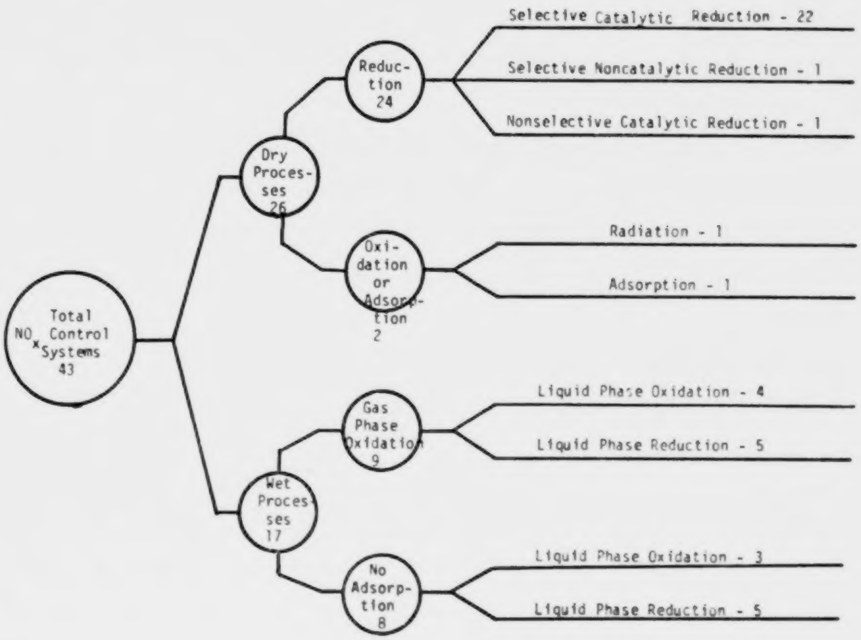
Total NO$_x$ Control Systems 43
Dry Processes 26
Reduction 24
Selective Catalytic Reduction - 22
Selective Noncatalytic Reduction - 1
Nonselective Catalytic Reduction - 1
Oxidation or Adsorption 2
Radiation - 1
Adsorption - 1
Wet Processes 17
Gas Phase Oxidation 9
Liquid Phase Oxidation - 4
Liquid Phase Reduction - 5
No Adsorption 8
Liquid Phase Oxidation - 3
Liquid Phase Reduction - 5

Figure 5. Classification of NO$_x$ flue gas treatment processes.

TABLE 2. EFFECT OF COMBUSTION MODIFICATION TECHNIQUES ON THE EMISSION OF POLYCYCLIC ORGANIC MATTER

	Concentration [μg/dscm]			
Compound	Baseline	Biased Firing	15% Recirculation	Biased Firing & Recirculation
Anthracene/Plenanthrene	115.0	119.5	92.8	157.3
Methyl Anthracenes	34.4	32.3	57.1	65.0
Fluoranthracenes	33.2	73.5	15.8	28.9
Pyrene	9.7	34.7	14.9	31.0
Total	192.3	260.0	180.6	277.2
% of Baseline	100	135	94	144

From: Thompson and McElroy, 1976.

Within a very narrow flue gas temperature range, reaction 4 is favored over reaction 5, thereby providing an opportunity for a net reduction in NO. Applied improperly, however, there is the potential for an increase in total NO_x levels. Unless injection is done within 150°F temperature range (Muzio and Arand, 1976), a number of undesirable conditions can result, including: (1) incomplete reduction of NO, (2) emission of excess NH_3, and (3) increase in total NO_x emissions due to NH_3 oxidation. This narrow optimum temperature range is illustrated in Figure 6. While it is possible to modify this temperature zone by combined use of NH_3 and H_2, the safety problems involved in the use of a highly explosive gas in a boiler may hamper H_2 use (Faucett et al., 1977). Thus, there is a serious unresolved problem. Further, gas temperature at any one injection port in the convective region of a boiler experiences swings of more than 200°F as boiler load varies in diurnal and seasonal cycles (Muzio and Arand, 1976).

Exxon, a developer of one such process, has estimated annualized costs for a 1000 MW coal-fired boiler with an initial NO_x level of 300 ppm (v/v) and a final desired level of 100 ppm (v/v) at 4.76 to 10.2 million dollars per year (Lyon as reported by Muzio and Arand, 1976). This is equivalent to 0.75 to 1.6 mills per kWh assuming an average capacity factor of 75% for a base loaded unit. Capital costs would be low since equipment requirements are limited to an NH_3 storage and distribution system. The principal operating cost is for NH_3, which is dependent on the rapidly rising cost of natural gas. The estimates of annualized costs provided above are for an ideal NO_x inlet concentration. Costs should rise proportionally to the inlet level of NO_x.

While this approach is the most straightforward, it is apparent that some serious operational problems and high operating costs discourage use in this country. Since NO_x reduction is limited to 50 to 70%, even at very high NH_3/NO_x ratios of 3 to 4 (Faucett et al., 1977), it is possible that this approach will serve primarily oil-fired boilers.

Selective Catalytic (Dry, Gas Phase) Reduction

This category includes the majority of processes under development, as demonstrated in Figure 5. Reduction of NO_x occurs in a catalytic re-

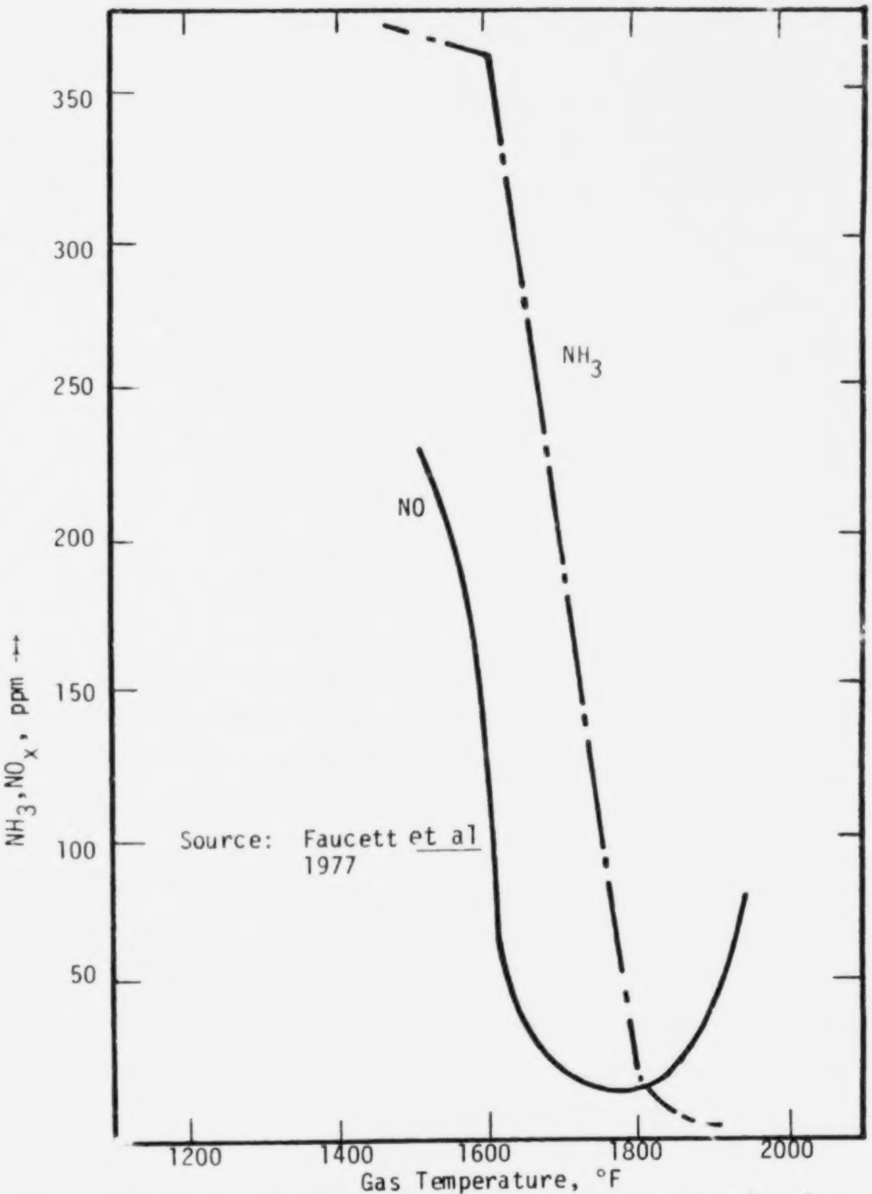

Figure 6. Effect of temperature on NO_x removal in the selective noncatalytic reduction process.

actor downstream of the boiler. By using a catalyst, it is possible to avoid the potentially crippling temperature sensitivity problems and fouling problems which plague the selective noncatalytic process performed in the boiler superheater. These catalytic reactions require only a 0.9 to 1.2 NH_3/NO stoichiometric ratio, thus minimizing sensitivity to rising NH_3 costs.

The two sets of composite reactions shown below generally illustrate the type of overall reactions responsible for NO reduction in the various catalytic processes (Faucett et al., 1977). The catalyst and design characteristics affect the actual overall stoichiometry of the processes.

$$4\ NH_{3(g)} + 2\ NO_{2(g)} + O_{2(g)} \xrightarrow{\text{Catalyst}} 3\ N_{2(g)} + 6\ H_2O_{(g)} \tag{6}$$

$$4\ NH_{3(g)} + 4\ NO_{(g)} + O_{2(g)} \xrightarrow{\text{Catalyst}} 4\ N_{2(g)} + 6\ H_2O_{(g)} \tag{7}$$

$$6\ NO_{(g)} + 4\ NH_{3(g)} \xrightarrow{\text{Catalyst}} 5\ N_{2(g)} + 6\ H_2O_{(g)} \tag{8}$$

$$6\ NO_{2(g)} + 8\ NH_{3(g)} \xrightarrow{\text{Catalyst}} 7\ N_{2(g)} + 12\ H_2O_{(g)} \tag{9}$$

$$4\ NH_{3(g)} + 3\ O_{2(g)} \xrightarrow{\text{Catalyst}} 2\ N_{2(g)} + 6\ H_2O_{(g)} \tag{10}$$

The catalytic process generally requires a high efficiency electrostatic precipitator on the "hot" side (before air preheater) to protect the catalyst from potential poisons and flyash coating. Malfunctions of these precipitators represent a serious threat to the catalyst life and long term NO_x reduction performance. In addition to the precipitator, a catalyst-containing reactor operating in a temperature range of 300 to 500°C is necessary. For these reasons, the capital costs for catalytic systems will probably be much higher than the previously discussed noncatalytic approach. A recent compilation of these processes include capital costs estimates ranging from \$10 to \$36 per kW (Mason et al., 1977). To put these numbers in perspective, consider that the boiler-turbine assembly costs \$400 to \$600 per kW and nonregenerative SO_2 control systems cost \$50 to \$150 per kW. The NO_x costs are low but certainly not insignificant. Annualized cost estimates range from a very low 0.2 mills per kWh to a moderate level of 1.8 mills per kWh. The lower NH_3 requirements offsets the higher capital costs involved in the catalytic approach. There is very little meaningful data concerning the possible useful life of the catalyst under conditions similar to coal-fired boilers, since almost all experimental work has concerned oil-fired boilers.

Radiation Oxidation

The EBARA-JAERI process is of interest in this report primarily because of the superficial similarity to the photochemical process. Acutally, the two radiation techniques are quite different with respect to chemical mechanisms used and to reaction products formed. The flue gas from the air preheater is treated in a cold side (after air preheater) electrostatic precipitator and then irradiated by electron beams to yield a highly corrosive particulate. This material is removed from the gas stream in a second precipitator (Acurex, 1977; Machi et al, 1975). Costs for this highly complex process range from a moderately high \$100 per kW to a phenomenal \$1000 per kW. The high value is probably most realistic for coal-fired boilers. Power plant derating of approximately 3.3% is required to satisfy energy demand. Due to limited size of presently available electron beam accelerators, large numbers (100 to 500) would be required for average sized coal-fired power plant applications.

It is readily apparent that this process is not a prime candidate for control of coal-fired boilers. The only advantage to the approach is the freedom from chemical additives and the simultaneous SO_2 and NO_x control without the use of wet scrubbers. It is doubtful that these advantages will outweigh the high costs and potential operational difficulties of electron beam accelerators.

Absorption of NO

There are at least eight processes under development which first absorb NO and then attempt to oxidize or reduce the nitrites and nitrates in solution. Very large absorbers are required to overcome the poor solubilities of NO. Performance appears partially sensitive to the highly variable SO_2 concentrations and to O_2 concentrations (Faucett et al, 1977). To date, this group of processes has only been studied on the bench and pilot scales. Development work has been directed toward oil-fired boilers.

Preliminary cost estimates suggest capital costs of \$65 to \$130 per kW and annualized costs ranging from 4.8 to 7.4 mills per kWh (Faucett et al, 1977). These represent ideal costs based on an absolute minimum NO_x reduction requirement of 125 ppm. All of these costs are for oil-fired boiler applications.

Oxidation of NO with Liquid Phase Oxidation or Reduction

This category of control techniques is most similar to the photochemical technique being studied. In each process, an additive is injected into the flue gas directly downstream of the air preheater. Additives such as ozone and chlorine dioxide are used to oxidize the NO to NO_2 while minimizing formation of N_2O_5 and other nitrogen compounds. By converting the very insoluble NO to the relatively soluble form of NO_2, it is possible to use much smaller absorbers than necessary for the direct NO absorption processes. This cost saving is partially offset by the much higher cost of the gas pnase oxidant. Harrison (1976) has estimated the capital and operating costs of an ozone plant for a 500 MW coal-fired power plant with 600 ppm inlet NO_x concentration at \$57.60/kW and 4.7mills/kWh respectively. Due to the cooling requirements of the ozone plant, the flue gas from the processes is increased by as much as 10%. The high concentration ozone stream presents serious safety problems which may not be adequately reflected in these costs.

Absorption processes range from \$84/kW to \$134/kW (Acurex, 1977). Corresponding annualized costs vary from 6.7 mills/kWh to 8.9 mills/kWh (Acurex, 1977). All of these costs are for oil-fired applications which require considerably less NO_x reduction than coal-fired boilers. Most of these processes have an optimal control efficiency of 60 to 70%. The potential for toxic secondary product formation due to ozone or chlorine dioxide side reactions has not yet been addressed.

PHOTOCHEMICAL NO_x CONTROL TECHNIQUES

A conceptual design of a photochemical control system for NO_x control at a coal-fired utility boiler is analyzed in this section. Based on anticipated light absorption characteristics and commercial lamp emission spectra, the potential energy requirements are calculated as a function of the net product quantum yield of the various photochemical reactions.

The reaction products and NO_2 quantum yields of four possible sets of reaction mechanisms are reviewed in this section. It is concluded that photochemical systems could be economically competitive. Major issues which need to be resolved in the experimental phase of the project are identified. Previous studies of photochemical techniques are discussed briefly to clarify possible reasons why this control approach has not been studied earlier.

Previous Studies

General Electric (Browne and Stone, 1965) tested the SO_2 control efficiency of ultraviolet light and corona discharges. Unfortunately, the energy calculations were not corrected for the 2% UV light absorption which occurred in the small diameter tubular reactor (path length of 1 inch). Because of this error, it was concluded that costs for a photochemical system were not competitive. Westinghouse (Hamm, 1965) performed a screening study of possible physiochemical means to collect sulfur dioxide, and photochemistry was only one of a large number of approaches tested. The researchers restricted the study to the infrared spectrum and not surprisingly reached the conclusion that "photochemistry" was not sufficiently energy efficient for use in SO_2 control. This study is of interest only because it may have limited research interest in the further evaluation of more reasonable photochemical techniques. Neither of the above studies considered NO_x control since at that time it was assumed that combustion modification techniques would be adequate for the modest NO_x reductions considered necessary.

Dols and Boknoven (1974) described a process for the oxidation of NO in coke oven gas to prevent pipeline gumming. This appears to be the first process developed for the photochemical oxidation of NO for commercial purposes. Oxidation is accomplished using a butadiene/NO ratio of two. The initial NO concentration is reported to be only 0.25 ppm (v/v), three orders of magnitude less than levels in coal-fired boilers. The gas stream was irradiated in the 2050 to 2200 Å absorption band of the butadiene. For these reasons, the system appears to be quite different from the photochemical system studied in this project.

Machi et al. (1975) developed a process for the simultaneous control of SO_2 and NO_x using either ionizing radiation or ultraviolet light. This process is the basis for the EBARA-JAERI system described earlier. This is probably the first photochemical-type system proposed for control of NO_x from a power plant. Irradiation is done with an electron beam which presumably results in hydroxyl and hydroperoxy radical formation by the dissociation of water vapor.

It is apparent that photochemical techniques have not been studied extensively. The work to date has been limited to several specialized or exotic applications. Considering the widespread nature of photochemical smog incidents involving the ambient level oxidation of nitrogen oxides, it is surprising that a system based on conventional smog-type reaction mechanisms has not been proposed.

Photochemical System Conceptual Design

A flowsheet for a photochemical treatment system on a coal-fired boiler is shown in Figure 7. This includes the existing equipment for particulate and sulfur dioxide collection plus the equipment needed to photochemically treat the nitrogen oxides. The photochemical reactor has been located downstream of the electrostatic precipitator in order to reduce erosion of lamp optical surfaces. Using a cylindrical design with the lamps centrally located, it is possible to achieve reasonable light absorption. The dimensions of the reactor are selected to obtain adequate path length and gas retention time. Irradiated effluent is then sent to the flue gas desulfurization system where the SO_2 and NO_2 are absorbed in an alkaline slurry. The lamps are mounted on vertical support rods running parallel to the reactor centerline. Due to the limited size of presently available ultraviolet lamps, over 700 units (length, 5 feet; diameter, 6 inches) would be required to get the intensities considered necessary. The average superficial gas velocity has been set at 5 feet per second so that the necessary retention time can be achieved without excessive reactor heights. Other assumed design parameters are summarized in Tables 3 and 4.

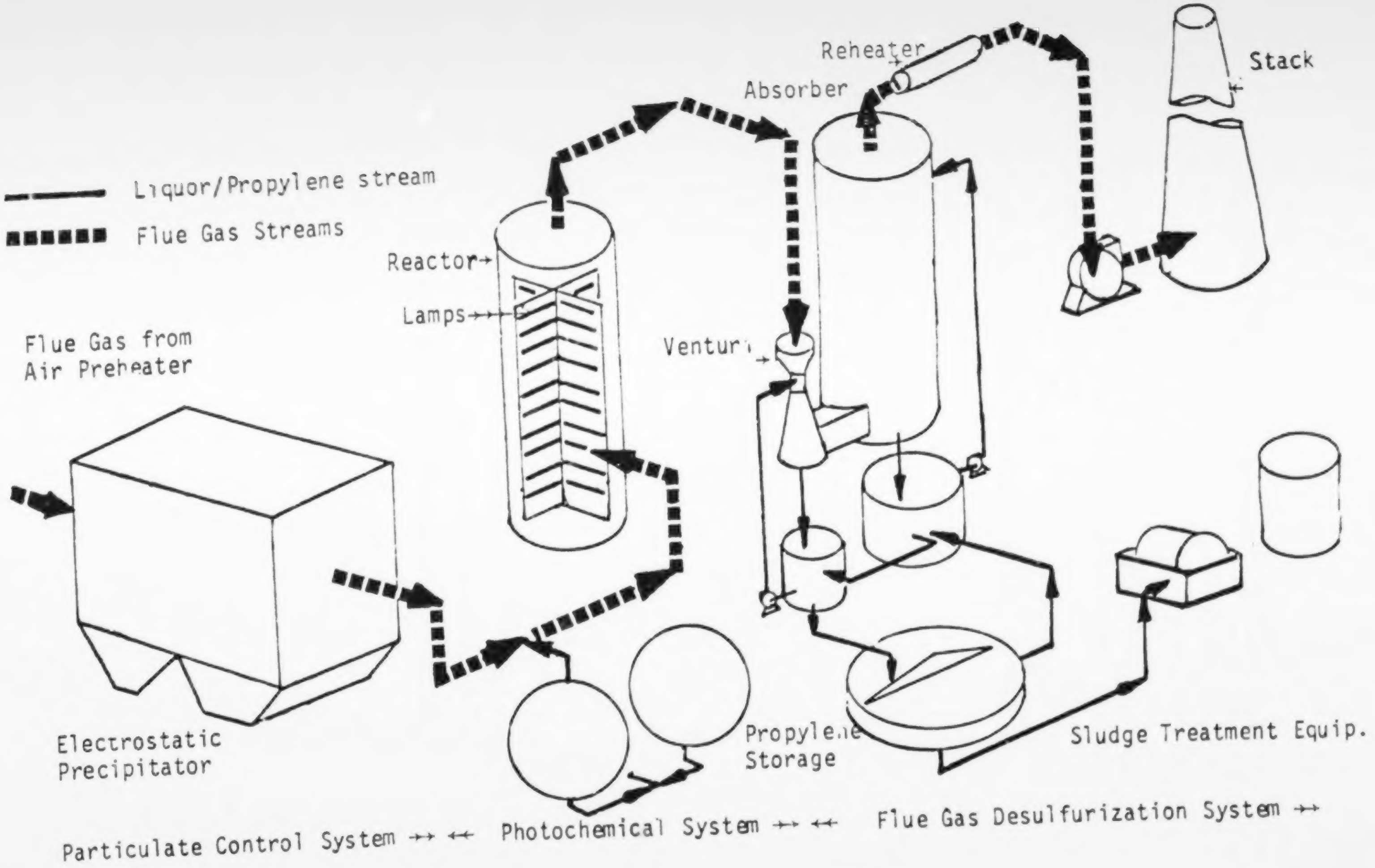
Liquor/Propylene stream
Flue Gas Streams
Reactor
Lamps
Flue Gas from
Air Preheater
Electrostatic
Precipitator
Venturi
Absorber
Reheater
Stack
Propylene
Storage
Sludge Treatment Equip.
Particulate Control System →→ ←←
Photochemical System →→ ←←
Flue Gas Desulfurization System →→

Figure 7. Photochemical system conceptual design.

TABLE 3. PHOTOCHEMICAL REACTOR DESIGN ASSUMPTIONS

Boiler Rating - 500 MW
Capacity Factor - 60%
Gas Flow Rate at Full Load - 1×10^6 scfm
Gas Temperature - 275°F
Gas Retention Time - 6 seconds
Gas Flow Characteristics - Well mixed
Lamp Type - Mercury doped xenon arc
Lamp Efficiency - 20%
Light Path Length - 10 feet

TABLE 4. EFFLUENT GAS COMPOSITION ASSUMPTIONS[a]

Pollutant	Inlet	Outlet
NO	450	100
NO_2	50	400
HNO_2	0	50
RCHO[b]	0	100
O_3	10	50
SO_2	1500	1500

[a] All concentrations in ppm.

[b] Includes formaldehyde and acetaldehyde

Photochemical System Operating Characteristics

The feasibility of photochemical systems is dependent on the efficiency of energy delivery/utilization and on the characteristics of the reaction products. These two subjects are reviewed using the conceptual design in the preceding section.

Energy Delivery Efficiency--

The energy cost of a photochemical system is the product of the energy delivery efficiency and the absorbed energy utilization efficiency. This is expressed in Equation 1.

$$C_p = \left(\frac{M_{NOX}}{\Phi_p E} \right) P_c \qquad \text{(Equation 1)}$$

Where: C_p = the total electrical power cost

M_{NOX} = moles of NOX treated per unit time

Φ_p = net product quantum yield of the combined reaction mechanisms

E = energy delivery efficiency for the specific reactor system and effluent gas composition

P_c = energy cost

Equation 1 indicates that energy cost is an inverse function of the net product quantum yield and the energy efficiency of generation/absorption. If either of these factors approach zero, the energy cost of a photochemical system would become prohibitive. Obviously, this is the case when deactivation of excited species occurs without chemical reaction and when there is a poor match between lamp emission spectrum and absorption bands of effluent compounds. Equation 1 also indicates that the energy is a linear function of the pollutant concentration. This is somewhat misleading since the energy delivery efficiency, E, should also be a function of the pollutant concentration in some cases. For example, if NO_x compounds are involved in an important primary photochemical process, then a reduction of the NO_x inlet concentration could reduce the overall energy delivery effectiveness. This would partially offset the cost savings of the initial NO_x inlet reduction.

In equation 2, the energy delivery efficiency factor has been expanded to specifically include the lamp generation efficiency across the middle and near UV spectrum, the average reactor pathlength, and the pollutant extinction coefficients. The net product quantum yield factor has been kept outside the summation sign since it is not strictly wavelength dependent.

$$\phi_p E = \phi_p \sum_{\lambda = 1800\ \text{Å}}^{\lambda = 12500\ \text{Å}} S_\lambda \left(e^{-\{\alpha_{\lambda 1} c_1 + \alpha_{\lambda 2} c_2 + \cdots + \alpha_{\lambda n} c_n\} L} \right) \qquad \text{(Equation 2)}$$

where S_λ = fraction of lamp input power emitted at wavelength λ

α_i = extinction coefficient of species i

c_i = concentration of species i

L = average pathlength for reactor

The parameter $\phi_p \cdot E$ has been estimated for the reactor configuration and effluent composition presented earlier. The data provided in Tables 3 and 4 has been combined with typical mercury-doped xenon arc emission spectra and the absorption spectra of the absorbing species (Figure 8). The results of the energy delivery calculations are shown in Table 5. The energy delivery to each of the absorbing species has been provided along with the total energy input to the gas stream. Almost complete light absorption is expected in the middle UV band of 2000 to 3000 Å, while only 60% absorption is achieved in the near UV band of 3000 to 3650 Å.

It is apparent that at the assumed pollutant concentrations, the aldehydes cannot compete effectively for the limited light available within its absorption spectrum. The middle ultraviolet band will be dominated by sulfur dioxide and ozone photolysis while the near ultraviolet band will be dominated by nitrogen dioxide photolysis.

The energy delivery estimates have been substituted back into equation 2 to derive a preliminary estimate of the net product quantum yield necessary for an economical control system. The desired energy demand is in the range of 0.5 to 2% of total station. It is apparent that the net product quantum yield must be greater than 0.5 to ensure reasonable

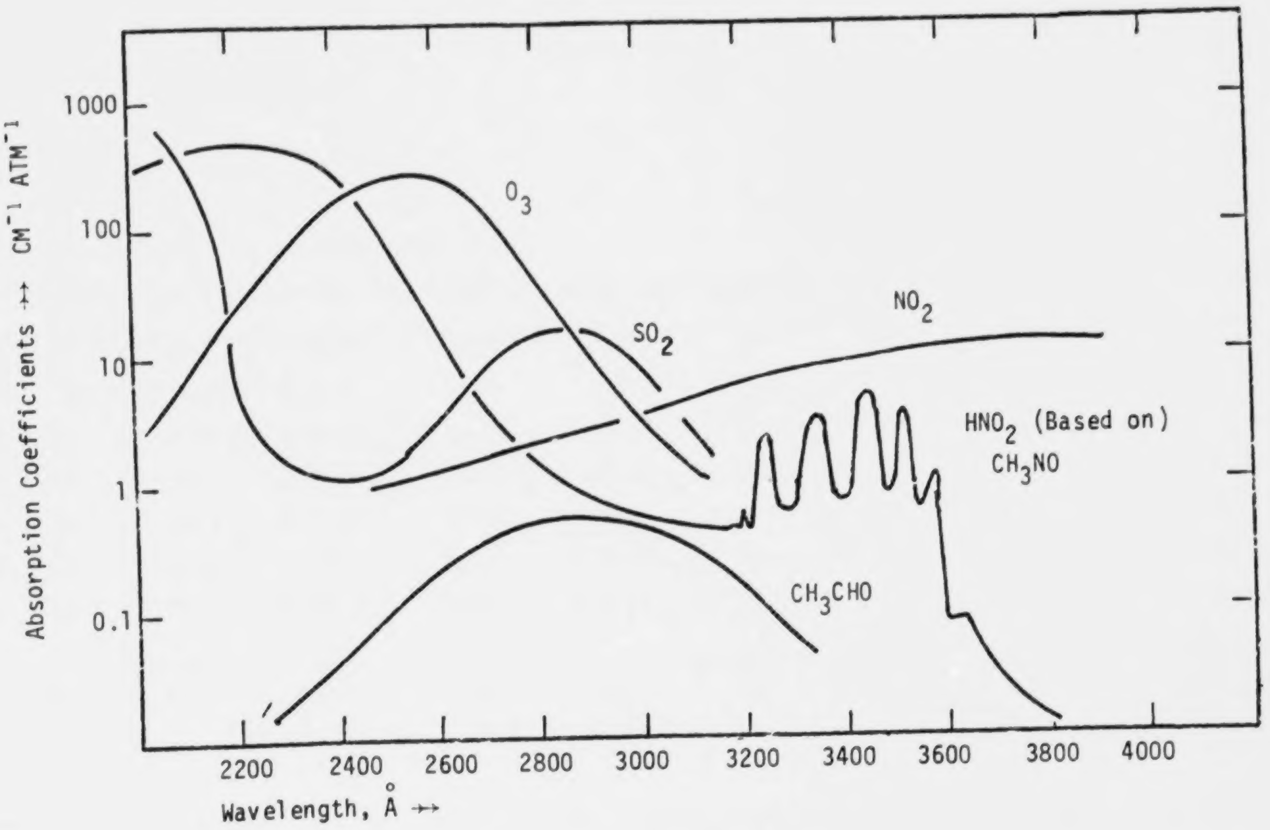

Figure 8. Absorption coefficients of flue gas components.

TABLE 5. ENERGY DELIVERY IN MODEL SYSTEM[a]

UV Band	S_λ	$c_i\alpha_i$ (moles/liter x liters/mole)						E	E_i, Quanta/Min				
Nm	Quanta/Min	NO_2	HNO_2	RCHO[b]	O_3	SO_2	Eff.	Quanta/Min	NO_2	HNO_2	RHCO[b]	O_3	SO_2
185-210	0	-	-	-	-	-	-	-					
210-240	26	$1.5\text{x}10^{-3}$	$6.4\text{x}10^{-4}$	Neg.	$3.2\text{x}10^{-3}$	$7.7\text{x}10^{-3}$	0.99	26	3	1.3	0	6.4	15.3
240-260	46	$3.9\text{x}10^{-4}$	$2.9\text{x}10^{-4}$	Neg.	$9.6\text{x}10^{-3}$	$2.9\text{x}10^{-3}$	0.99	46	1.4	1.0	0	33.5	10.1
260-280	39	$5.2\text{x}10^{-4}$	$6.5\text{x}10^{-4}$	$1.4\text{x}10^{-5}$	$6.4\text{x}10^{-3}$	$9.6\text{x}10^{-3}$	0.99	39	1.2	0.1	0	15.0	22.6
280-300	29	$7.7\text{x}10^{-4}$	$3.2\text{x}10^{-4}$	$2.6\text{x}10^{-5}$	$9.6\text{x}10^{-4}$	$9.6\text{x}10^{-3}$	0.99	29	2.0	0.1	0.1	2.4	24.4
300-320	74	$1.0\text{x}10^{-3}$	$4.8\text{x}10^{-5}$	$2.0\text{x}10^{-5}$	$3.2\text{x}10^{-5}$	$1.9\text{x}10^{-3}$	0.65	48	16.4	0.8	0.3	0.5	30.2
320-340	9	$1.8\text{x}10^{-3}$	$6.7\text{x}10^{-6}$	Neg.	Neg.	$1.0\text{x}10^{-4}$	0.47	4	4.0	0	0	0	0.2
340-380	85	$2.6\text{x}10^{-3}$	Neg.	Neg.	Neg.	Neg.	0.80	68	51.6	17.0	0	0	0

[a] Applicable to 500 MW station, 2% derating for lamp power and 20% lamp efficiency in spectral band <4000 Å

[b] Includes formaldehyde and acetaldehyde

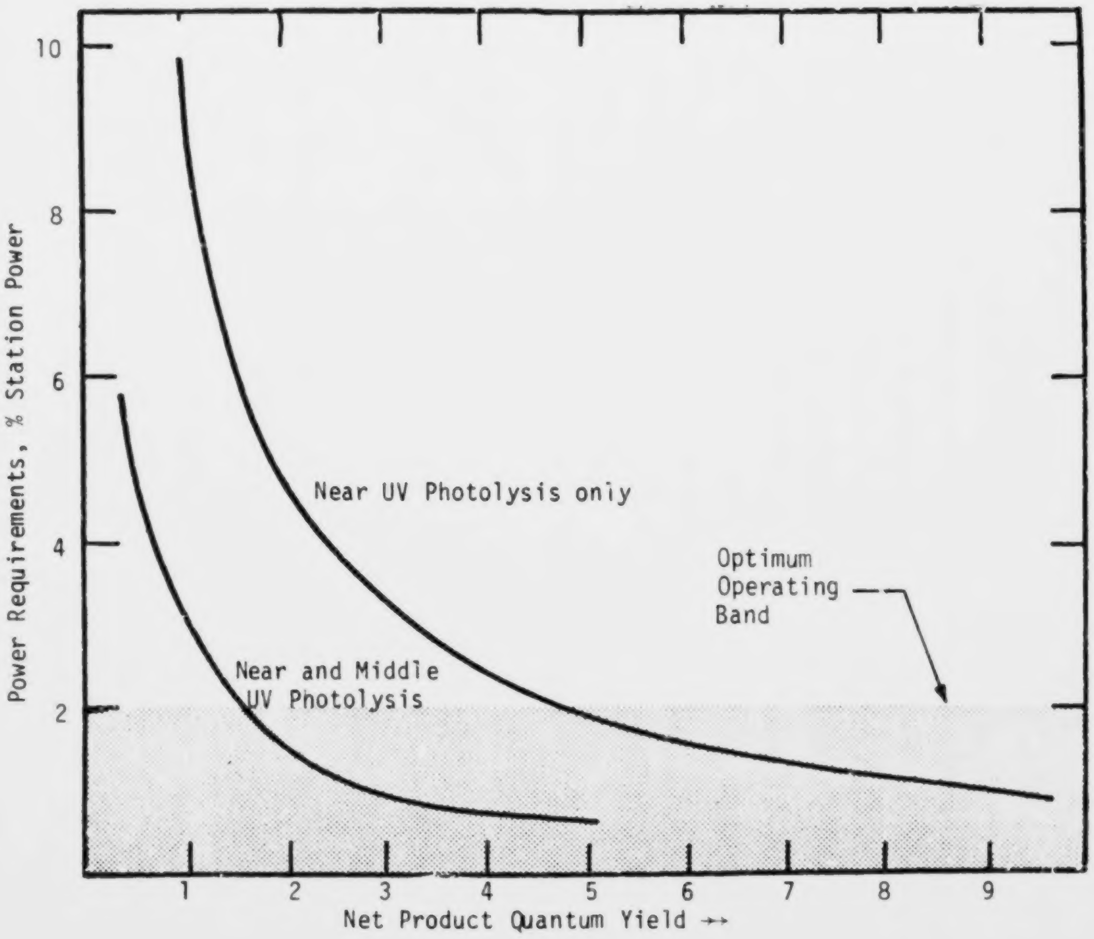

Figure 9. Power requirements as a function of net product quantum yield.

energy demands. If NO_2 photolysis is the only important reaction mechanism, then the product quantum yield requirements are considerably more severe as indicated by the upper curve. Without any contribution from reactions initiated in the middle UV, the quantum yield of NO_2 photolysis reactions must be greater than 5.

Energy Utilization--

The preceding section concerned the problems in the delivery of energy to an effluent gas stream. Results of this analysis indicate that the economical feasibility of photochemical systems depends directly on the net product quantum yield which can be achieved. The reaction mechanisms which will be initiated in such a system are now reviewed with respect to the possible product quantum yields and with respect to the possible types of reaction products.

It should be noted that the term reaction mechanism is used in a very broad sense. It applied to an entire assembly of reactions initiated by the absorption of ultraviolet light in a specific spectral band by a specific compound. Some of the possible mechanisms are identified in the list below:

	Mechanism	Spectral Band	Absorbing Species
1.	Vacuum UV Reactions	1700 - 2000 Å	O_2, H_2O
2.	Excited State Chemistry	2400 - 12500 Å	SO_2, NO_2, O_2
3.	Molecular Complex Photolysis	2400 - 3400 Å	EDA Complexes
4.	NO_2 Photolysis	2400 - 4000 Å	NO_2, HCHO, CH_3CHO

Each of these "mechanisms" could consist of thousands of individual chemical reactions involving large numbers of distinct species. NO_2 photolysis is emphasized since it is possibly the dominant reaction mechanism in the photochemical system.

NO_2 Photolysis--The irradiation of coal-fired boiler effluent in the near UV spectral band can promote several simultaneous cyclic free radical processes. Simplified illustrations of the three major sets of reactions are provided in Figures 10a, b, and c.

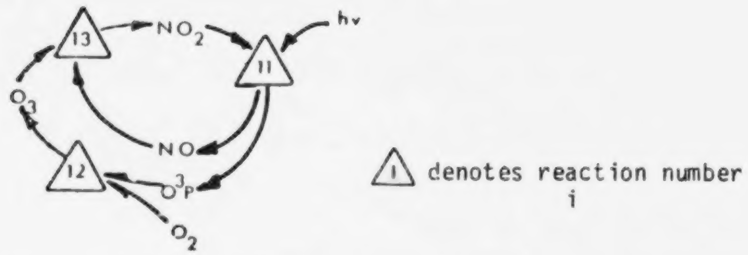
13
NO_2
hv
11
O_3
NO
12
O^3P
O_2
1 denotes reaction number i

Figure 10a. Photostationary state reactions.

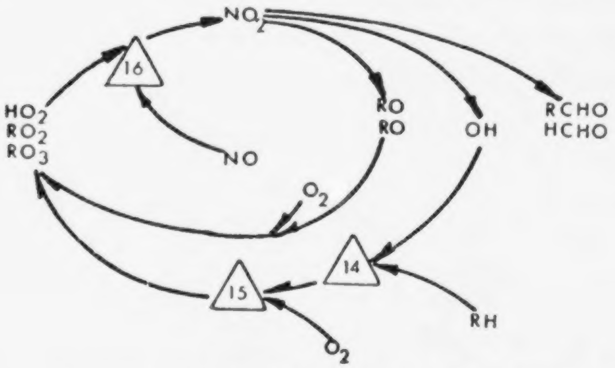
NO_2
16
HO_2
RO_2
RO_3
NO
RO
RO
OH
RCHO
HCHO
O_2
14
15
RH
O_2

Figure 10b. Simplified olefin/NO_x photochemical reactions.

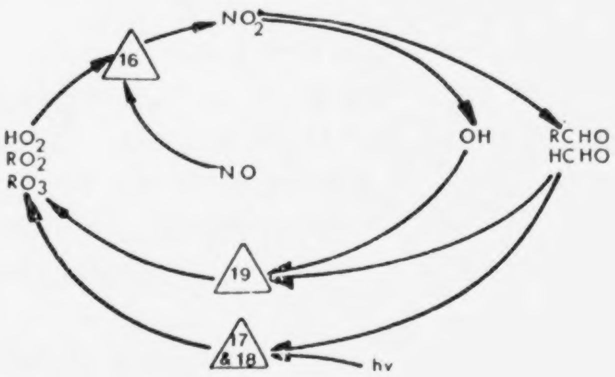
NO_2
16
HO_2
RO_2
RO_3
NO
OH
RCHO
HCHO
19
17 & 18
hv

Figure 10c. Simplified aldehyde photochemical reactions.

In the absence of appreciable olefin concentration, the reactions are limited to the photostationary state conditions of Figure 10a. Reactions 11 to 13 are involved in this cycle.

$$NO_2 + h\nu(3000\text{-}4000\ \mathring{A}) \rightarrow NO + O(^3P) \tag{11}$$

$$O(^3P) + O_2 + M \rightarrow O_3 + M \tag{12}$$

$$O_3 + NO \rightarrow NO_2 + O_2 \tag{13}$$

Unless there is sink for the ozone formed in reaction 12, there is little change in the NO/NO_2 ratio. The NO_2 product quantum yield of this set of reactions is zero.

When olefins are added to the flue gas, several additional free radical cycles are initiated. Basic elements of these processes are the hydroxy radical attack on virgin olefin and the peroxy radical oxidation of NO to yield NO_2 plus additional hydroxy and peroxy radicals. Three general types of reactions are listed below:

$$\cdot OH + C_3H_6 \twoheadrightarrow R\cdot + H_2O \tag{14}$$

$$R\cdot + O_2 \twoheadrightarrow RO_2\cdot \tag{15}$$

$$\left\{\begin{matrix} HO_2\cdot \\ RO_2\cdot \\ RO_3\cdot \end{matrix}\right\} + NO \twoheadrightarrow \left\{\begin{matrix} OH\cdot \\ RO\cdot \\ RO_2\cdot \\ RCHO \\ HCHO \end{matrix}\right\} + NO_2 \tag{16}$$

Reaction 14 involves addition of the OH· group to the olefin. The resulting radical will react with oxygen to yield the peroxy radical. The oxidation of NO in reaction 16 can result in the formation of one or more of the products listed in the brackets. The organic radicals can undergo further reaction with oxygen to give additional peroxy radicals. While hydroxy attack of propylene accounts for most of the olefin consumption, the reaction with ozone also could yield many similar organic radicals.

The aldehydes formed in reaction 16 can photolysis directly if there is sufficient energy available in the 2400 to 3400 A band. As shown in reactions 17 and 18 , the products include the formyl radical, or simply ethane and CO. The latter reaction becomes important only at the high energy side of the absorption spectrum. The aldehydes may also react with hydroxy radicals by means of hydrogen abstraction to give products analogous to those formed in reaction 17. Due to the limited light available in the middle UV, reaction 19 will probably be the principal reaction path for the aldehydes.

$$\mathrm{RCHO} + h\nu(2400\text{-}3400\ \mathrm{\mathring{A}}) \rightarrow \mathrm{R}\cdot + \mathrm{HCO}\cdot \qquad (17)$$

$$\mathrm{RCHO} + h\nu(2400\text{-}3400\ \mathrm{\mathring{A}}) \rightarrow \mathrm{R}\cdot + \mathrm{R}\cdot + \mathrm{CO} \qquad (18)$$

$$\mathrm{RCHO} + \mathrm{OH}\cdot \rightarrow \mathrm{RO}\cdot + \mathrm{H_2O} \qquad (19)$$

The aldehyde reactions listed above could be important free radical propagation reactions.

The NO_2 product quantum yield of the NO_x-olefin reaction system can conceivably be high. As shown in the propylene and aldehyde degradation steps, the attack of one ozone molecule or one hydroxy radical can result in the direct oxidation of NO and can result in the formation of numerous hydroperoxy radicals. The latter react almost exclusively with NO to yield NO_2. While the yield is a function of olefin and total NO_x concentration, the value at high concentrations could be in the range of 2 to 10.

The combined result of these free radical cycles is a gradual depletion of the NO and the formation of NO_2. Once the NO is exhausted, ozone is no longer consumed in reaction 13, it builds up to appreciable concentrations. Other stable secondary products such as peroxyacyl nitrate, nitric acid and organic aerosols also accumulate in the latter stages of the reactions. An example concentration profile during the course of the photochemical reactions is provided in Figure 11.

With time limited and light limited conditions, it should be possible to avoid the latter stages of the overall process during which most of the toxic secondary products are formed. By designing the reactor to reach the NO_2 peak, an optimum reaction product composition should be obtained. At this stage of the reaction, however, there potentially is incomplete consumption of the olefin. Some olefin could be emitted from the process.

Vacuum ultraviolet reactions -- Both water vapor and oxygen compounds absorb strongly in the 1700 to 1900 Å band and undergo dissociation to

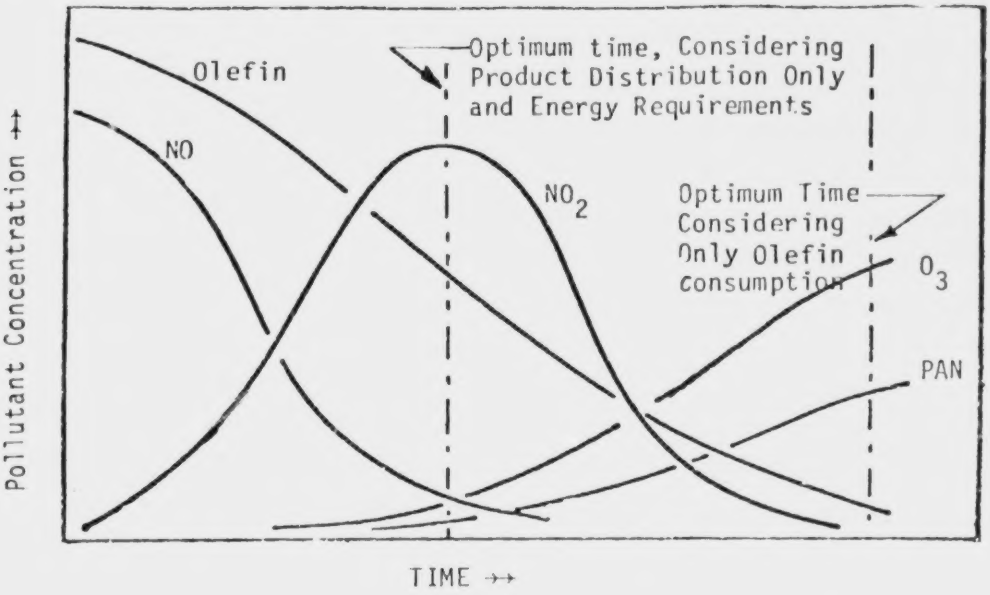

Figure 11. Typical pollutant concentration-time profile for photochemical reactions in batch reactor.

yield free radical species. The applicable reactions are presented below:

$$\mathrm{H_2O} + h\nu\ (1700 - 1900\ \mathring{A}) \longrightarrow \mathrm{H\cdot} + \mathrm{OH\cdot} \qquad (20)$$

$$\mathrm{H\cdot} + \mathrm{O_2} \longrightarrow \mathrm{HO_2\cdot} \qquad (21)$$

$$\mathrm{O_2} + h\ (1700 - 1900\ \mathring{A}) \longrightarrow 2\ \mathrm{O(^3P)} \qquad (22)$$

$$\mathrm{O(^3P)} + \mathrm{O_2} + \mathrm{M} \longrightarrow \mathrm{O_3} + \mathrm{M} \qquad (23)$$

These reactions could result in the oxidation of NO to NO_2 with or without the addition of olefins. In the absence of hydrocarbons, the NO_2 product quantum yield would be in the range of 1 to 2 assuming that radical recombination is not a serious problem. With olefins, the product quantum yield and the reaction products would be very similar to those discussed in the previous section.

Molecular complex photolysis -- The formation of molecular complexes between SO_2 and either NO or NO_2 would create the possibility of a primary photochemical process involving absorption within the charge transfer band. Based on a review of the ionization potentials of the NO_x compounds, it has been suggested (Richards, Fox, and Reist, 1976) that this absorption could be in the middle UV band. The reactins involved are entirely speculative at this time since only one SO_2 gas phase complex has been studied (Christian and Grundnes, 1967). The importance of this reaction mechanism depends on the equilibrium constant of the complex and the extinction coefficient of the complex, neither of which are presently known. The product quantum yields of these reactions are probably less than 1 since non-volatile reaction products are formed. There is no reason to believe that a free radical chain reaction process can be initiated by molecular complex photolysis.

Excited state reactions--The absorption of long wavelength UV and visible light could result in the formation of various excited state species. Generally, these species revert rapidly to the ground state and do not participate in chemical reactions. The product quantum yields for the possible reactions would be quite low unless at high concentrations the excited species are temporarily stabilized within a cluster or a complex.

Study Requirements

The preliminary analyses suggest that photochemical systems are an economically viable technique for NO_x control assuming that the net product quantum yield of the combined reaction mechanisms is in the range of 1 to 5. Factors which influence quantum yields, such as olefin concentration and pollutant concentrations are potentially important. The extent of hydrocarbon consumption at the point of optimal NO_2 concentration is a third possible issue.

CHAPTER 5

EXPERIMENTAL

GENERAL DESIGN OBJECTIVES

The experimental apparatus was designed to simulate anticipated field conditions. An artificial flue gas and components more sophisticated than necessary for a full system were used to gain maximum control of the independent variables.

A continuous stirred tank reactor (CSTR) was chosed as the irradiation chamber since this was most compatible with the geometric configuration of the high quality ultraviolet (UV) lamps. Light absorption path length and light distribution are more favorable in a CSTR than in a plug flow reactor (PFR). Due to the offsetting factors of holding time and light intensity in the CSTR, it was possible to match light energy per gram mole levels in this study with levels considered achievable in commercial units. Thus, the CSTR results can be related to conditions to be expected in larger systems. Risks inherent in scale-up are also minimized since non-zero order reactions proceed more rapidly in real gas streams represented by dispersed plug flow conditions than in the well-mixed conditions of this study.

Conditions within the experimental unit and those expected on a commercial scale are compared in Table 6. Two typical utility boilers have been listed: one without NO_x controls and one with state-of-the-art combustion controls. With two exceptions, all variables are adequately represented in the quartz CSTR system. Despite its high concentration in flue gases, CO_2 was not considered important either as a third body or as a direct photochemical reactant; and therefore, it was omitted. Humidity was purposely minimized since the reactants would have been partially removed in the impingers. Preliminary test work indicated that the reactions are not highly sensitive to humidity.

TABLE 6. COMPARISON OF EXPERIMENTAL SYSTEM AND FULL SCALE SYSTEMS

Parameter	Quartz Reactor Bench Scale System	Utility Boiler Full Scale System Uncontrolled	Utility Boiler Full Scale System State of the Art Combustion Controls
Dominant Flow Characteristics	Completely Mixed	Dispersed Plug Flow	Dispersed Plug Flow
Gas Retention Time, Seconds	45	6-12	6-12
Gas Flow Rate, SCFM	0.04	2×10^5-2×10^6	2×10^5-2×10^6
Flue Gas Composition			
CO_2, %	0	11-15	11-15
O_2, %	0-8	4-8	2-5
H_2O, %	1-3	3-8	3-8
NO_x, PPM	0-2000	400-1200	300-600
SO_2, PPM	0-3000	1000-3000	1000-3000
HC, PPM	0-2000	10-100	10-100
CO, PPM	0-3000	10-200	10-2000
Particulate, gr/dscf	0	0.5-2	0.5-2
Gas Temperature, °F	250-350	250-325	250-325
UV Absorption, % Input			
2400-3000 Å	20	99	99
3000-4000 Å	6	70	70
Watts UV Absorbed per Gram Mole NO_x	0-100	50-100	50-100
NO_2, Photolysis Rate, K_1, min^{-1}	0-5.0	0.2-2.0	0.2-2.0

REACTOR DESIGN AND PERFORMANCE

The dual CSTR system shown in Figure 12 was used in this study. The outer reactor is a 22" diameter, 1/2" thick titanium sphere originally built for use as a helium storage tank for a NASA Lunar Rover. Access holes were cut in the sphere and brass flanges were permanently mounted using Armstrong 612 Epoxy resin. A front brass plate was built to serve as the lamp house and reactor carrier. A 1/2" diameter SS 304 support rod attached to this front plate was used to mount and align the inner reactor. Whenever cleaning of the inner reactor was necessary, it was possible to remove the entire assembly from the outer sphere without disconnecting any gas lines, lamp power cords or thermocouple leads.

The inner reactor had an internal volume of 1.39 liters and was composed of commercial grade quartz. The front and back windows were made of Suprasil 2 quartz with UV transmission extending down to 1800 Å. A ground glass fitting was mounted on the back extension of the reactor so that the inner surfaces of the reactor could be flushed with distilled water for cleaning.

Light Source

An Illumination Industries model XL-2009-150 mercury-doped xenon arc was used as a light source. This was selected after a preliminary survey of various high pressure mercury arcs, compact xenon arcs and mercury-doped xenon arcs. The latter group was found to be highly temperature dependent with strong shifts in output spectrum with only 5-10°F changes in lamp house temperature. Standard xenon arcs without mercury-doping had insufficient energy output despite superior temperature stability and start-up characteristics. The mercury-doped xenon lamp was a compromise choice that allowed reasonable energy output with only minor temperature dependence. None of the lamps had any significant output in the 1700 to 1850 Å band; therefore, study of vacuum ultraviolet reaction mechanisms was impossible. The spectrum of the mercury-doped xenon arc as measured by an Optronic Model 400 Radiometer is illustrated in Figure 13. It exhibits the peaks characteristic of mercury, specifically 2537, 2860, 2960, 3030, 3130 and 3660 Å. Small quantities of 1930 Å light are also emitted

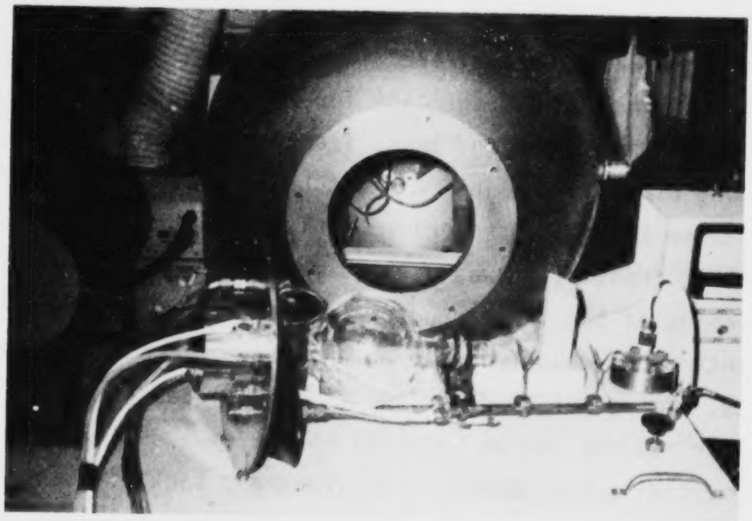

Figure 12a. View of quartz reactor on support rod.

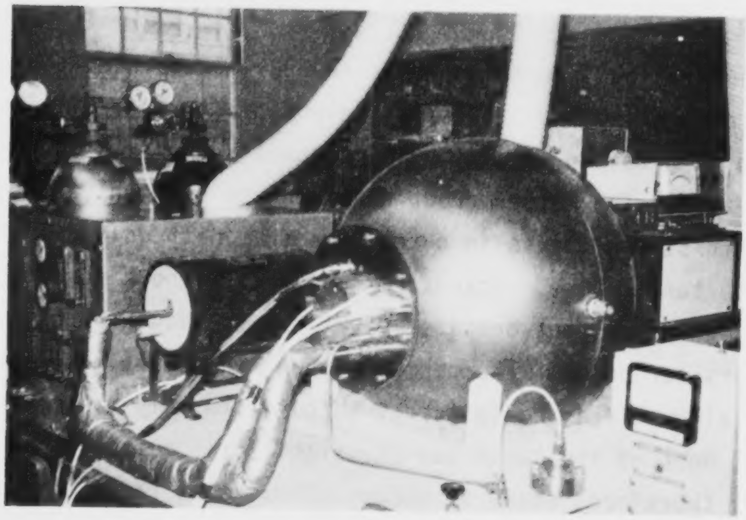

Figure 12b. View of outer CSTR.

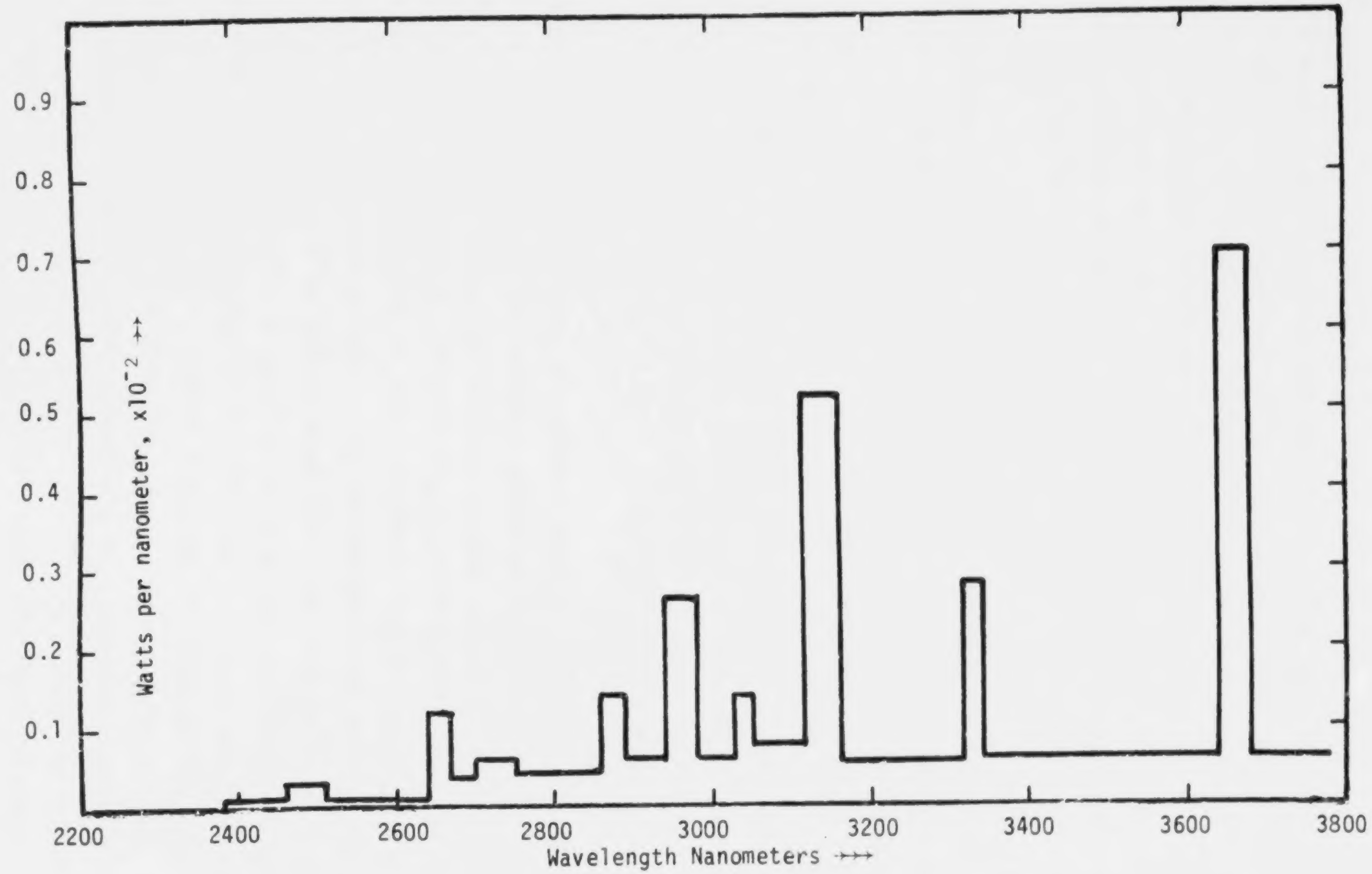

Figure 13. Mercury doped xenon arc output spectra.

due to the choice of Suprasil quartz lamp envelopes. This type of lamp achieves 90% full output in 2 minutes and 98% in 3 minutes based on radiometer and spectrometer readings. An Electronic Measurements Model 308 Power Supply was used to operate the lamp. Starting voltages were approximately 35 kv and operating conditions were 20vdc and 6-8 amps. The lower value was used in most of the tests so that the 150-watt lamp was actually operating at 120-130 watts. This minimized temperatures at the base of the xenon arc and at the nylon insulators surrounding the anode.

Lamp House

The xenon arc lamp is mounted with the anode 10° off vertical which is within the manufacturer's specifications. The lamp bulb is 1-3/8" from the front window of the inner CSTR.

A polished aluminum conical reflector is located directly behind the xenon arc to improve energy delivery to the reactor. NO_2 photolysis tests indicated that 40 to 60% of the total near UV energy absorbed in the reactor was reflected from the aluminum cone. Aluminum was chosen due to its high reflectivity in the middle UV band. The lamp bulb was never touched or cleaned with solvents. A dry piece of lens tissue was used daily to clean the bulb.

The distribution of light within the quartz reactor was measured qualitatively using thermocouples mounted on a flexible, movable rod. The millivolt difference between a black thermocouple directly in the light path and a white thermocouple shielded from direct light was taken as a measure of light intensity. Due to the mounting equipment necessary to support the thermocouple rod inside the quartz reactor, it was impossible to perform the light distribution tests inside the large sphere. Reflected light from the titanium surfaces may moderate the light intensity gradients shown in Figure 14. It is apparent that light intensity is low near the walls of the quartz reactor.

Lamp operating currents were monitored with a Simpson Microampmeter connected parallel to a 0.25 ohm shunt. Meter values represent 1.7×10^{-6} of actual currents.

A set of 3 aperture plates was constructed of multiple layers of decorative metal foil of 1/16" thickness. The conventional diaphragm aperture was considered inappropriate since the intense lamp house tem-

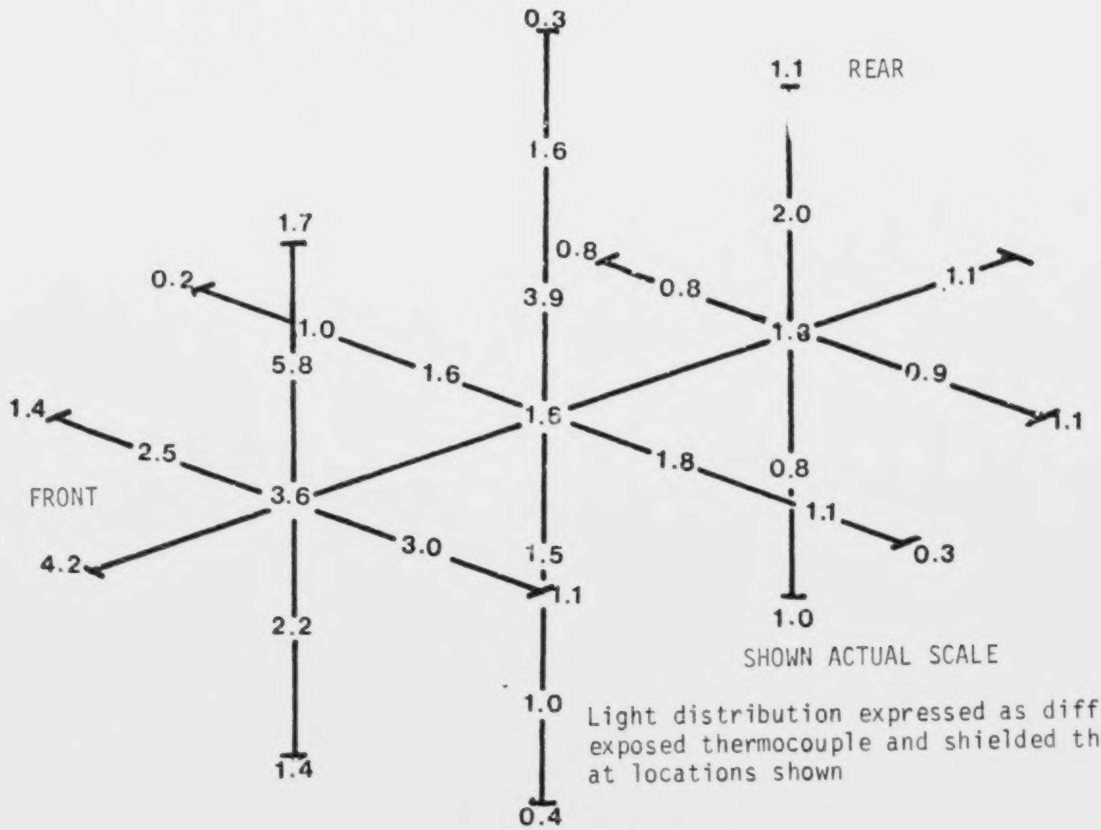
0.3
1.1
REAR
1.6
2.0
1.7
0.8
0.8
1.1
0.2
3.9
1.0
1.3
5.8
1.6
0.9
1.4
1.6
1.1
2.5
1.8
0.8
FRONT
3.6
1.1
3.0
1.5
0.3
4.2
1.1
2.2
1.0
1.0
1.4
0.4

SHOWN ACTUAL SCALE

Light distribution expressed as difference in exposed thermocouple and shielded thermocouple at locations shown

Figure 14. Light distribution in quartz reactor.

peratures would have vaporized the lubricating oil and warped the shutter blades. NO_2 photolysis tests on various occasions indicated the following intensity ratios:

Plate 1	0.16
Plate 2	0.30
Plate 3	0.57
Open (Basis)	1.00

These plates were used to select the general light intensity range desired.

The lamp electrodes extended through the interior walls of the filter house. Cylindrical nylon was used to prevent sparkover of the high voltage starting pulse. A constant stream of commercial grade N_2 at a rate of 15-20 liters per minute aided lamp house heat dissipation and precluded ozone formation. The N_2 flowed axially around the lamp, per manufacturer's recommendations. During certain tests when heat dissipation was inadequate, slight vaporization of the nylon insulators occurred. This was readily apparent on the relatively "cold" surfaces within the filter house such as the aluminum reflector and the interior brass walls. No discoloration was ever noted on the lamp or reactor face.

For certain runs, it was necessary to filter out a portion of the UV emission spectrum. A 3" O.D. Suprasil quartz window was used for full spectrum (>1800 Å) runs and a commercial glass window was used to isolate the near UV (>3200 Å).

Lamp current was the principal independent variable affecting ultraviolet energy output. The k_1 data for both lamps used in the experimental run indicated a consistent relationship with lamp current. The linear regression equation representing this data of Figure 15 is shown below. This equation was calculated after throwing out the March 16th and March 18th data points. These low values were contributed to visi-

$$y = 0.96 + 2.52\ (x-10)$$

where: $y = k_1$, min^{-1}
x = lamp current, amps (as read by Simpson Microampmeter.)

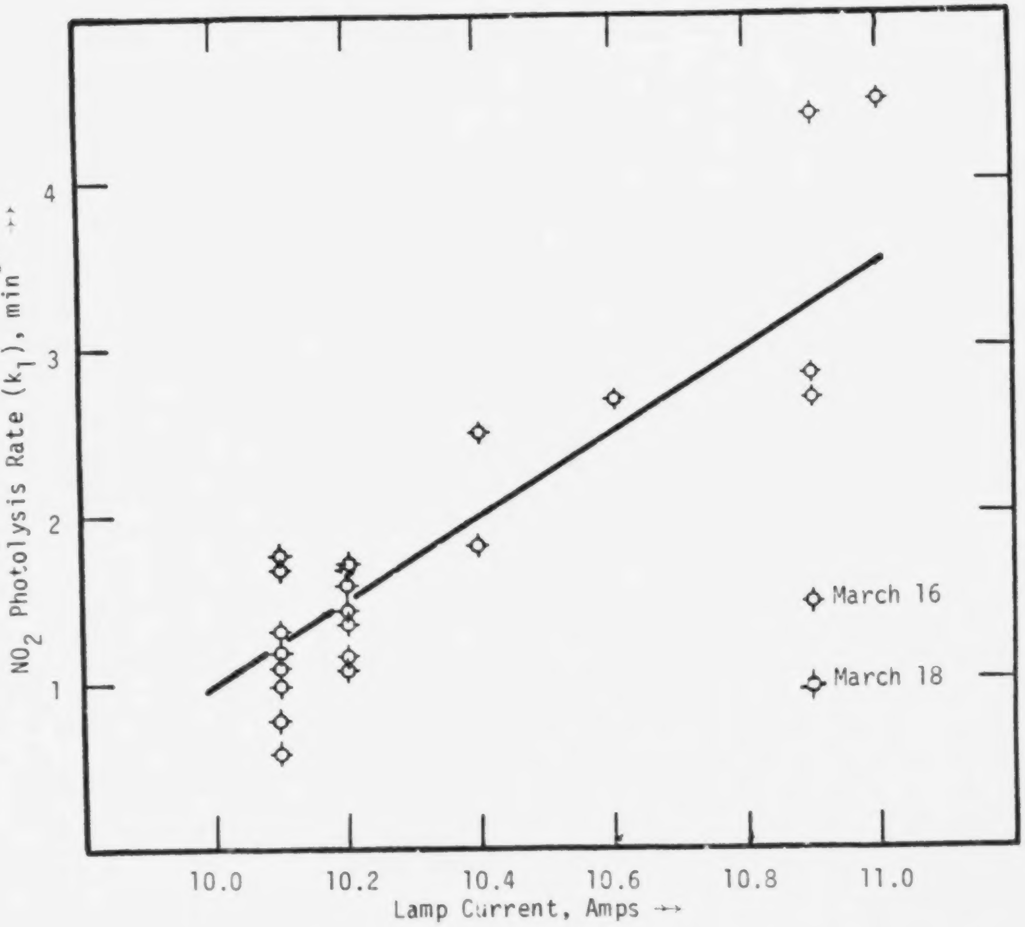

Figure 15. NO_2 photolysis rate as a function of lamp current.

ble deposits on the inner surfaces of the reactor during high SO_2 concentration runs (>3000 ppm SO_2). The slope of the k_1 plot of Figure 15 is slightly higher than corresponding plot of total UV volts versus current as determined by the Radiometer.

Reactor Gas Flow Characteristics

The gaseous mixing characteristics determine the average local reactant concentrations in the reactor zones where secondary thermal reactions are proceeding. The resulting influence on competitive reaction mechanisms is prejudiced against second and third order reactions when non-plug flow conditions occur (Levenspiel, 1972). The inner reactor was purposely designed with minimum possible plug flow conditions since this minimizes several non-photochemical NO_2 formation reactions and since it represents the slowest possible reaction times for all mechanisms.

A set of tracer tests were performed in order to evaluate flow pattern characteristics as a function of flow rate. The procedures of Wolf and Resnick (1963) were used. After a steady state NO_x concentration was established in the reactor for a period of five bed volumes, the NO_x flow was abruptly stopped. The response to this step change in inlet NO_x flow was measured using the TECO chemiluminescent monitor. The basic equation (3) of Wolf and Resnick was used to analyze the data.

$$F(t) = 1 - \exp\left\{\left[-\frac{(1-f)}{(1-d)a\theta}\right]\left[t - L - \left\{\frac{p(1-d)\theta}{(1-f)}\right\} + a(1-d)m\theta\right]\right\} \quad \text{(Equation 3)}$$

where: $F(t)$ = fraction of material which remains in the reactor

f = fraction of gas flow short circuiting

d = fraction of reactor volume with only diffusion mass transfer (dead space)

r = residence time correction factor

a = fraction of non-dead space which is well mixed

p = fraction of non-dead space which is in plug flow

θ = average residence time

t = elapsed time

L = lag

m = lag factor

By assuming lag is negligible and that the average residence time is known, Equation 3 can be rearranged to give Equation 4. This was used to match results from the tracer tests.

$$F(t) = 1 - \exp - \left[\frac{(1-f)}{(1-d)\mathbf{a}}\right]\left[\frac{t}{\theta} + p\right] \quad \text{(Equation 4)}$$

Since one equation with three independent variables cannot yield a unique solution, some judgment is necessary to derive a reasonable solution. The reactor configuration studied in these tracer runs is shown in Figure 16. The small diameter Teflon tube on the inlet side was added after preliminary tracer work indicated serious short circuiting. This tube plus the outlet tubing leading to the NO_x instrument added a plug flow section to the "reactor". The long neck near the outlet tube introduces a potential dead space of up to 5 percent. These factors were considered in the trial and error solutions.

Results are summarized in Table 2. Corresponding graphs illustrating the match between Equation 4 values and the observed 1-F(t) versus t/θ curves are provided in Appendix A.

TABLE 7. TRACER RESULTS

Flow Rate (lpm)	% CSTR	% Plug Flow	% Dead Space	% Short Circuiting
1.0	92	8	2	6
1.5	91	9	2	6
2.0	92	8	2	6
2.5	85	15	4	1
3.0	72	28	8	1

Mixing characteristics within the 1 to 2 liters-per-minute range closely approach design objectives. Dead zones are somewhat smaller than expected while shortcircuiting is slightly greater. At the higher flow rates, it is apparent that some plug flow character can be maintained across the quartz sphere. An increase in dead space at 3.0 liters per minute is probably due to isolation of gases in the outlet neck. Over the range of flow rates used in the study, CSTR conditions can be assumed to prevail with only slight error.

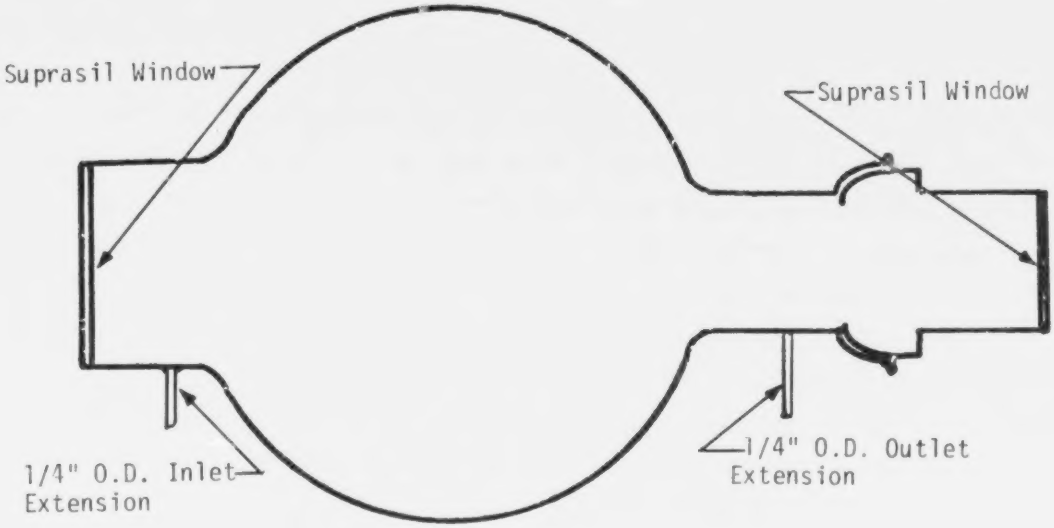
Suprasil Window
Suprasil Window
1/4" O.D. Inlet Extension
1/4" O.D. Outlet Extension

Figure 16a. Initial inlet configuration.

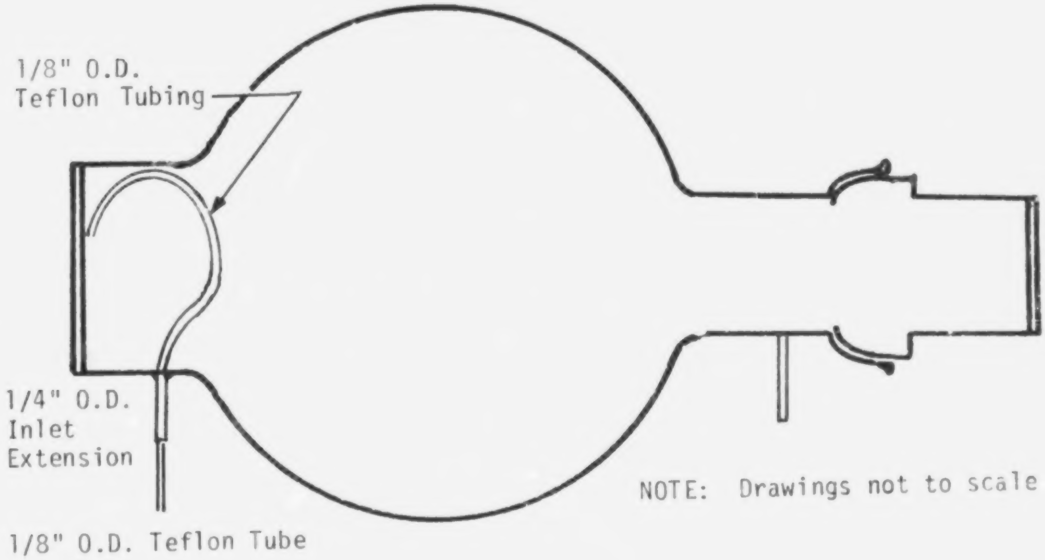
1/8" O.D. Teflon Tubing
1/4" O.D. Inlet Extension
1/8" O.D. Teflon Tube

NOTE: Drawings not to scale

Figure 16b. Reactor inlet configuration.

ACTINOMETRY

The experimental apparatus included actinometer systems for both the near UV (3000 to 4000 Å) and the middle UV (2400 to 3000 Å) spectral bands. The function of these actinometry systems was to provide a measure of light absorption so that the NO_2 net product quantum yield defined in equation 1 could be calculated. Quantum yield can be related

$$\Phi_{NO_2} = \frac{(N_{NO_2}/t)}{[(N_{NEAR}+N_{MIDDLE})/t]} \qquad \text{(Equation 5)}$$

where: N_{NO_2} = Gram moles of NO_2 formed in CSTR

N_{NEAR} = Quanta of UV light absorbed in the 3000 to 4000 Å band.

N_{MIDDLE} = Quanta of UV light absorbed in the 2400 to 3000 Å band.

t = Unit of time

to the overall energy requirements using the lower curve in Figure 9. The rate of NO_2 formation in the CSTR (numerator of Equation 5) can be calculated using the steady state NO_2 concentration in the reactor effluent and the effluent flow rate. This is shown in Equation 6.

$$(N_{NO_2}/t) = \left(G\,\frac{\text{liters}}{\text{min}}\right)\left(\frac{70°\text{F}}{T}\right)\left(\frac{\text{Gram Moles}}{22.4\text{ liters}}\text{ total}\right)\left(NO_{2_{ss}}\right)\left(\frac{1\text{gram mole }NO_2}{10^6\text{ ppm }NO_2}\right)$$

(Equation 6)

where: G = the CSTR effluent flow rate

T = the gas temperature at the reactor outlet

$(NO_2)_{ss}$ = steady state NO_2 concentration in the reactor

Acetone photolysis was used to measure middle UV energy penetrating through the quartz sphere. The difference between runs with and without reactive gases in the quartz sphere served as a measure of the N_{MIDDLE} term of Equation 5.

The acetone pressure was chosen to maximize UV absorption within the outer CSTR. Over the 2400 to 3000 Å spectral range, UV absorption ranged from 75 to 94%. The results of Howe and Noyes (1936) indicate that the CO quantum yield of the overall set of reactions is approximately equal to one at the acetone vapor pressure, gas temperatures and UV spectral bands used in the actinometry system. Thus, with only minor corrections the CO yield provided a direct measure of middle UV energy input to the quartz sphere. The CO was measured in a Miran Dispersive Infrared Analyzer. A complex system of dry ice and liquid nitrogen baths were used to remove interfering vapors, particularly acetone. Numerous cold trap designs were evaluated, however, none could operate for longer than 45 minutes without plugging due to acetone freezing. Because of this problem the middle UV actinometry system was abandoned.

The inability to measure light absorption in the middle UV forced a redefinition of the NO_2 product quantum yield term to be measured in the study. This new definition is given in Equation 7. Since the contribution of middle UV light is ignored in the revised definition, the calculated product quantum yield should be greater than or equal to the actual quantum yield for the entire UV spectrum of 2400 to 4000 Å. The values would be equal only in the case that UV absorption in the middle UV band does not enhance or reduce NO_2 formation.

$$\Phi_{NO_2}(\text{calc}) = \frac{(N_{NO_2}/t)}{(N_{NEAR}/t)} \qquad \text{(Equation 7)}$$

$$\frac{\Phi_{NO_2}(\text{calc})}{\Phi_{NO_2}} \geq 1 \qquad \text{(Equation 8)}$$

The revised definition of NO_2 product quantum yield can be related to the overall energy requirements of the system using the upper curve of Figure 9. This approach overestimates the actual energy requirements by the factor represented by the ratio of quantum yields (Equation 8).

The N_{NEAR} term was determined using the NO_2 photolysis procedures of Sickles and Jeffries (1975). The NO_2 photolysis is measured by irradiating a NO_2-N_2 gas stream and observing the steady state concentrations of NO and NO_2 in the reactor effluent. The photolysis rate, k_1 is calculated using Equation 9 provided in their paper.

$$K_{1_{ss}} = \frac{\Delta[NO_2]}{2\tau[NO_2]_{ss}}\left[1 + R_1 + \frac{R_2([NO]_o + \Delta[NO_2])}{[NO_2]_{ss}}\right] \quad \text{(Equation 9)}$$

where: $\Delta(NO_2)$ = the drop in NO_2 concentration between inlet and outlet streams

$(NO_2)_{ss}$ = the steady state NO_2 concentration in the reactor average residence time

$(NO)_o$ = concentration of NO in the reactor influent

R_1 = 0.27

R_2 = 0.25

The k_1 tests were done in the actual CSTR to account for internal light reflection and the non-ideal light distribution conditions discussed earlier. Tests were done at least once per day. An attempt was made to perform the k_1 determination at the temperatures expected in the runs, however, some deviation generally existed. Results of three successive tests indicate a drop in observed k_1 values of 20% over a temperature range of 275 to 125°F. Based on these results, corrections were considered unnecessary for the relatively small temperature variation between the runs and the applicable k_1 test.

The k_1 value was used in Equation 10 to calculate the N_{NEAR} term of the product quantum yield. Substitution of the right side of this equality and the right side of Equation 6 leads to a very simple definition of the NO_2 product quantum yield.

$$(N_{NEAR}/t) = V_{liters}\left(\frac{70°F}{T}\right)\left(\frac{\text{Gram Moles Total}}{\text{22.4 Liters}}\right)(NO_2)_{ss}\left(\frac{\text{Gram Mole } NO_2}{10^6 \text{ ppm } NO_2}\right)\bullet \left(k_1 \frac{\text{Quanta/min}}{\text{Gram Mole } NO_2}\right) \quad \text{(Equation 10)}$$

where: k_1 = the NO_2 photolysis rate

T = the gas temperature in the CSTR

V = the volume of the CSTR

$$\Phi_{NO_{2(calc)}} = G/V \cdot k_1 = 1/\tau k_1 \qquad \text{(Equation 11)}$$

Equation 11 suggests that the NO_2 product quantum yield is a dependent variable of the NO_2 photolysis rate, k_1. This unusual condition results because the photochemical system utilizes NO_2 photolysis to produce NO_2. Equation 11 provides a very convenient means to relate the observed steady state NO_2 concentration with the energy requirements of the system as indicated on the upper curve of Figure 9.

REACTANT AND PRODUCT MEASUREMENT

The diluted effluent stream in the outlet manifold was analyzed with a set of gas analyzers shown in Figures 17 and 18. All of these instruments were calibrated by preparing a known gas concentration in a 40-liter Teflon bag. In initial tests, all the components in the system used were mixed together during calibration. There appeared to be essentially no interferences at the undiluted concentrations of initial components.

Nitrogen Oxides Analysis

A Thermo Electron Model 10A Chemiluminescent NO-NO_x Analyzer was used. This instrument utilizes the reaction between NO and O_3 which results in light emission at 3100 Å. The light intensity measured by the photomultiplier assembly is linearly related to the concentration of NO. The concentration of combined NO_x species is determined by reduction to NO in a metal coil at 650°C-700°C. The difference between the NO and NO_x values is representative of the NO_2 concentration plus an unknown number of other species such as nitrous acid, nitric acid and peroxyacylnitrate.

The chemiluminescent instrument was calibrated routinely using Teflon bag mixtures containing known quantities of NO, O_2, SO_2 and propylene. The instrument was operated using laboratory air instead of O_2 since the diluted outlet concentrations rarely exceeded 500 ppm.

Sulfur Dioxide Analysis

It was necessary to use a pulse fluorescent technique in order to ensure SO_2 specificity. A Thermo Electron Model 40 Analyzer was chosen.

Figure 17. Gas analyzers for NO_x, SO_2, and condensation nuclei.

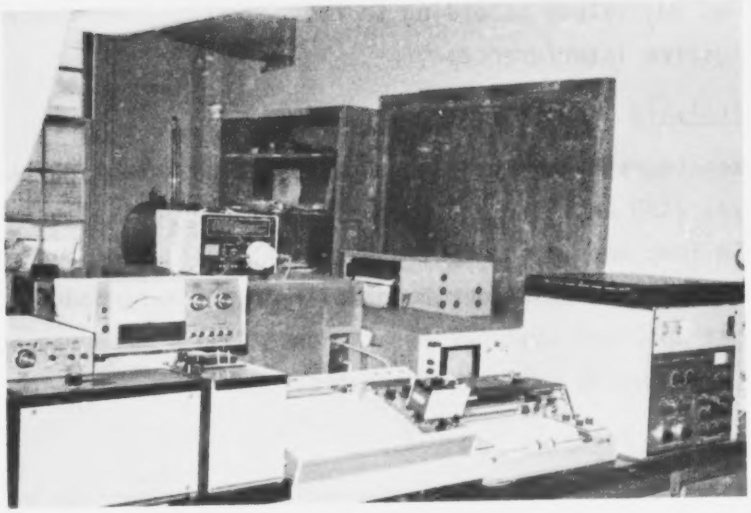

Figure 18. Gas analyzer for hydrocarbons.

It operates by excitation of SO_2 to the singlet state by irradiation at 2200-2300 Å using a pulsed UV source. The excited molecules decay to the ground state by two possible pathways - fluorescent at 3400 Å and quenching. Light from the fluorescence reaction is linearly related to the SO_2 concentration.

$$\begin{array}{lll} SO_2 + h\nu(2200\text{-}2300\ \mathring{A}) & \xrightarrow{I} SO_2^* & (24) \\ SO_2^* & \rightarrow SO_2 + h\nu & (25) \\ SO_2^* + m & \rightarrow SO_2 + m & (26\ ) \end{array}$$

Using the Teflon bag mixtures with typical (diluted) reactor effluent, it was observed that the fluorescence is sensitive to NO_2 concentration, a product of the photochemical reactions. The significance of this interference is illustrated in Figure 19. It is proposed that this previously unreported negative interference is due to increased quenching efficiency via a contact molecular complex, as indicated in reactions 27 and 28.

$$\begin{array}{lll} SO_2^* + NO_2 & \rightleftarrows [(SO_2)(NO_2)]^* & (27) \\ [(SO_2)(NO_2)]^* + m & \rightleftarrows SO_2 + NO_2 + m' & (28) \end{array}$$

The molecular complex would provide additional vibrational degrees of freedom which would facilitate radiationless decay. It was necessary to adjust observed SO_2 values according to the prevailing NO_2 concentration due to the negative interference.

Hydrocarbon Analysis

Gas chromatography analyses were performed on a routine basis using a Varian Series 2440 Analyzer equipped with a flame ionization detector. A 10 cc sample loop was purged continuous with outlet manifold gas and injections were then done twice during each irradiation period. A polypax 3 meter column at 80°C was used for separation. Calibration was again done using Teflon bag samples of known concentrations.

Condensation Nuclei Analysis

An Environment/One Rich 100 condensation nuclei monitor was used to evaluate possible aerosol formation. For a portion of the irradiation period, the Millipore filter was taken off line to permit unfiltered gases

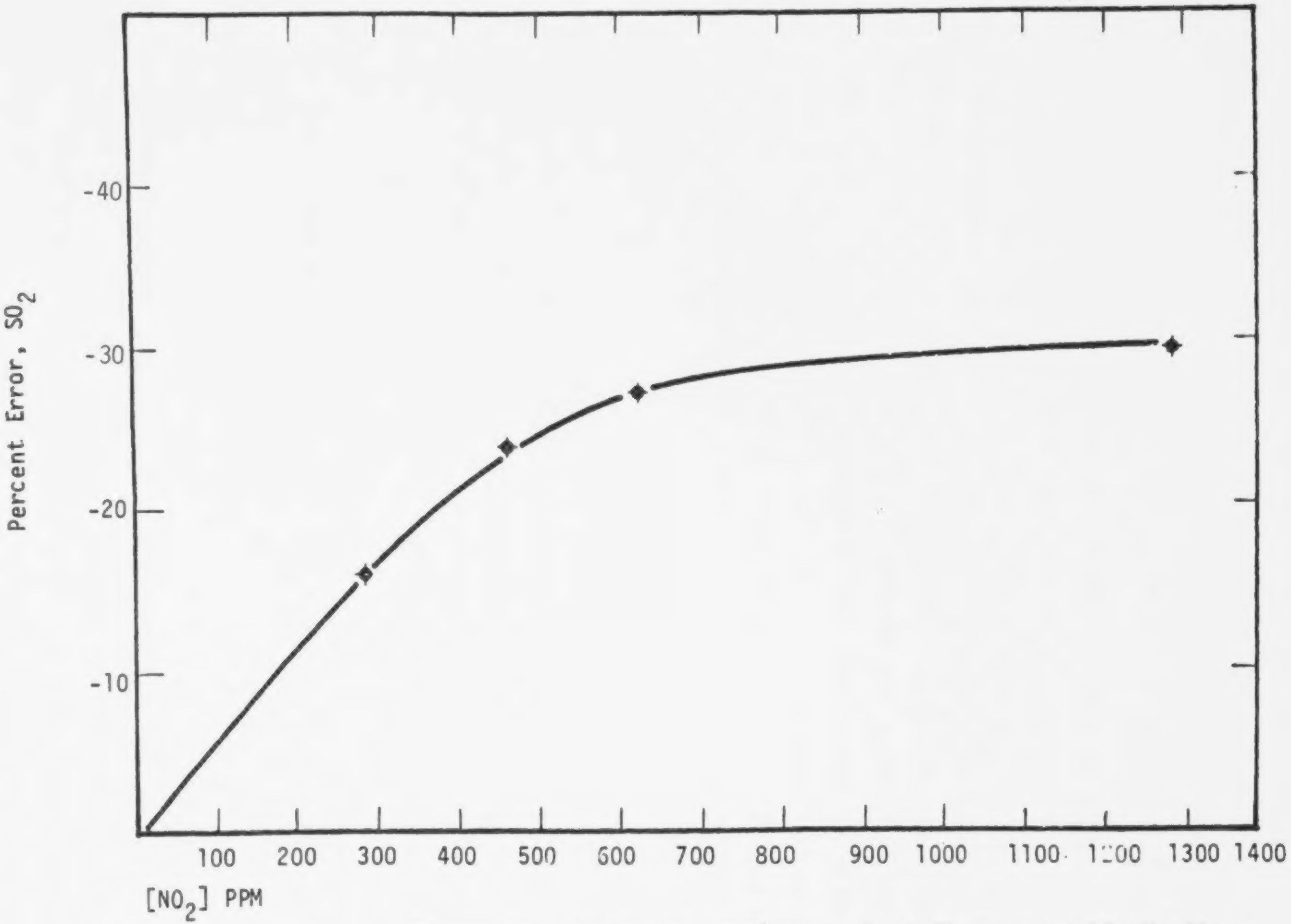

Figure 19. Influence of NO_2 on pulsed fluorescent SO_2 Readings

to enter the outlet manifold. This instrument exposes the sample gas to a 300% supersaturated condition which causes condensation of water vapor on condensation nuclei. A portion of these grow into the light scattering size region causing a reduction in light transmission in a tubular cell. This instrument qualitatively indicated the presence or absence of large quantities of condensation nuclei.

Spectral Analysis

A number of spectral changes were anticipated due to aging of quartz windows, lamp deterioration and reactor cleanliness. The k_1 responds to a relatively broad spectral band and would not serve as a useful indicator of such developing problems. For this reason, a Heath Model 703 IR/UV spectrometer was used. The PM tube detector module was placed on the centerline defined by the xenon arc and reactor (see Figure 20). A Hewlett Packard x-y plotter was used to record spectra from 2400 to 3700 Å for N_2 and during actual test situations. A set of spectra was generally taken once per run. Relative peak height values on the N_2 spectra revealed the deterioration effects listed earlier. The differences in the two spectra indicated major absorbing species.

GAS HANDLING APPARATUS

The experimental apparatus was designed to maximize flexibility in and to facilitate routine checks for nonoptional performance caused by leaks, surface mediated catalytic reaction or other factors. The system was composed of a number of separate units including:

(1) gas blending
(2) heaters
(3) temperature measurement
(4) ventilation
(5) humidification

Gas Blending

The simulated flue gas was prepared by blending of pollutant gases and oxygen into a nitrogen carrier gas stream. This permitted complete flexibility in the concentrations of all components. The blending box is shown in Figure 21. All gas lines from the cylinders

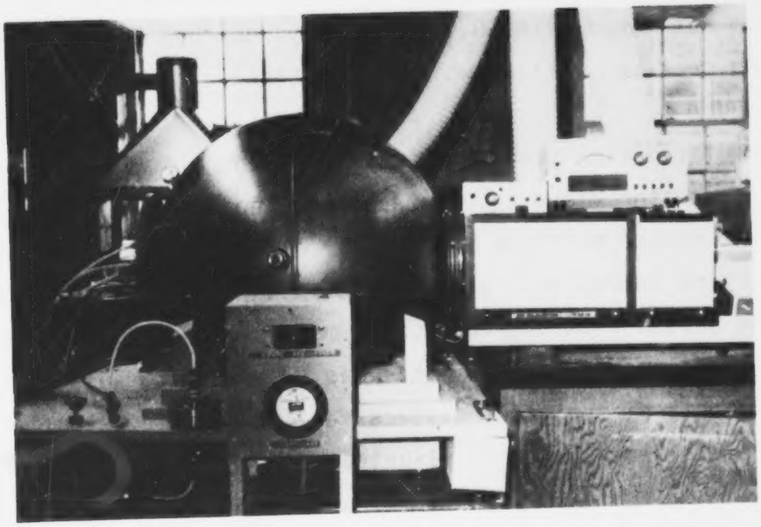

Figure 20. Side view of reactor and spectrometer.

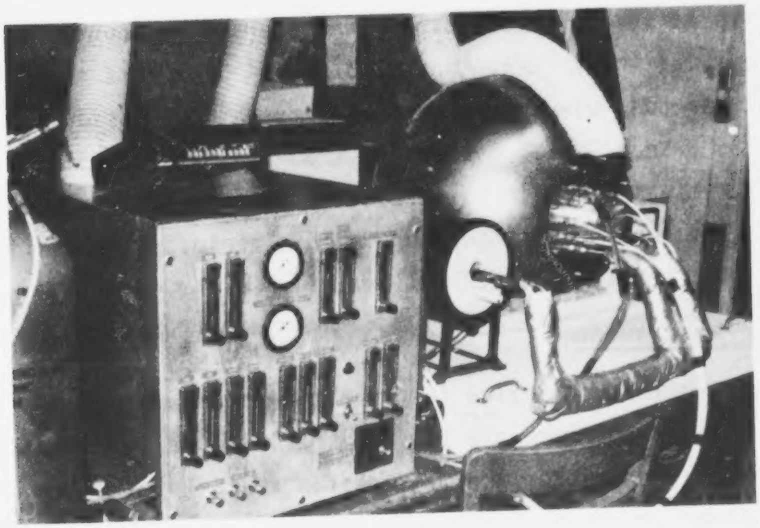

Figure 21. Front view of blending box.

to the blending box and within the blending box were Teflon so that hydrocarbon contamination could be minimized. As shown in Figure 22, the N_2 and O_2 were mixed first followed by humidification in Greenberg-Smith impingers filled with distilled water. Part of the humidified gas stream was drawn off to a Dew Point Hygrometer for measurement of humidity. The N_2-O_2 stream was mixed with SO_2, NO_x and hydrocarbon lines to complete the blending process. All flows were monitored with calibrated rotameters shown in Figure 21.

The simulated flue gas stream was split in half with one portion going to the reactor via a tube furnace and the other half proceeding directly to the outlet manifold solenoids. A pressure gauge on the reactor side of the line served as a very sensitive indicator of flow variations.

The gas stream entering the outlet manifold was diluted a factor of 2 to 5 by dried laboratory air. This was necessary to support the large flow requirements of the gas analyzers feeding off of the outlet monitor. The complete gas flow system is illustrated in Figure 22.

Heaters

A tube furnace shown in the center of Figure 21 served as the initial reactor gas heating system. The temperature of the heated gas generally was 125-150° F at the front flange of the large reactor.

A series of seven 100-watt power resistors were mounted in the outer CSTR. By varying the voltage from 0 to 85 V.A.C. across the parallel circuit, it was possible to control gas temperatures inside the quartz CSTR from 125°F to >300°F. By heating from the outside walls of the quartz CSTR, it was possible to keep the reactor walls at least 10°F higher than the inner gas temperature. This minimized deposition of aerosols on the reactor's inner walls.

Temperature Measurement

The gas temperature inside the quartz reactor was measured using a Chromel-Constantin thermocouple (Type E thermocouple). The zero to 10 multivolt signal generated were measured on a Model 10A Fluke digital Multimeter (see top right, Figure 21).

The thermocouple probe was located on the quartz reactor centerline,

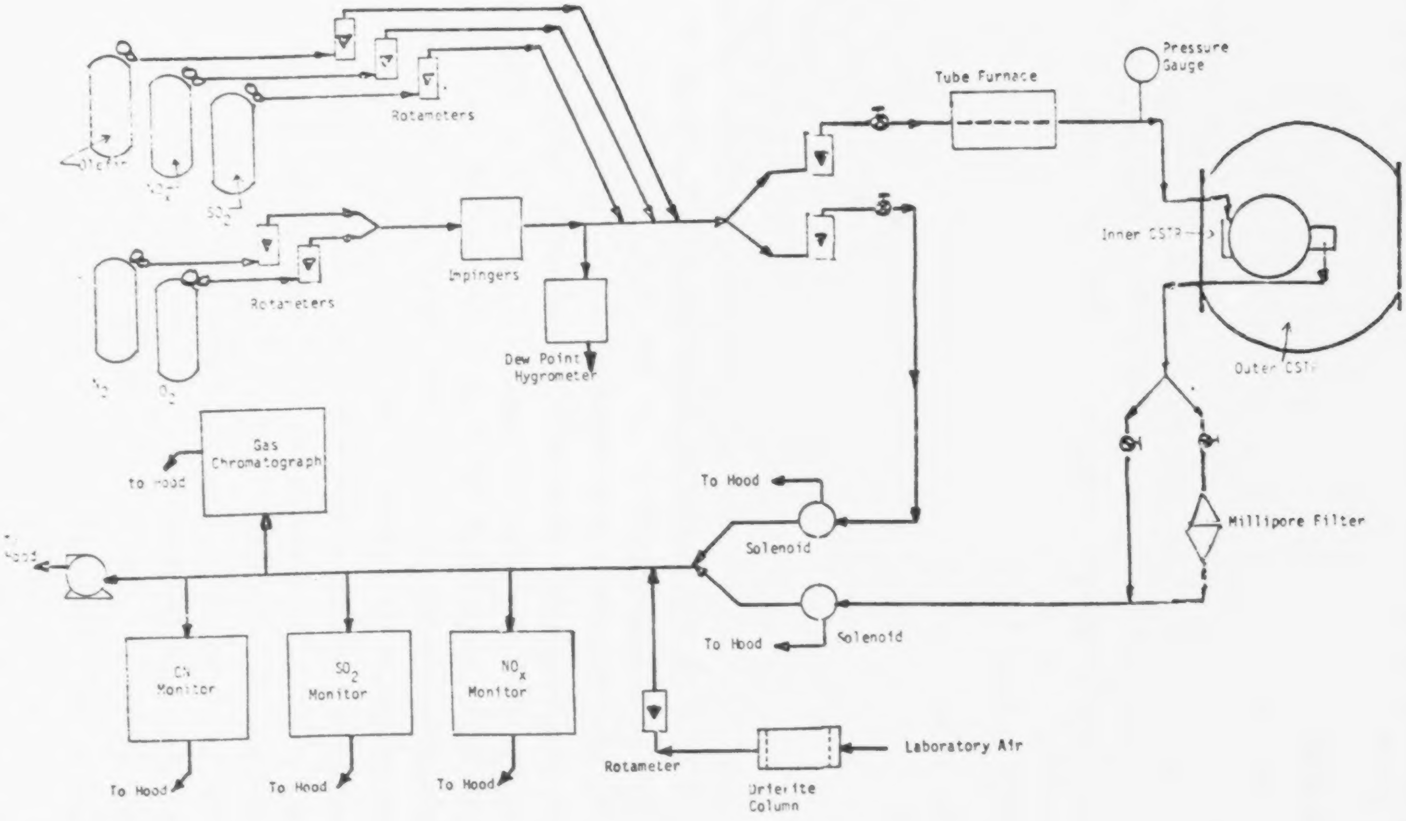
Olefin
NO_x
SO_2
Rotameters
N_2
O_2
Rotameters
Impingers
Dew Point Hygrometer
Tube Furnace
Pressure Gauge
Inner CSTR
Outer CSTR
Millipore Filter
To Hood
Solenoid
To Hood
Solenoid
Gas Chromatograph
to Hood
Hood
CN Monitor
SO_2 Monitor
NO_x Monitor
To Hood
To Hood
To Hood
Rotameter
Drierite Column
Laboratory Air

Figure 22. Gas flow system.

directly above the gas exit port. The probe was loosely wrapped with several layers of white Teflon tape so that radiant energy would not bias the results.

Humidification

The combined N_2 and O_2 streams were humidified in a set of 2 500-ml impingers filled with distilled water. Desired humidities were achieved by bypassing some of the gas around the impingers. Treatment of the simulated flue gas would have allowed higher humidity; however, the reservoirs would have collected soluble gases such as SO_2 and NO_2.

EXPERIMENTAL DESIGN

A preliminary test series was performed to aid in the preparation of the experiments. Considering that over 10 major variables were considered of possible importance, a complete factorial design was not considered feasible. Even with the rapid turnaround capabilities of CSTR systems, the maximum number of tests which could reasonably be done with available resources was estimated to range from 150 to 200. It was necessary to screen the variables and subdivide the test program so that this limitation was not exceeded.

The very rough initial tests indicated that the variables of most importance with respect to NO oxidation were the UV light intensity and the hydrocarbon concentration. Accordingly, a 5 x 5 x 2 factorial design was used to study these variables at NO_x levels of 600 and 1000 ppm (v/v). The ranges of the variables roughly approximate the levels considered achievable in commercial systems. Hydrocarbon concentrations well beyond stoichiometric requirements were used in order to identify the point, if any, that the system becomes hydrocarbon insensitive. Specifics concerning this major test series are provided in Table 8. The test series was repeated once so that interactions among these three variables could be identified.

A number of small factorial test series were devoted to secondary variables also observed to influence NO oxidation in the preliminary test work. These runs were done at equal light intensities and hydrocarbon levels so that the sensitivity of the system to each variable could be qualitatively compared. Specifics concerning these studies are also covered in Table 8.

Most of the series in Table 8 provided information concerning variations expected in commercial systems. The range in SO_2 levels, O_2 levels and gas temperatures were selected to correspond to the anticipated levels at utility boilers. The spectral characteristics study (series 5) was intended to aid in the selection of lamps for subsequent pilot plant stuies. The hydrocarbon comparison study (series 6) served to evaluate relative advantages of each compound in terms of NO conversion efficiency. This information would be of use in cost estimation and design of subsequent work.

Despite the high concentrations of CO_2 in boiler effluent it was assumed that there would be no relationship between the NO oxidation efficiency and the level of CO_2. Series 7 was included in the study to check this assumption. The possible beneficial impact of carbon monoxide was studied in Series 8.

TEST PROCEDURE

Each run consisted of three distinct phases: (1) establishment of dark phase steady state conditions with respect to gas flow rates, reactor temperature and pollutant concentrations, (2) a 15- to 20-minute irradiation period, and (3) a recheck of dark phase steady state conditions. In this manner, it was possible to check for drift of pollutant concentrations, temperature, and other factors which would have influenced the reactions during the irradiation period. During the initial dark phase period the rotameter readings, temperatures, and gas analyzer values were recorded along with information concerning the run. After this data was recorded in the project notebook, the lamp was started. Immediately after lamp start-up, the reactor effluent was diverted to the Millipore filter. After a warm-up period of 4.0 minutes, the Heath Spectrometer was started on a scan beginning at 2450 Å and extending to 3700 Å. The complete scan required 11 minutes. At the 5.0-minute point after lamp start-up, a GC injection was made and the NO_x and SO_2 analyzer data was recorded. Rotameter settings, temperatures, lamp currents, and other

TABLE 8. EXPERIMENTAL DESIGN

Series No.	Variable 1	Levels	Variable 2	Levels	Variable 3	Levels	REPS	Total Number of Tests
1	Light Intensity	0 (min^{-1}) 0.25 0.50 1.00 2.00		0 250 500 1000 2000 ppm (v/v)	$[NO_x]_o$	600 1000 ppm	2	100
2	$[SO_2]_o$	0 ppm 500 1000 1500 3000	$[NO_x]_o$	600 1000	-	-	1	10
3	$[O_2]$	0 % 1 3 5 10 %	$[NO_x]_o$	600 1000	-	-	1	10
4	Temperature	125°F 175 225 275	$[NO_x]_o$	600 100	-	-	1	8
5	Spectral Characteristics	2400Å 3200Å	Light Intensity	0 (min^{-1}) 0.25 0.50 1.00 2.00	-	-	1	10

TABLE 8 (continued)

Series No.	Variable 1	Levels	Variable 2	Levels	Variable 3	Levels	REPS	Total Number of Tests
6	Hydro-carbon Type	Propylene Ethylene	Hydrocarbon Concentration	250 500 1000 2000	-	-	1	8
7	$[CO_2]$	0% 8 12 20	-	-	-	-	1	4
8	CO	0 1000 ppm 1500 2500	-	-	-	-	1	4

data of interest was then checked. At the 10.0 minute point, another GC injection was made and the NO_x and SO_2 analyzer data was recorded. Rotameter settings, temperatures, lamp currents and other data of interest was then checked. Near the completion of the irradiation period, the Millipore filter was taken off line to prevent exposure to dark phase conditions. The CN counter was observed for several minutes to determine if aerosol formation was detectable. When all necessary data had been recorded, the lamp was shut down and time was allowed to reestablish dark phase steady state conditions. All flow rates, and pollutant concentrations, and gas temperatures were then rechecked and recorded.

After each run, the lamp filters and/or aperture plates were changed. At the beginning of each day, the lamp condition was checked using the k_1 level. After each day's run, cumulative lamp operating hours and the number of starts was recorded. The xenon-mercury arc was replaced when operating time exceeded 100 hours or when the number of starts exceeded 200.

CHAPTER 6

RESULTS AND DISCUSSION

The experimental program has been designed to address five basic factors concerning photochemical system operating characteristics and cost. These principal issues are listed below:

1. What is the relative importance of UV absorption in the middle UV spectrum?
2. What olefin concentrations are necessary to achieve adequate NO oxidation?
3. At the point of optimal NO_2 formation, what fraction of the olefin has not reacted?
4. To what extent do the flue gas chemical and physical characteristics affect the photochemical system performance?
5. What secondary products are emitted from the reactor?

Data from the 159 runs performed have been divided into five sections, each one of which is devoted to one of the issues listed above. These analyses culminate in an assessment of order-of-magnitude annualized costs.

While the primary purpose of this project is simply to evaluate the competitive potential for photochemical NO_x control, some attention is also given to the identification of possible reaction mechanisms. This is useful in transferring information gained in this study to consider other industrial applications.

SPECTRAL EFFECTS

NO Oxidation Effectiveness

Filters were used to test the relative effectiveness of near UV and middle UV light. A standard piece of window glass was used to eliminate light of wavelengths 3000 Å and a piece of Suprasil® or quartz was used for full spectrum tests. Use of a Suprasil quartz filter was not strictly necessary since the front window of the CSTR is composed of similar material. The filter was added to equalize the effects of light reflection. Each of these filters were 1/4" thick, 2" diameter and were placed between the lamp and the CSTR front window.

Heath Spectrometer scans indicated that the window glass filter reduced UV light of <2960 Å by 99%. It also significantly reduced radiation of 3030 Å and 3130 Å (two major peaks in the lamp output spectra) and it moderately attenuated the entire near UV spectrum entering the CSTR. This unintended impact on the near UV band was quantitatively accounted for by performing k_1 tests with each of the filters. The ratio between the observed k_1 values was 2.04 (>1800 Å/>3000 Å) ±0.40 based on 3 separate determinations done over a 4-week period.

Differences in NO Oxidation

The extent of NO oxidation at equivalent k_1 levels is the criteria used to evaluate spectral effects. The aperature plates were used to vary the incident light intensities to give 4 distinct levels. Results of eight tests, four with each filter, are presented in Figure 23. The upper curve is the NO conversion in ppm (v/v) using the Suprasil® quartz filter while the lower curve is the NO conversion using the window glass filter. Other variables such as propylene concentration, oxygen concentration and gas temperature were held relatively constant as indicated by the data summary table included within Figure 23. The eight tests were performed in random order.

The shaded region between the two curves represents the contribution of middle UV light. At the UV light intensities which will be typical of commercial installation, namely 0.2 to 0.4 min^{-1} adjusted k_1, the middle UV appears responsible for 65 to 85% of the NO converted. This is remarkable considering that the middle UV output from a mercury doped xenon arc is only 15% of the output in the near UV band (see Section 4, Figure 13).

The $\Phi_{NO_2}(calc)/\Phi_{NO_2}$ factor introduced earlier appears to be a function of the total light intensity entering the reactor. At low levels of

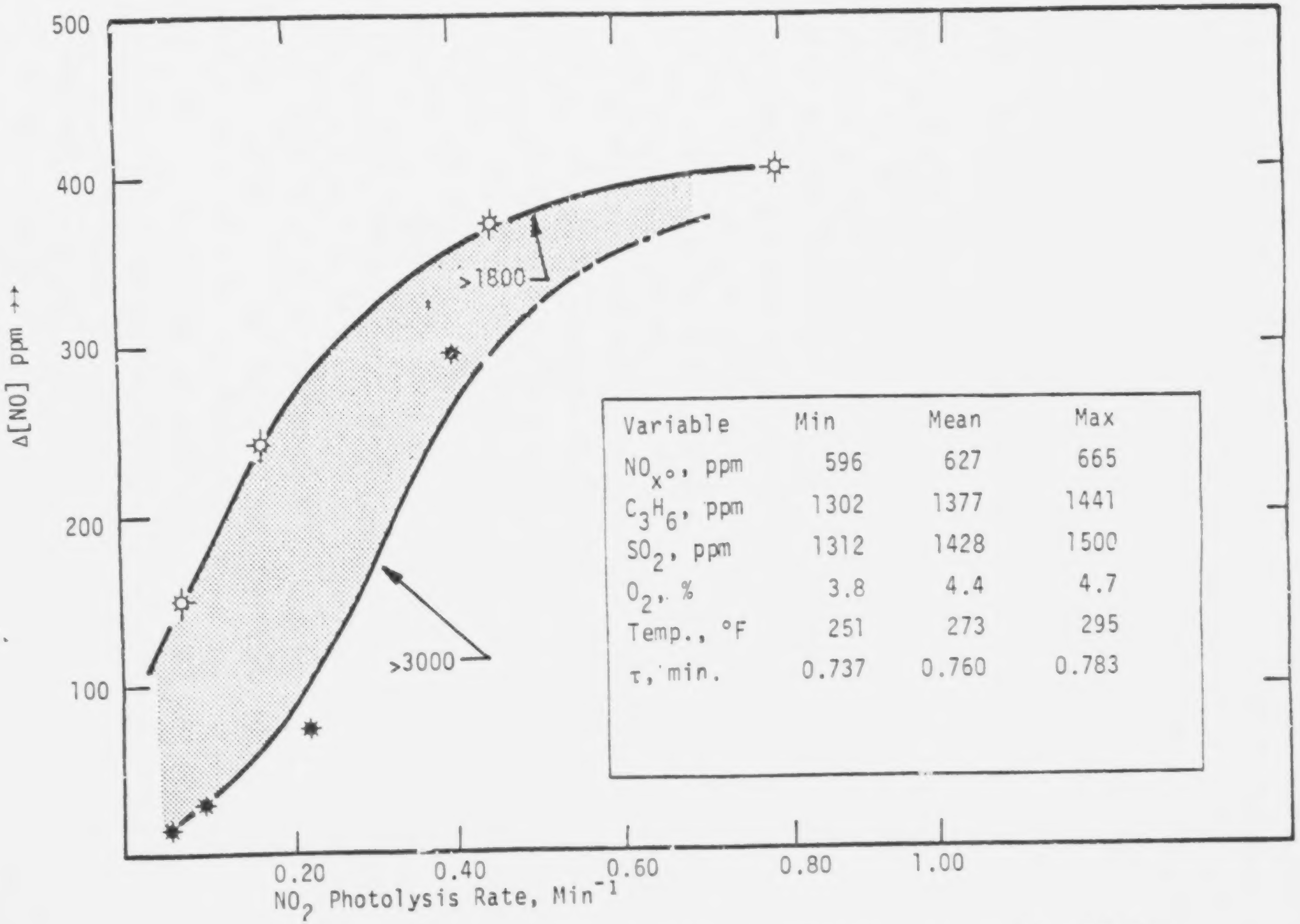

Variable	Min	Mean	Max
NO_{x°, ppm	596	627	665
C_3H_6, ppm	1302	1377	1441
SO_2, ppm	1312	1428	1500
O_2, %	3.8	4.4	4.7
Temp., °F	251	273	295
τ, min.	0.737	0.760	0.783

Figure 23. Influence of middle ultraviolet light on NO oxidation.

light, this ratio is 1 to 3. The ratio approaches 1 at very high light intensities presumably because reactions initiated in the near UV are sufficient to convert the available NO. This revised data indicates that the k_1 must be in the range of 0.2 to 0.4 min^{-1} in order to keep energy demand less than 2% of station power.

Possible Causes of Spectral Effects

The Heath Spectrometer was used to identify possible absorbing species in the middle ultraviolet band of 2400 to 3000 Å which could be responsible for the enhanced NO conversion. It was necessary to analyze experimental runs performed without the filters.

Figure 24 includes two separate spectra; one taken during the actual run and one taken after all gas streams except the dry N_2 stream have been turned off. Strong UV absorption is apparent in the band from 2600 to 3030 Å. This set of comparative spectra is characteristic of virtually all spectra obtained during the experimental program. For a small set of the runs, however, attempts were made to determine what fraction of the middle UV absorption could be assigned to SO_2 and what fraction was the result of other primary absorbers such HCHO, CH_3CHO, HNO_2, and EDA Complexes. This was accomplished by modifying the procedure used in taking the second, "baseline" spectra. In this set of runs, the SO_2 injection rate was kept constant and only the NO_x inlet stream was turned off. Since the latter volumetric flow rate was quite small relative to the total, the SO_2 concentration in the "baseline" spectra was almost equal to that used in the run. The result of these comparative spectra is shown in Figure 25. SO_2 obviously accounts for essentially all middle UV absorption measurable by means of the Heath Spectrometer.

Considering the apparent dominance of SO_2 absorption, it is logical to propose that SO_2 participates in one or more primary photochemical processes which contribute to NO oxidation. Possible reaction mechanisms include EDA comples reactions and singlet SO_2 reactions (excited state possibly stabilized within a complex or cluster). A series of 10 experimental runs were performed to check for the role of SO_2 in the overall reaction scheme. The SO_2 content in the reactor influent was varied from 0 to 3000 ppm to correspond to the general range in coal-fired boilers of 500 to 3000 ppm. The tests were divided into five low

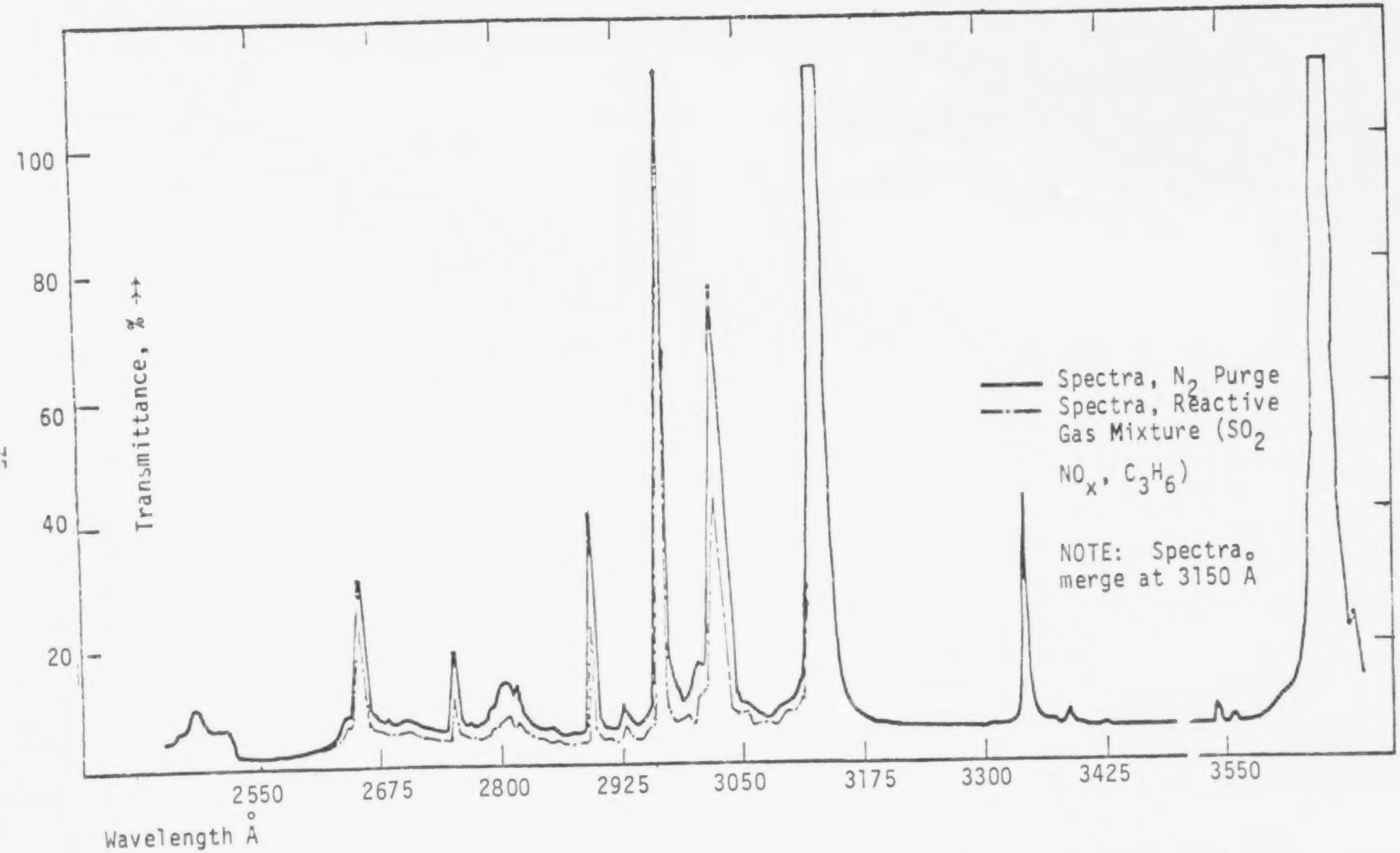

Figure 24. Typical comparative spectra; during and after experimental run.

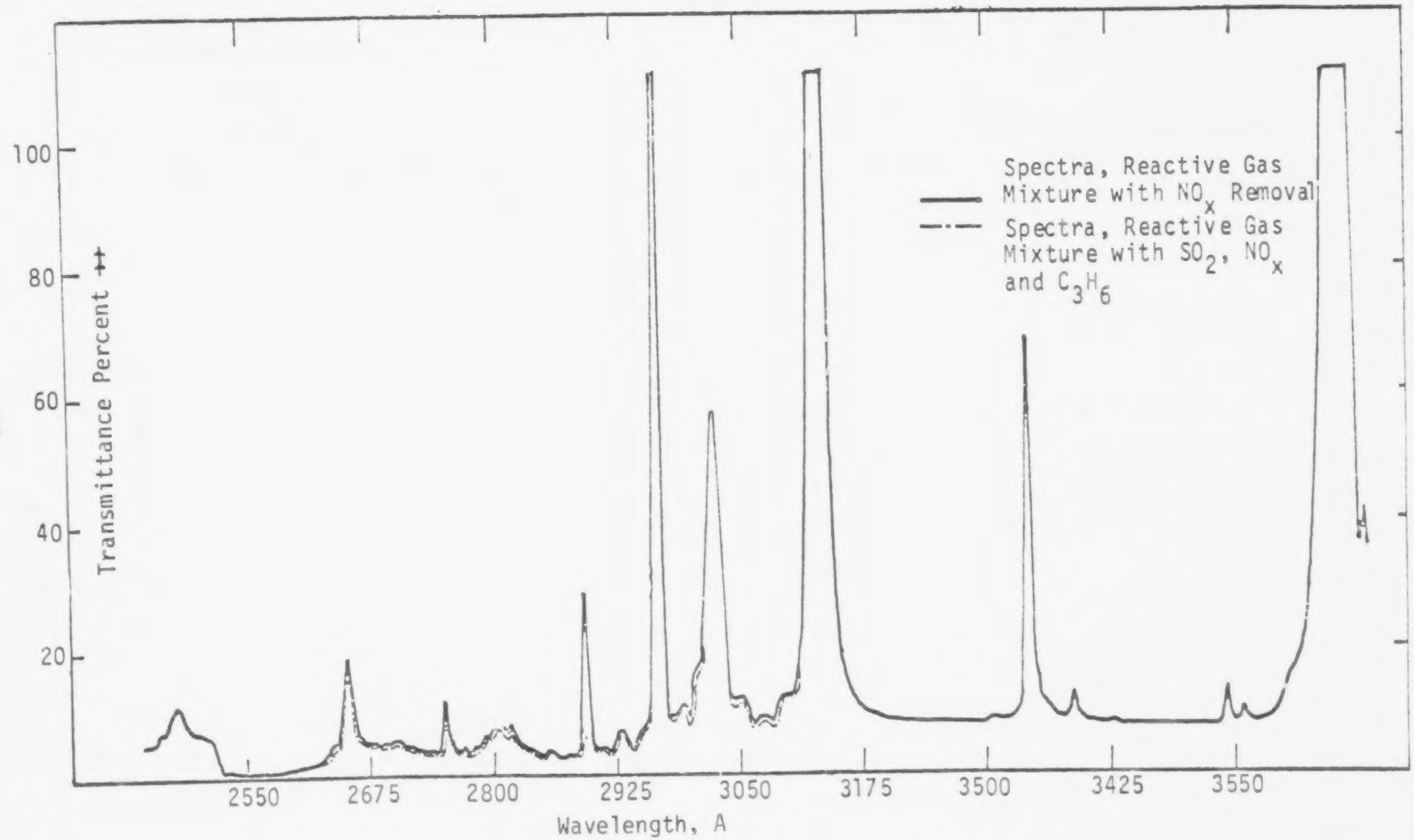

Figure 25. Influence of NO_x on spectra.

NO_x inlet runs and five high NO_x inlet runs. The results of interest were the extent of NO oxidation across this wide range of SO_2 concentrations. These are presented in Figure 26 along with a summary of the variability of other factors.

The upper line of Figure 26 is the observed SO_2 effect on NO oxidation with the inlet NO_x concentrations averaging 544 ppm. While there may be a discernable association, the influence of SO_2 on this type of system is insignificant. In the case of the high NO_x inlet tests (average of 1165 ppm), there is a definite suppression of NO oxidation at the higher SO_2 concentrations. This is contrary to the trend which could be inferred from the spectral band tests. The probable reason for the negative effect of SO_2 on the overall system is the hydroxy radical reaction listed below:

$$\cdot OH + SO_2 \overset{M}{\rightarrow} OHSO_2 \qquad (29)$$

This reaction would compete with hydroxy attack on the propylene which is important in maintaining the free radical chain process resulting in NO oxidation. The $HOSO_2$ radical formed in the above reaction would react further to form probably sulfuric acid, peroxysulfuric acid, and related compounds according to the reactions proposed by Calvert et al. (1977). At the high SO_2 concentrations tests, aerosol deposits containing considerable sulfur were observed. This confirms that SO_2 is being oxidized and the above reaction is the only known reaction fast enough to account for the conversion to aerosol precursors.

The SO_2 test series demonstrate that SO_2 absorption is not responsible for the strong effect of middle UV light. Based on these results, it appears very unlikely that EDA complexes composed partially of SO_2 or that excited SO_2 reactions have a significant impact on NO conversion. It is necessary to identify other possible middle UV absorbers to account for the spectral effects. Three possible species are O_3, HNO_2 and H_2O_2. All of these absorb strongly in portions of the middle UV spectrum, and the photolysis reaction yield free radicals which could enhance the oxidation process. The reactions are provided below:

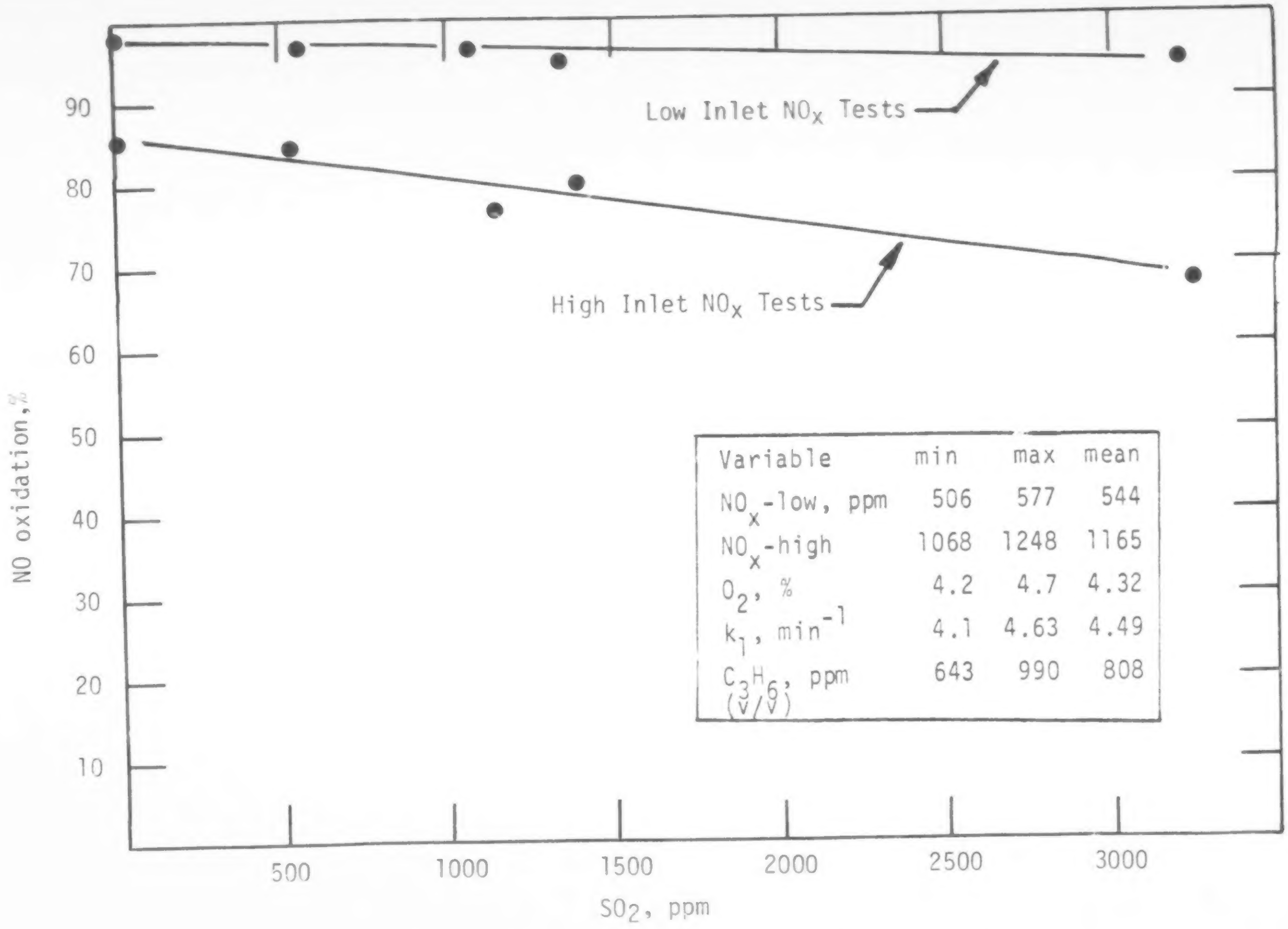

Variable	min	max	mean
NO_x-low, ppm	506	577	544
NO_x-high	1068	1248	1165
O_2, %	4.2	4.7	4.32
k_1, min^{-1}	4.1	4.63	4.49
C_3H_6, ppm (v/v)	643	990	808

Figure 26. Influence of SO_2 on NO oxidation

$$O_3 + h\nu(2400\text{-}2800\ \text{Å}) \longrightarrow 2O(^3P) \xrightarrow{O_2} 2O_3 \qquad (30)$$
$$HNO_2 + h\nu(2400\text{-}3600) \longrightarrow OH\cdot + NO \qquad (31)$$
$$H_2O_2 + h\nu(1900\text{-}4000) \longrightarrow 2OH\cdot \qquad (32)$$

The presence of these absorbing species cannot be dismissed on the basis of the comparative spectra discussed earlier. A check of the Heath Spectrometer using Equation 12 indicates that the minimum detectable concentrations are quite high. For this analysis, minimum detectable was arbitrary (MDC) defined as the concentration which would result in 2% transmittance change at a specific wavelength. The results indicates that the MDC's for O_3 is 17 ppm, for HNO_2 is 145 ppm and for H_2O_2 is 740 ppm.

$$\frac{\text{Ln}(0.98)}{\alpha_{2660}\,L} = C \qquad \text{(Equation 12)}$$

It is conceivable that one or more of the above species does exist at steady state concentrations below those detectable, and that these photolyze to produce free radicals which support NO oxidation.

In summary, the analyses of possible causes of the middle UV enhancement did not conclusively indicate what species were responsible. It is clear, however, that SO_2 does not participate in any primary photochemical processes which significantly effect the overall system.

HYDROCARBON REQUIREMENTS

The energy requirements and the hydrogen requirements are considered two major components of the photochemical system operating costs. A large test matrix was performed to determine the extent of NO oxidation over wide ranges of both variables. These tests were done using propylene. The relative effectiveness of ethylene and propylene was tested in a separate set of tests.

Propylene Tests

The efficiency of NO oxidation at 5 levels of hydrocarbon concentration and 5 levels of UV light intensity were tested in two sets of matrices. One set was done at an approximate inlet NO_x concentration of 600 ppm which is representative of many coal-fired boilers without combustion modifications for NO_x suppression. The second set of tests was done at an inlet NO_x concentration of approximately 1200 ppm which is an upper limit concentration probably representative of cyclone fired boilers or units firing coal of very high fuel nitrogen content. The entire test series was repeated.

Propylene was a convenient hydrocarbon to use since the reactions are fairly well understood and since it does not degrade into light scattering aerosol which could deposit on the optical surfaces within the CSTR. Propylene is also an attractive candidate for commerical systems, because it is a readily available bulk chemical of reasonable cost.

Results are presented in a series of 4 figures (27 to 30). The first and the third are for the low NO_x tests and the second and the fourth are for the high NO_x tests. In each case, the observed NO is plotted with respect to the prevailing k_1 level and the inlet propylene concentration. Isopleths have been drawn to indicate conditions of equal NO oxidation.

There are several outlying points in each of the four figures. It is believed that this is due to errors inherent in the k_1 measurement and in the propylene measurement. Light deposits on the inside window of the CSTR could reduce k_1 values by as much as 50% based on NO_2 photolysis tests before and after reactor cleaning. There were also random fluctuations in the lamp current caused by variation of lamp operating temperature. After the first 40 runs, a series of electrical problems caused by construction in adjacent labs resulted in the premature failure of the xenon-mercury arc. It was replaced by a supposedly identical unit; however, operating characteristics were different. Due to a higher operating temperature, it was necessary to reduce the lamp current so that volatilization of the nylon insulator around the lamp electrodes would not significantly affect the light intensity levels.

Gradual deterioration of the capillary used to inject the gas sample to the Varian Gas Chromatograph resulted in some error in the propylene measurement. Calculated propylene concentration based on the cali-

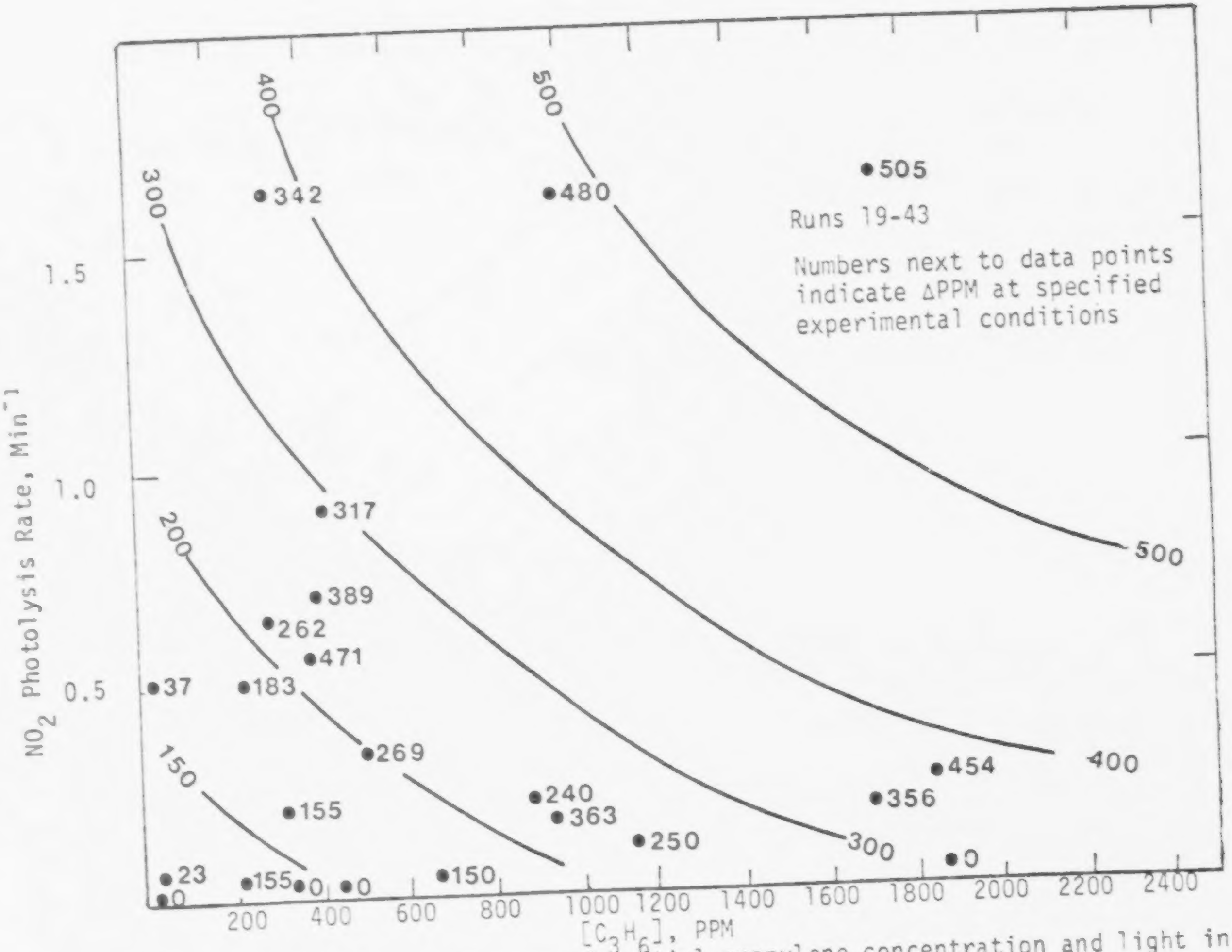

Figure 27. NO oxidation, influence of initial propylene concentration and light intensity, low initial NO_x concentration (∿600 ppm (v/v))

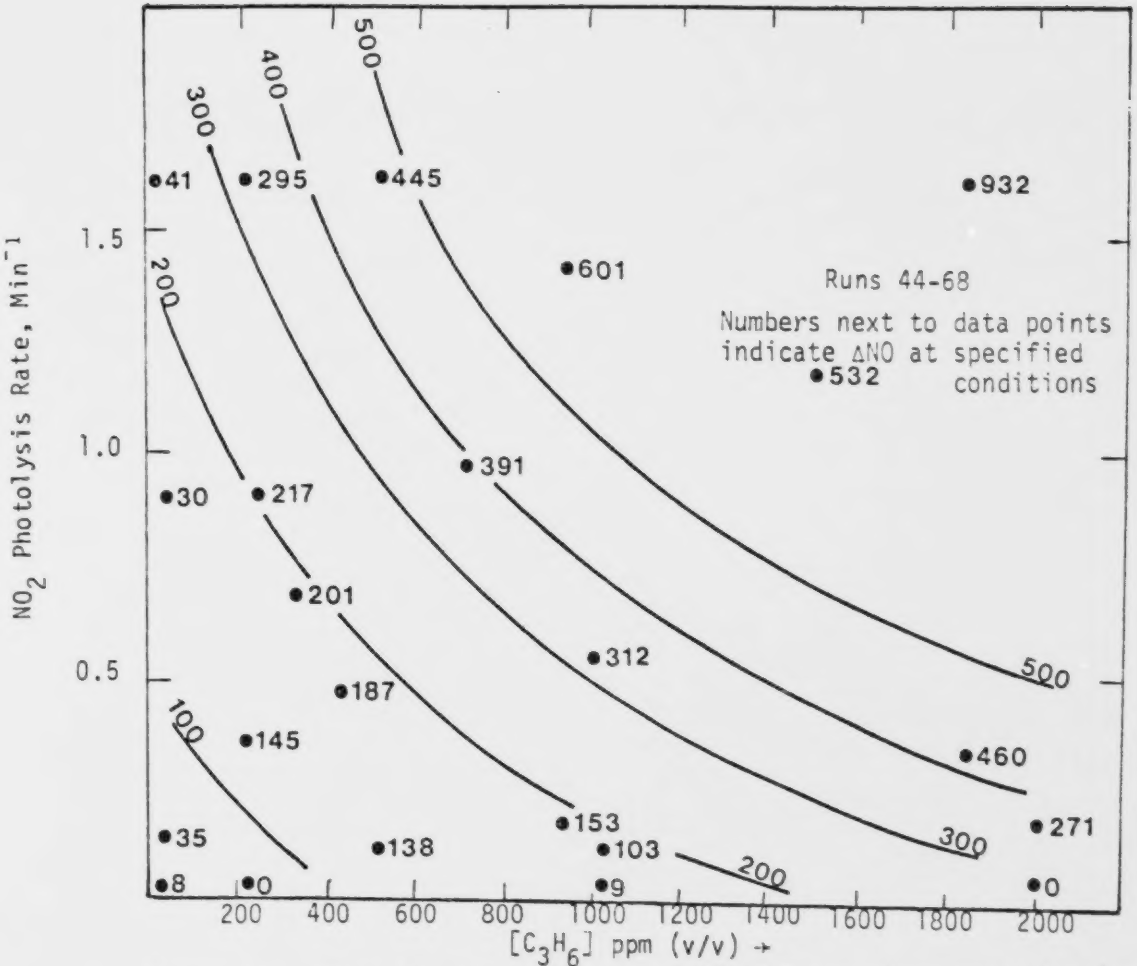

Figure 28. NO oxidation, influence of initial propylene concentration and light intensity, high initial NO_x concentration (1200 ppm v/v)

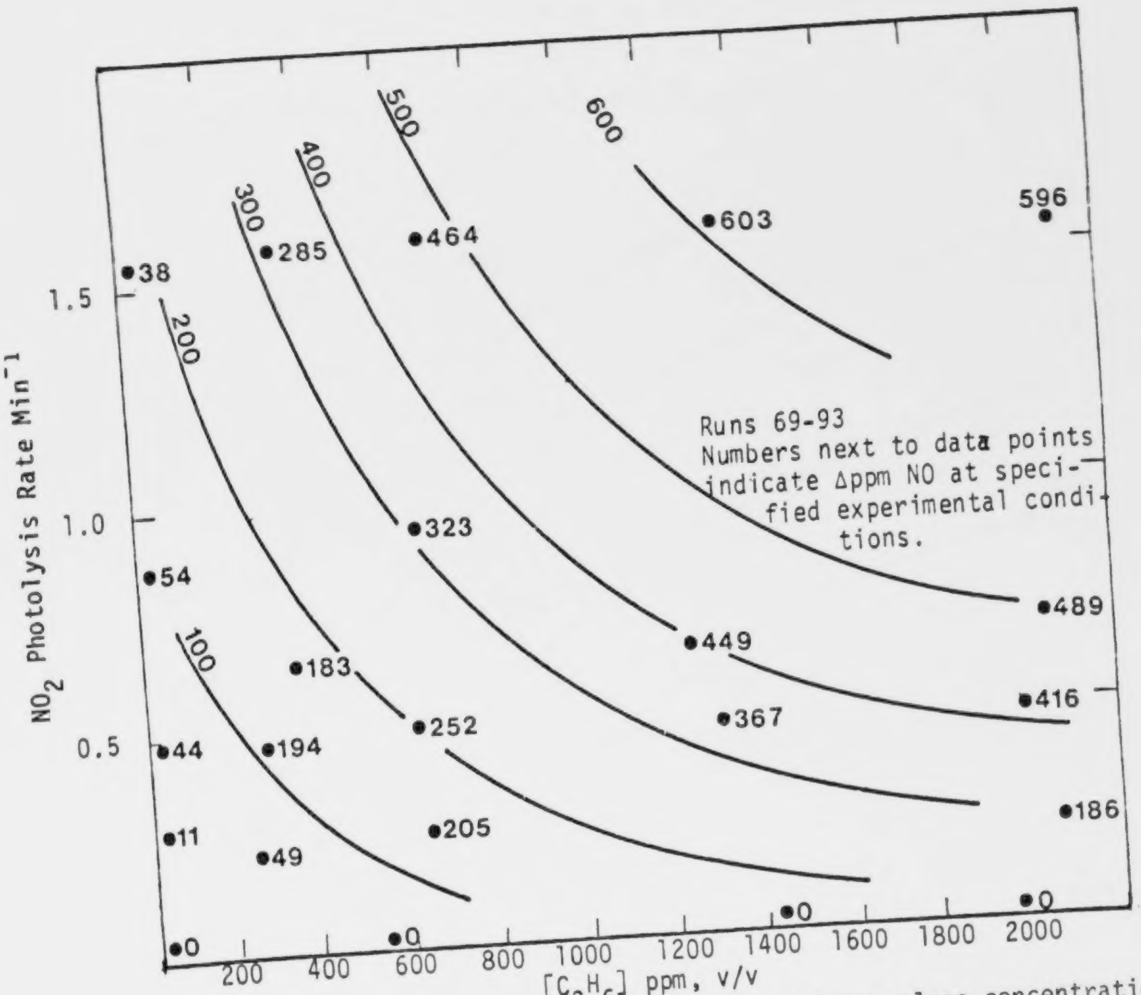

Runs 69-93
Numbers next to data points indicate Δppm NO at specified experimental conditions.

Figure 29. NO oxidation, influence of initial propylene concentration and light intensity, low initial NO_x concentration (600 ppm v/v)

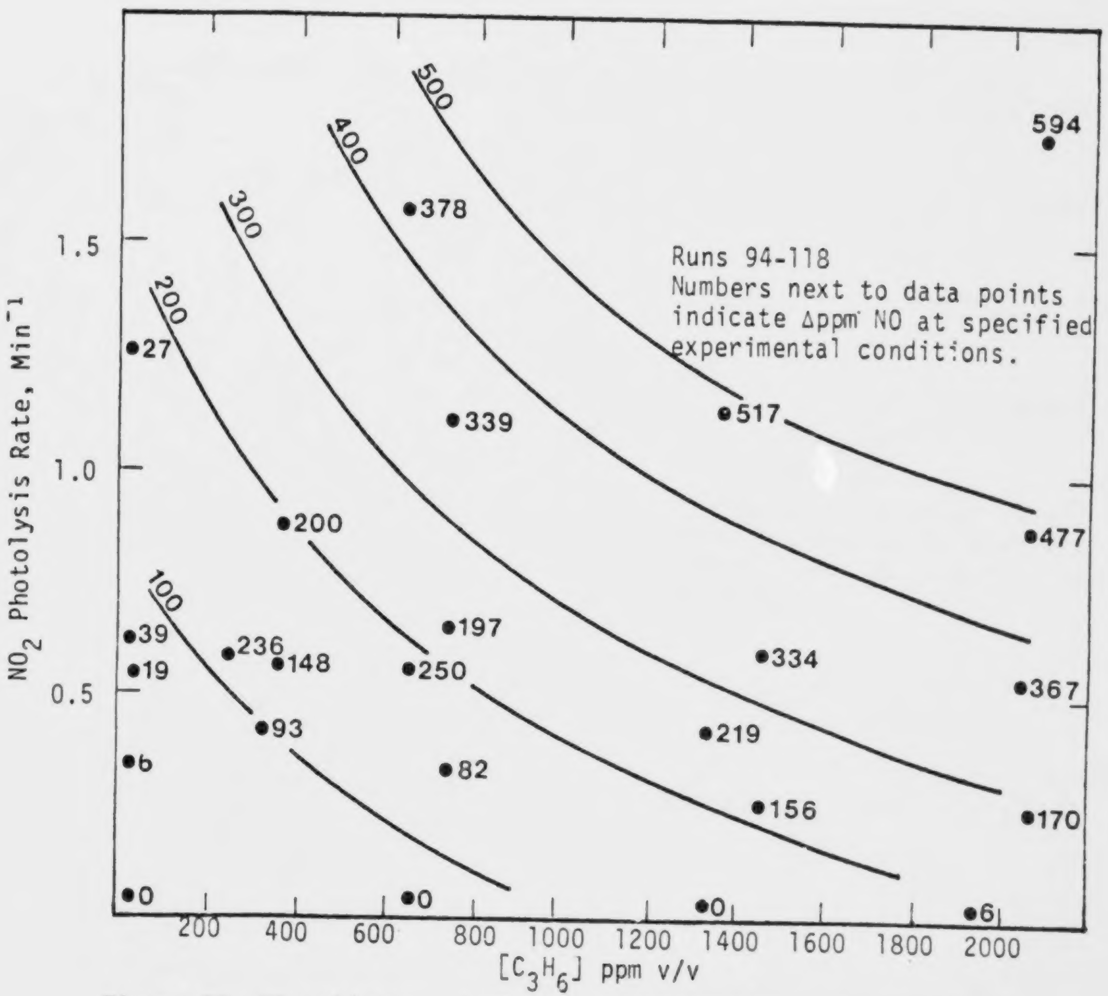

Figure 30, NO oxidation, influence of initial propylene concentration and light intensity, high initial NO$_x$ concentration (1200 ppm v/v) brated rotameter values indicated up to a 25% error due to these problems.

The low NO_x inlet k_1-olefin plots have three distinct regions, (1) an area of apparent UV light insensitivity below 500 ppm (v/v) of olefin, (2) an area of olefin insensitivity at UV intensities below 0.5 k_1, and (3) a central region where both variables exert an influence.

The light insensitive region is obviously unattractive due to the high cost of electrical power. Selection of an optimum operating point in the remaining two regions depends on the necessary control efficiency and the relative costs of propylene and energy. To achieve an outlet NO concentration of 100 ppm it appears necessary to use propylene concentrations greater than 500 ppm with k_1 values of approximately 1 to 2.

A comparison of the high and low NO_x test series shows the efficiency of NO conversion appears to be 10 to 25% better in the low NO_x tests. Because of this unexpected result, an additional series of tests were performed to study the relationship between inlet NO_x concentration and the efficiency of NO oxidation. These runs are described in a later section.

In the high NO_x series, there is a light insensitive region; however, there does not appear to be a propylene insensitive region. At the same stoichiometric NO/C_3H_6 ratio; however, the UV light requirements are close to those for the low NO_x test program.

Comparison of Propylene and Ethylene Effectiveness

One of the principal design requirements is the selection of the most effective hydrocarbon on a cost per unit NO converted basis. A screening of possible hydrocarbons is beyond the scope of this project; nevertheless, tests using ethylene were considered useful to evaluate the differences in performance.

A set of eight runs were performed, four with propylene and four with ethylene. The extent of NO conversion is presented in Figure 31 along with a summary of variability in the run conditions. There is a clear difference between the two compounds on a Δppm NO basis. This could be due to the reactivity of the alkyl radical in the propylene reactions or due simply to a difference in the reaction rate constants

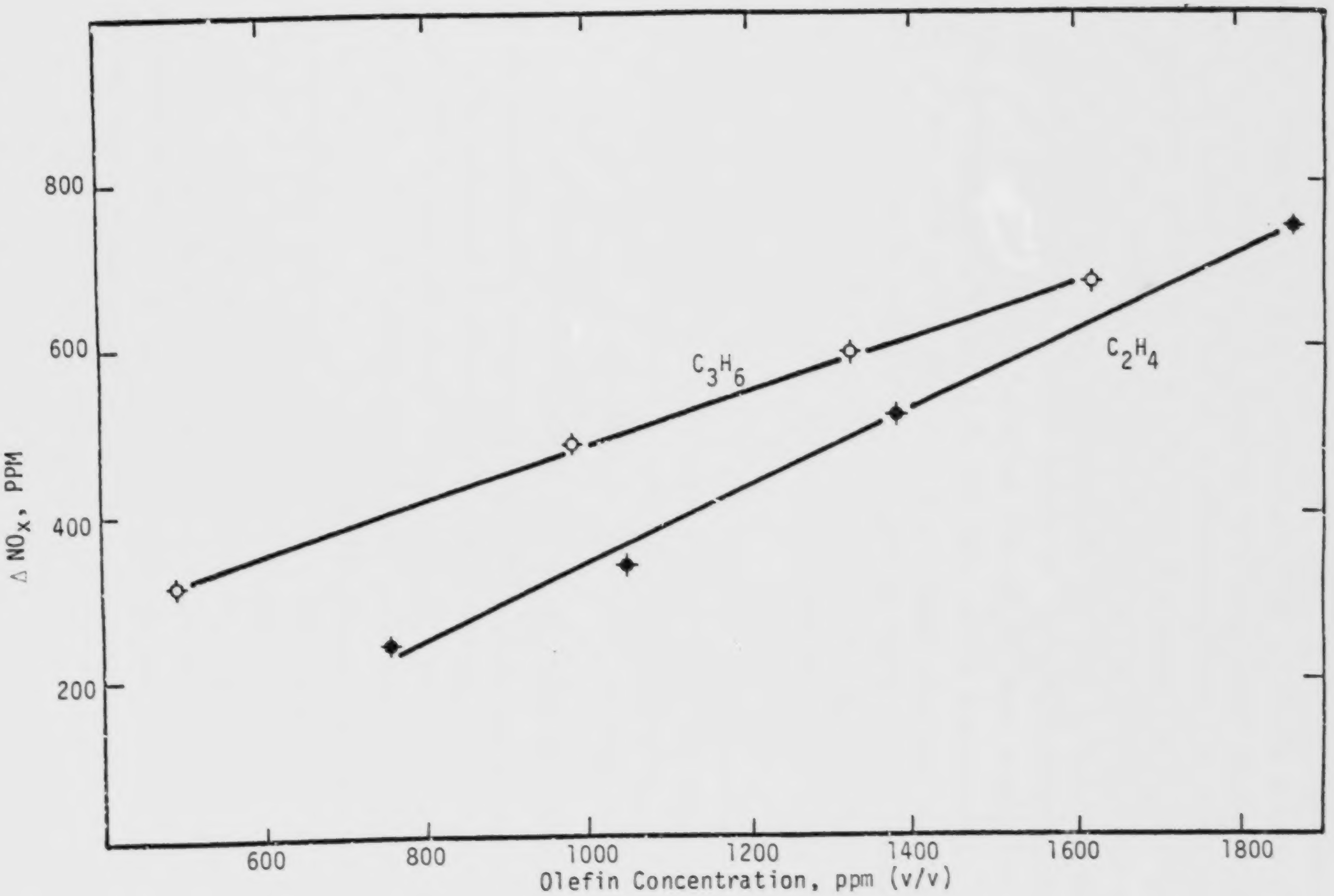

Figure 37. Comparison of propylene and ethylene

of the two compounds with hydroxy radicals. The convergence of the two curves of Figure 31 supports the reaction rate explanation. At the high olefin concentrations, there should be more effective competition for the reactive species.

Unreacted Hydrocarbon Emissions

The environmental acceptability of the photochemical process is partially dependent on the fraction of injected olefin which does not react and is emitted from the control system. The downstream flue gas desulfurization system would not be effective in removing these hydrocarbons.

The fraction of propylene consumed at various light intensity levels and various inlet propylene concentrations was evaluated using the data of runs 74 to 93. The purpose was to determine if there was an optimal operating range in which the emission of unreacted hydrocarbon is not a problem. The data are displayed in Figures 32a-d, each of which presents results at a distinct k_1 level. The top line of these figures is the inlet propylene concentration and the bottom line is the reactor outlet concentration. Unreacted olefin is represented as the shaded portion. The run number adjacent to each data point corresponds to the run summaries of Appendix B.

Unreacted propylene emissions are a significant problem across the range of propylene inlet concentrations used in these runs. Even at very low concentrations, a major fraction of the olefin remains unconsumed. Light intensity does have a favorable impact as demonstrated by the shrinking unreacted hydrocarbon concentrations evident by comparing Figures 32a-d. Based on these results, it appears that control of the hydrocarbon/NO_x stoichiometric ratic is not effective in preventing the emission of unreacted hydrocarbon. There are only three options remaining: (1) increase light intensity, (2) alter propylene reactivity, and (3) select more reactive hydrocarbon. The first option can be evaluated using the same data set presented in Figure 32.

The percent propylene consumption derived from the data of Figure 32 has been combined with the observed percent NO oxidation for the same runs to derive a second set of four Figure 33a-d. The purpose of these is to determine operating point of the system with respect to the NO_2 peak (re-

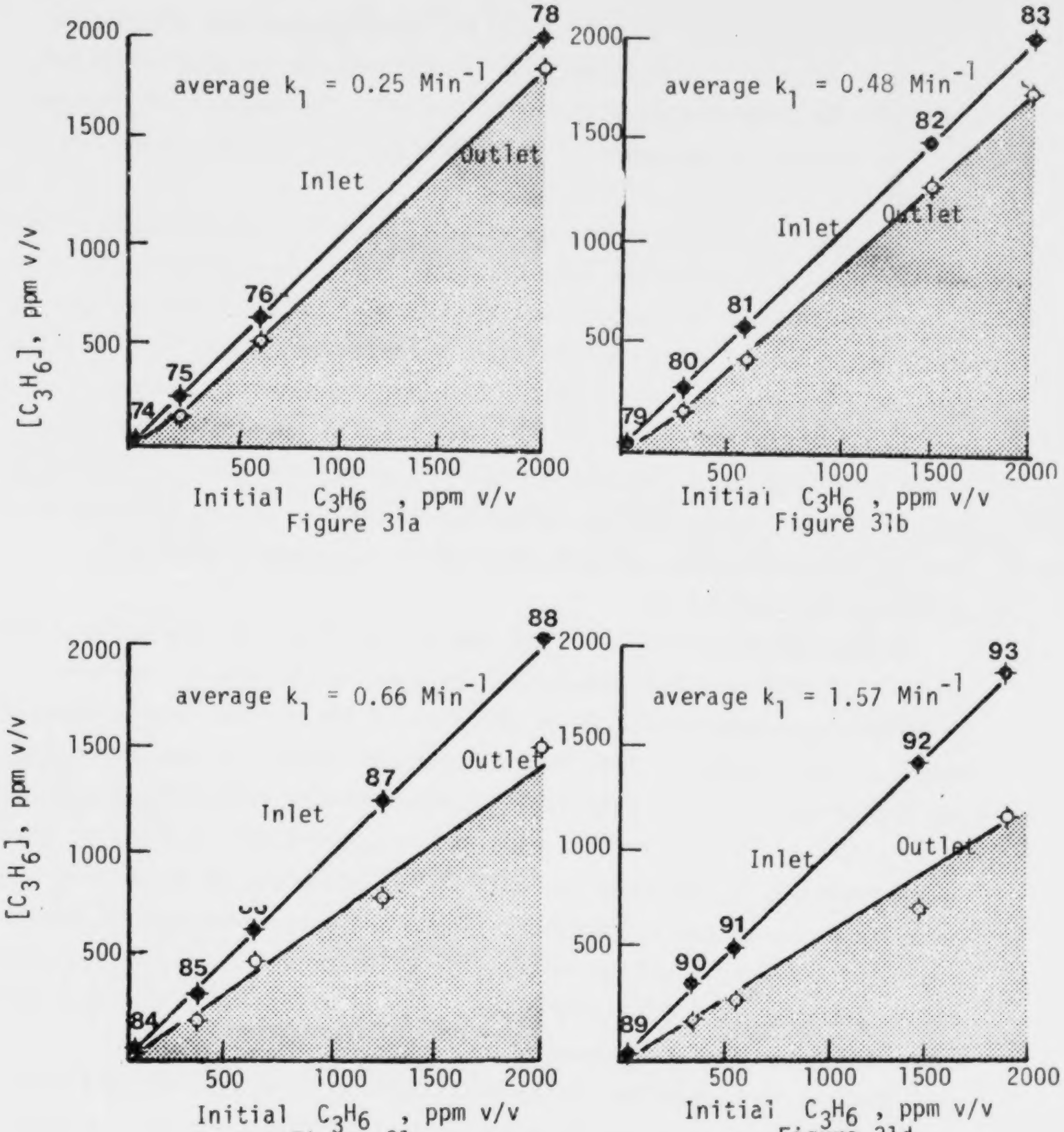

Figure 31a

Figure 31b

Figure 31c

Figure 31d

Figure 32. Unreacted propylene concentration at various inlet NO_x levels and light intensities

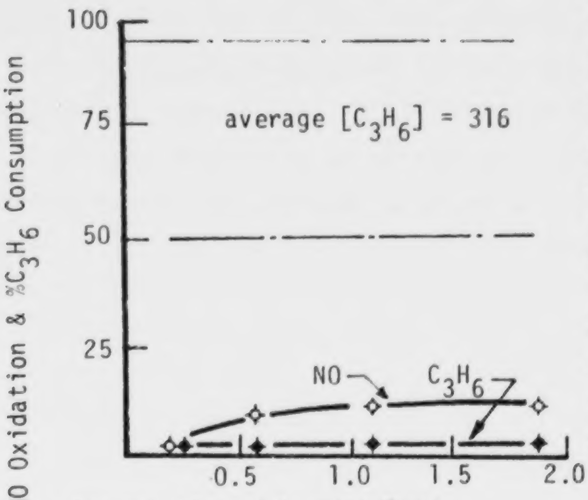

Figure 33a. NO_2 photolysis rate, min-1

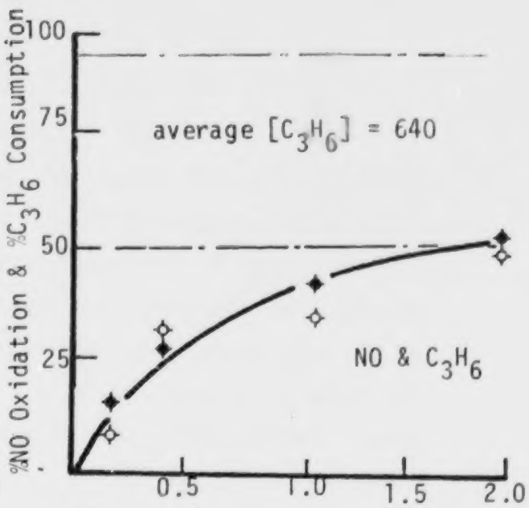

Figure 33b. NO_2 photolysis rate, min-1

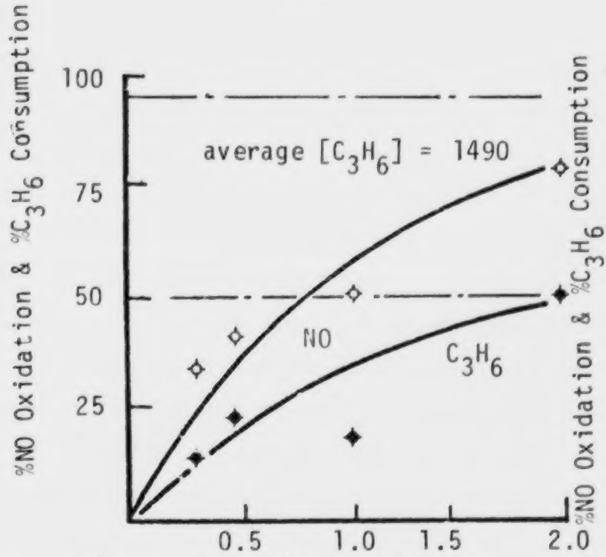

Figure 33c. NO_2 photolysis rate, min-1

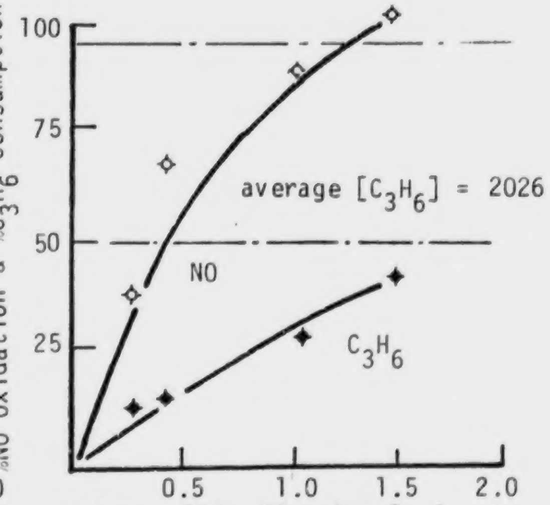

Figure 33d. NO_2 photolysis rate, min-1

Figure 33. NO oxidation and propylene consumption as a function of NO_2 photolysis rate.

fer to Figure 11), and to extrapolate the possible light energy requirements to achieve low olefin emissions. On these graphs, the point of $NO-NO_2$ crossover is shown as a horizontal line at the 50% conversion level and the point of the NO_2 peak is arbitrary shown as a horizontal line at the 95% conversion level.

At the low propylene concentration test series, Figure 33a, it is apparent that the reaction system does not begin to even approach the $NO-NO_2$ crossover point. The extrapolated light requirements approach positive infinity since the operating conditions are within the light insensitive region described in the previous section. As the propylene concentration is increased stepwise in the set of four figures, it is apparent that the operating point approaches and then goes beyond the point of the NO_2 peak. The extrapolated light energy requirements gradually decrease to a level of $k_1 = 1.5\ min^{-1}$(this can be converted to station power requirements using Figure 9). In the case of propylene, control of unreacted emissions using increased light energy requires undesirably high energy levels.

Assuming that the energy costs were tolerable, use of increased light energy to control hydrocarbon emissions entails a second risk. As illustrated in Figure 11 of Chapter 4, secondary reaction products form readily when ambient-type photochemical systems pass the NO_2 peak. Some of the compounds which could be expected include peroxyacylnitrate (PAN), ozone (O_3), nitric acid (HNO_3) and hydrogen peroxide (H_2O_2). Fine particulate composed of sulfates, nitrates, and organic particulate could also form. All of these reaction products would strain the control capability of the scrubbers used the downstream flue gas desulfurization systems. The fine particulate would be especially difficult to remove. In the case of propylene, the data presented in Figures 33a-d. demonstrates that control of unreacted emissions using light energy is done at the risk of secondary pollutant generation, assuming that reaction schemes at stack concentrations generally resemble those at ambient concentrations.

Solutions more fundamental than just control of the C_3H_6/NO_x stoichiometric ratio or the increased use of light appear necessary to prevent emissions of unreacted hydrocarbons. The alteration of effluent conditions to improve the propylene competition for reactive species such as O_3 and OH will be analyzed in a subsequent section. Generally, the reaction rates with OH radicals, ozone or atomic oxygen increase with the molecular weight of the hydrocarbon; however the potential for aerosol formation also increases. Presumably, a compromise choice will be required.

VARIABLES INFLUENCING NO OXIDATION

The effect of various physical and chemical variables are analyzed to determine the operating limitations of the photochemical system and to evaluate the extent to which propylene reactions can be optimized. Possibly the most important variable is the oxygen concentration since this is essential to the free radical chain reactions and since NO_x suppression techniques can lead to reduced flue gas oxygen content. Such modifications can also lead to increased CO levels; therefore, this is examined over the concentration range anticipated. Due to the unexpected difference between the high and low NO_x test series discussed in a previous section, a set of tests have been devoted to this subject. Other variables considered are effluent gas temperature and CO_2 concentration. All of the experiments described in this section were done at reaction conditions resembling as close as possible those used in the large test matrices of runs 19 to 118. Each test program is discussed with respect to the influence of the NO conversion efficiency and with respect to the possible underlying chemical reasons for the observed effect.

Influence of Oxygen Content

The principal questions of interest are: (1) whether the reduced oxygen content of NO_x suppressed boilers interferes with photochemical oxidation, and (2) whether the increase of oxygen would reduce the unreacted propylene concentration. These were evaluated in a set of 10 runs (numbers 127 to 136), five of which were done at high NO_x levels and five of which were done at moderate NO_x levels. The oxygen content of the reactor feed stream was modified by adjusting the balance between the

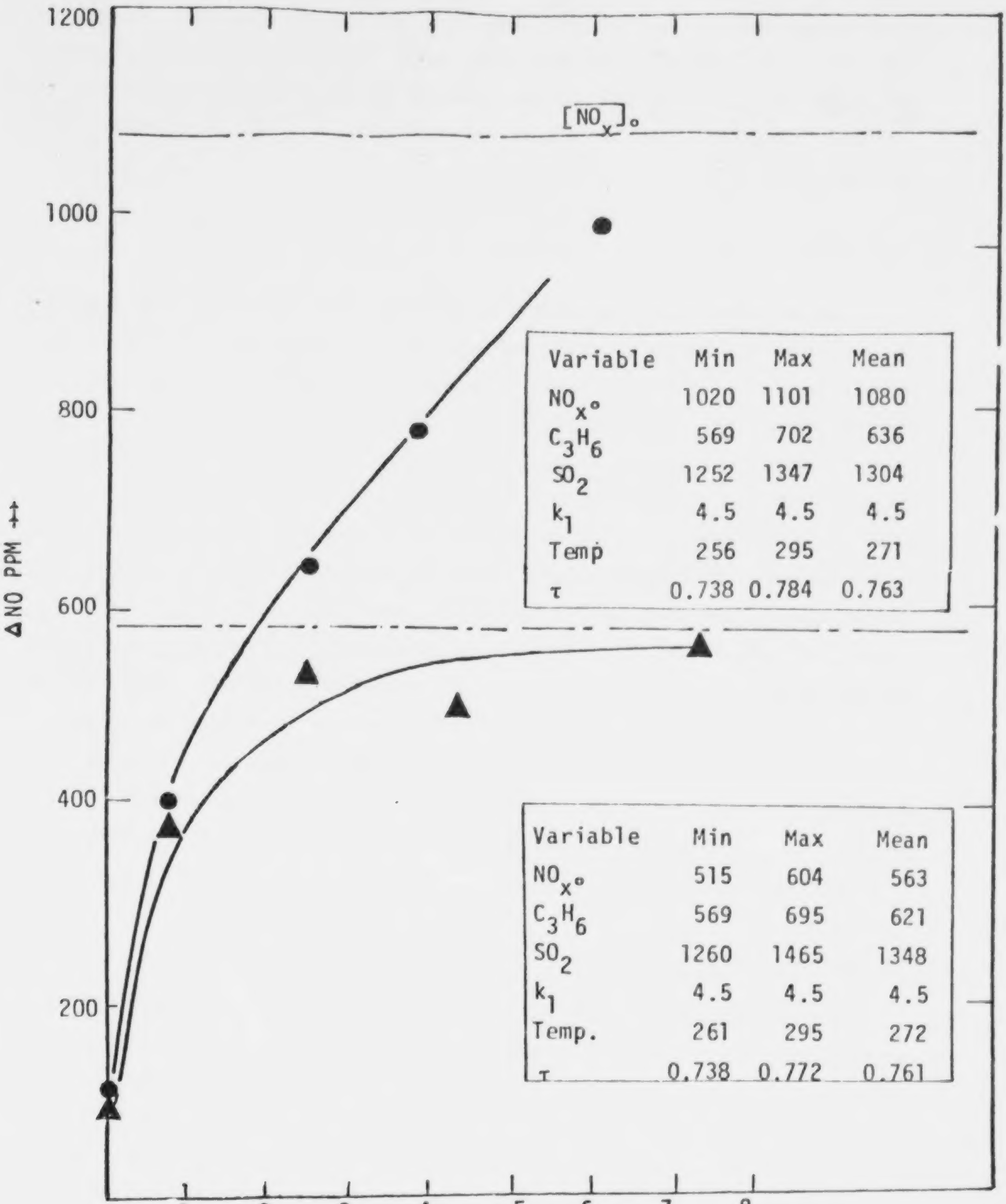

Variable	Min	Max	Mean
NO_{x_o}	1020	1101	1080
C_3H_6	569	702	636
SO_2	1252	1347	1304
k_1	4.5	4.5	4.5
Temp	256	295	271
τ	0.738	0.784	0.763

Variable	Min	Max	Mean
NO_{x_o}	515	604	563
C_3H_6	569	695	621
SO_2	1260	1465	1348
k_1	4.5	4.5	4.5
Temp.	261	295	272
τ	0.738	0.772	0.761

Figure 34. Effect of oxygen content on NO oxidation

dry nitrogen and dry air streams in the blending box. The prevailing oxygen concentrations were calculated based on the rotameter values as calibrated at the operating pressure of the particular run. Other variables were held as constant as possible in the set of runs.

The results are presented in Figure 34. For each set of five, the average inlet NO_x concentration is shown as a horizontal line. The typical oxygen contents for high NO_x emitting boilers are shown as a range of 3 to 5% by volume. The corresponding values for more typical boilers with and without NO_x suppression capability are shown as a range of 1½ to 4%. Those units with low excess air capability would be in the low end of the range and unmodified boilers would be close to the 3 to 4% range. With respect to the lower curve, it is apparent that below an oxygen concentration of 2% there is rather severe oxygen starvation of the free radical cycles. However, within the region typical of most installations, this loss in NO oxidation capability is limited to 5 to 15%. This is a very important result in that it appears that a photochemical system is compatible with low excess air combustion modifications. It is desirable, but not necessary, to add oxygen through flue gas dilution.

At high inlet NO_x levels, the extent of oxygen starvation is severe throughout the range studied. NO oxidation effectiveness is impaired to the extent of 10 to 90% with the latter value occurring at extremely low oxygen content. For such applications, it may be advantageous to either reduce inlet NO_x concentrations and/or dilute the effluent stream prior to the photochemical reactor.

The influence of oxygen content on the utilization of propylene is unclear. The data presented in Table 9 indicate that the untreated olefin concentration varies from 67 to 95% of the inlet concentration over the oxygen range of 0 to 7%. High oxygen content such as in run 128 did not significantly improve the propylene emissions problem. In fact, the extent of propylene conversion at the k_1 level of 2.84 min^{-1} appears to be slightly lower than comparable values discussed in the previous section (refer to Figures 32a-d). Conversely, low oxygen content did not drive propylene emissions any higher than would be expected for the quantity of NO oxidized.

TABLE 9. INFLUENCE OF OXYGEN CONTENT ON PROPYLENE CONSUMPTION

	Oxygen Content (% by Vol.)	C_3H_6 (ppm)	Unreacted C_3H_6 Emissions (% of $[C_3H_6]_\circ$)	ΔNO (ppm)
High	0	102	82	126
$[NO_x]_\circ$	0.86	108	83	404
Tests	2.54	234	67	626
	3.88	N/D	N/D	781
	6.14	210	70	990
Low	0	26	95	120
$[NO_x]_\circ$	0.81	117	79	392
Tests	2.45	190	67	558
	4.43	157	78	493
	7.42	N/D	N/D	559

The NO oxidation in the absence of O_2 (runs 133 and 134) is interesting because it indicates the extent of conversion possible in the absence of the free radical chain reaction mechanisms and other mechanisms dependent on oxygen. One possible reaction mechanism is the oxidation of NO by atomic oxygen as shown in reactions 33 to 38.

$$\begin{array}{llr}
NO_2 + h\nu(3000\text{-}4000\ \text{Å}) & \rightarrow NO + O(^3P) & (33) \\
O(^3P) + NO & \xrightarrow{M} NO_2 & (34) \\
O(^3P) + C_3H_6 & \rightarrow \dot{C}H_2CH = CH_2 + OH & (35) \\
 & \rightarrow \cdot C_3H_6O \cdot & (36) \\
\dot{C}_3H_6\dot{O} + NO & \rightarrow C_3H_6ONO & (37) \\
O(^3P) + NO_2 & \rightarrow NO + O_2 & (38)
\end{array}$$

The NO_2 product quantum yield for such a mechanism must be small due to the rate of the reverse reaction, 38.

Influence of Carbon Monoxide Concentration

The typical levels of carbon monoxide in the effluent of coal-fired boilers is 10 to 50 ppm. With certain combustion modifications for NO_x suppression, however, increased CO levels can result. The maximum expected concentration is 2000 ppm since above this point there is probably unacceptable carbon carryover and there is a risk of explosive conditions (Acurex, 1978). A set of four runs (numbers 137 to 140) were performed to examine the possible effect of CO within the 0 to 3000 ppm range. The purposes of this work was to determine the extent to which CO enhances the NO conversion efficiency and to determine if unreacted hydrocarbons are reduced at high CO levels.

CO was injected into the influent gas stream using the SO_2 line, and the prevailing CO concentration was calculated based on the rotameter calibration. Except for the absences of SO_2, the effluent conditions were similar to those used in the large test series (runs 19 to 118). The variability of reaction conditions is presented in the table included with Figure 35. This figure illustrates the NO oxidation effectiveness in terms of ppm NO converted at the corresponding CO inlet concentration. The run numbers shown adjacent to each of the data points corresponds to the data compilation in Appendix B.

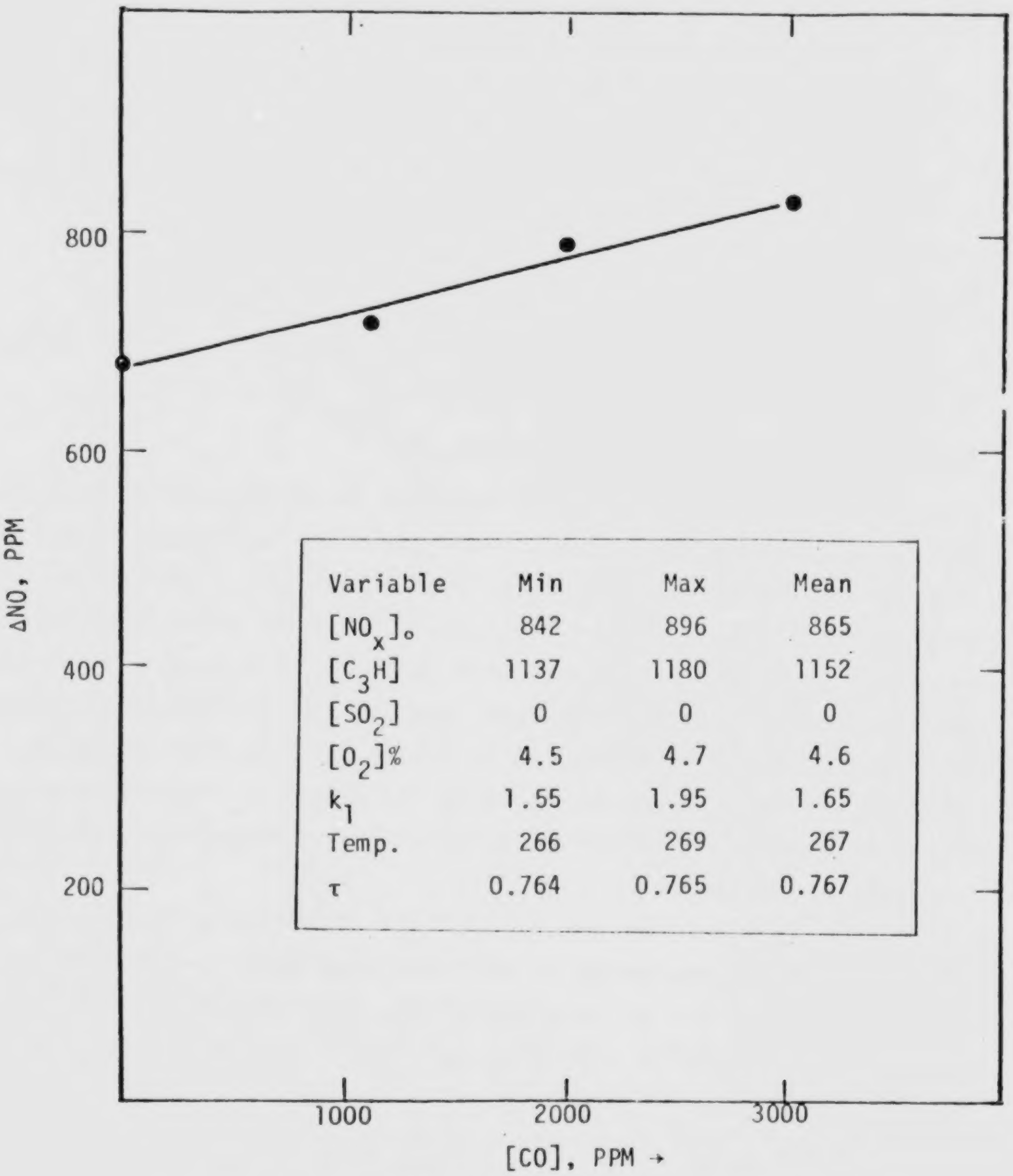

Variable	Min	Max	Mean
$[NO_x]_o$	842	896	865
$[C_3H]$	1137	1180	1152
$[SO_2]$	0	0	0
$[O_2]$%	4.5	4.7	4.6
k_1	1.55	1.95	1.65
Temp.	266	269	267
τ	0.764	0.765	0.767

Figure 35. Effect of CO on NO oxidation

The results displayed in Figure 35 show that CO enhances the oxidation of NO. There is a 22% increase in the ppm of NO converted at 3000 ppm CO relative to 0 ppm CO. This effect is attributed to the reaction of CO with hydroxy radicals which ultimately results in the hydroperoxy radical attack of NO.

$$CO + OH\cdot \rightarrow CO_2 + H\cdot \qquad (39)$$

$$O_2 + H\cdot \overset{M}{\rightarrow} HO_2 \qquad (40)$$

$$NO + HO_2\cdot \rightarrow NO_2 + OH\cdot \qquad (41)$$

The effectiveness of the chain process is limited by the competition for the hydroxy radicals. This competition primarily comes from the reactions listed below:

$$OH\cdot + C_3H_6 \rightarrow CH_3CHOH{=}CH_2\cdot \qquad (42)$$

$$OH\cdot + NO_2 \rightarrow HNO_3 \qquad (43)$$

$$OH\cdot + NO \rightarrow HNO_2 \qquad (44)$$

The fraction of hydroxy radicals retained in the CO chain reaction can be approximated using the ratio of Equation 13. The summation term in the denominator accounts for OH sinks not expressly considered in the above set of reactions.

$$F_{OH} = \frac{k[CO]}{k[CO] + k[C_3H_6] + k[NO_2] + k[NO] + \sum_{i=1}^{N} \overline{k_i[C_i]}} \qquad (13)$$

where: F_{OH} = the fraction of hydroxy radicals reacting according to reaction 39

k_i = the rate constant for the reaction number i

Assuming that the summation term is neglible, and using the reaction 39 rate constant of 2.50×10^2 ppm^{-1} min^{-1} and constants of Demerjian, Kerr and Calvert (1975) for the other hydroxy reactions, indicates that CO utilizes 5% of the hydroxy radicals at 3000 ppm. This small fraction apparently accounts for the 22% increased in NO oxidation. These results confirm previous conclusions that hydroxy radical utilization is an important factor in the overall reaction scheme active in the photochemical process. CO has a moderate influence on NO conversion due to its OH reaction and resulting free radical chain reactions. This positive effect again demonstrates that the photochemical system is compatible with conditions expected at boilers modified to suppress NO_x generation.

The high concentrations of NO and NO_2 in addition to the large rate constants for hydroxy radical reaction may hinder the optimal utilization of hydroxy radicals. In time-limited and light-limited conditions, both reactions 43 and 44 may represent free radical termination steps. The adverse impact of high NOx levels on system performance has already been discussed earlier concerning the large test series and is evaluated specifically in the next section.

Influence of Initial NO_x Concentration

During the course of other experimental subsets, it was observed that there was a moderate negative correlation between the extent of NO conversion and the initial NO concentration. This was studied in a special series of runs with initial concentrations varying from 400 to 2000 ppm. Obviously, the high levels are not representative of any commonly encountered fossil-fuel fired boiler. Unlike most of the experimental work, this set of tests has been done specifically to evaluate mechanistic questions and not to evaluate technical/economic feasibility of the technique.

A series of 7 runs (numbers 141 to 147) were performed under nearly identical conditions. The influence of initial NO_x concentration was indicated by the difference in ppm NO converted. Results are presented in Figure 36. The probable reasons for the negative slope are the reactions listed below:

$$OH\cdot + NO_2 \rightarrow HNO_3 \qquad (43)$$

$$OH\cdot + NO \rightleftarrows HNO_2 \qquad (44a,b)$$

$$OH\cdot + HNO_2 \rightarrow NO_2\cdot + H_3O \qquad (45)$$

$$OH + HNO_3 \rightarrow NO_3 + H_2O \qquad (46)$$

$$HNO_2 + h\nu(<4000\ \text{Å}) \rightarrow NO + OH\cdot \qquad (47)$$

$$HNO_3 + h\nu(<3400\ \text{Å}) \rightarrow NO_2 + OH\cdot \qquad (48)$$

Reactions 43 and 44 should be important sinks for the hydroxy radicals. With the time and light limited conditions, it is unlikely that the photolysis of nitrous acid and/or nitric acid would significantly offset the overall dampening effect of increased NO_x.

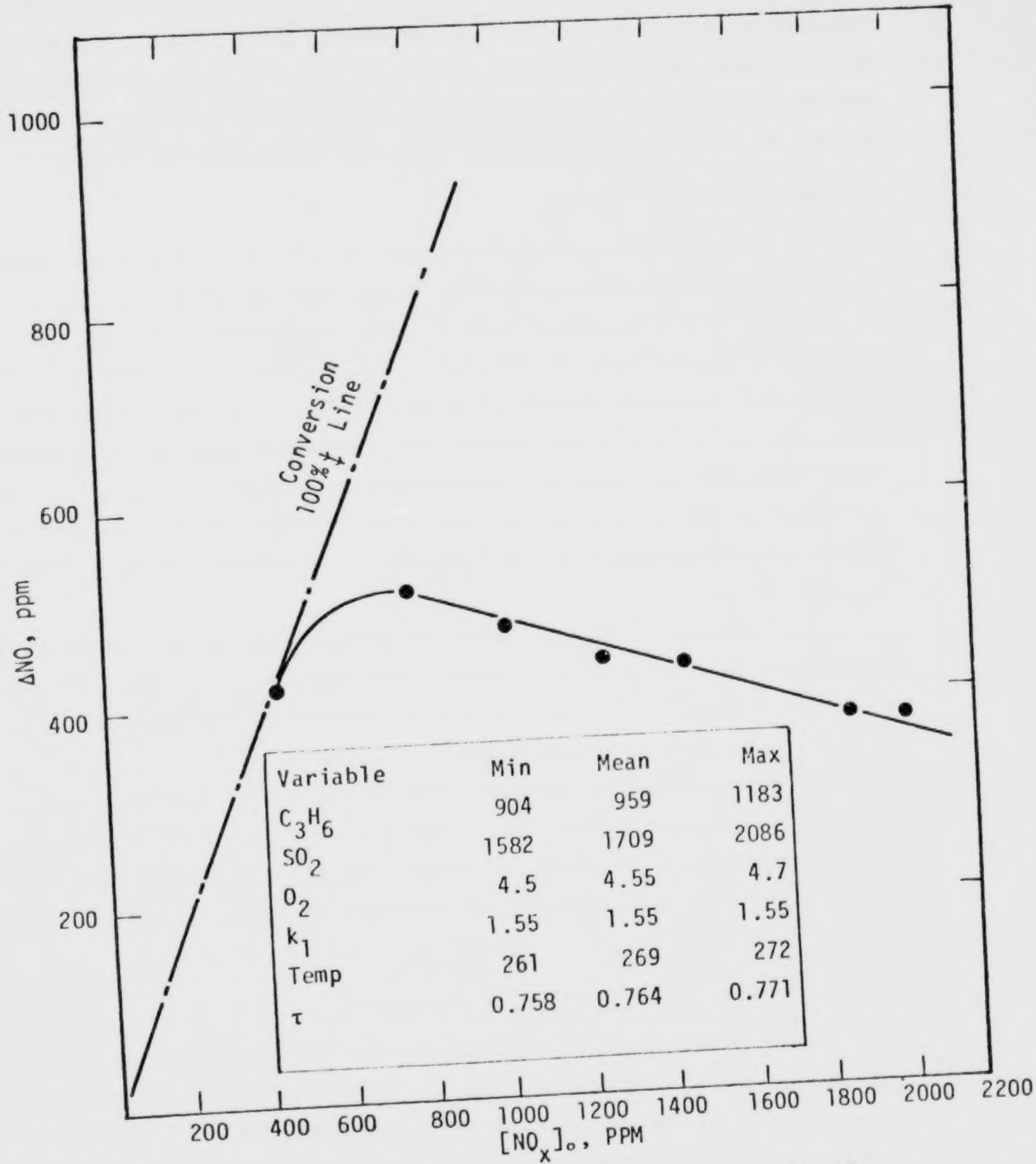

Variable	Min	Mean	Max
C_3H_6	904	959	1183
SO_2	1582	1709	2086
O_2	4.5	4.55	4.7
k_1	1.55	1.55	1.55
Temp	261	269	272
τ	0.758	0.764	0.771

Figure 36. Effect of initial NO_x concentration on NO oxidation

It should be noted that this is not a problem for the photochemical system since both nitrous acid and nitric acid should be effectively removed downstream in the flue gas desulfurization system. These results could suggest that the difference between the high concentration runs and the low concentration runs is partially due to the increased presence of nitrous acid and nitric acid in the high concentration tests.

Influence of Carbon Dioxide

The simulated flue gas streams used in this project did not include CO_2 since photolysis was negligible in the lamp emission spectra and since CO_2 does not actively participate in known dark phase reactions. Suspected chemical activity is limited to enhancement of the atomic oxygen-nitric oxide reaction (Demerjian *et al*., 1975). This relatively minor third body activity did not warrant the additional complexity involved with adding another component to the reactor influent stream. This assumption was tested in a set of four runs (numbers 148 to 151) done at CO_2 concentrations ranging from 0 to 20%. Typical CO_2 levels are in the range of 10 to 15%.

The influence of CO_2 was measured with respect to the change in NO concentration at various CO_2 levels. The results of the four tests are presented in Figure 37. Variability of experimental conditions is reported in the table enclosed within this Figure.

The observed NO concentration drop varied 3% for the tests and there is no apparent trend. It is concluded that CO_2 does not exert any appreciable influence on the overall photochemical process and that the system can in fact be operated successfully in the high CO_2 environment of coal-fired boiler effluent.

Influence of Gas Temperature

There are three possible locations where hydrocarbons could be injected and the irradiation performed: following the FGD system presaturator, preceding the presaturator, and preceding the air preheater. A series of tests were done to evaluate system performance at the various temperature levels characteristic of these possible locations. Due to physical limitations of the reactor, it was impossible to approach the 500-700°F range representative of the air preheater inlet. In these runs,

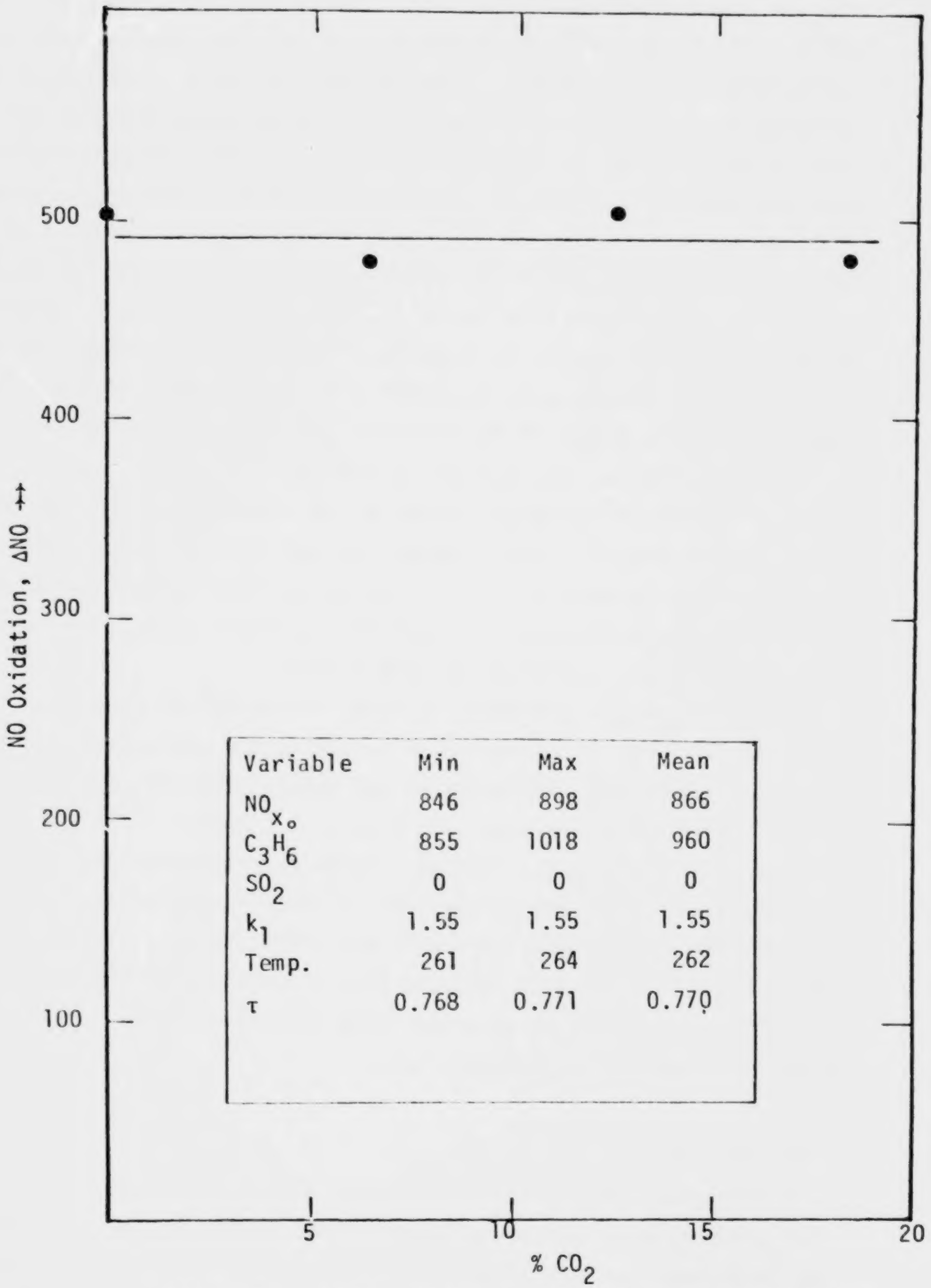

Variable	Min	Max	Mean
NO_{x_o}	846	898	866
C_3H_6	855	1018	960
SO_2	0	0	0
k_1	1.55	1.55	1.55
Temp.	261	264	262
τ	0.768	0.771	0.770

Figure 37. Effect of CO_2 concentration on NO oxidation

the gas temperature was varied from a low of 115 F to a high of almost 300 F. The latter value is characteristic of older boilers with minimal air preheater surface areas. Newer boiler designs have maximized thermal efficiency by reducing air preheater exit temperature from 300 to 275 F. This is possible due to the common use of low sulfur western coals with low acid dewpoint. After the presaturator, which sometimes accompanies a flue gas desulfurization system, the gas temperature is reduced to adiabatic saturation levels of approximately 125 F. These two common temperature ranges are illustrated on Figure 38. Effluent temperature between these two regions is uncommon. Data points have been taken in this temperature range only to obtain a clearer picture of the relationship between the extent of NO oxidation and the gas temperature.

The test series was divided in high NO_x and low NO_x subsets. The flow rate of the blended gas stream to the reactor was adjusted to account for the density changes occurring upon heating in the tube furnace and CSTR. The purpose of this was to ensure that the energy per gram mole of gas was approximately equal for the eight tests. The runs (numbers 152-159) were performed in random order.

The results are presented in terms of percent NO oxidation. This was chosen instead of change in NO concentration since there was considerable unintentional variation in the initial NO_x concentrations as indicated in the tables provided with Figure 38. Conversion of NO at high temperatures is obviously favored. There is a considerable loss of system effectiveness as the temperature if reduced; therefore, the preferred location for the system is prior to the presaturator. It is conceivable that performance could be improved with the reactor on the "hot side" of the air preheater if the observed trend continues. This should be examined in subsequent bench scale tests.

REACTION PRODUCTS

The quantities and characteristics of the photochemical system reaction products will partially determine the commercial acceptability of the technique. Ideally, the system would operate at the point of the NO_2 peak and there would be a minimum of secondary reaction products such as ozone, PAN, and aerosols. The formation of submicron aerosols would be

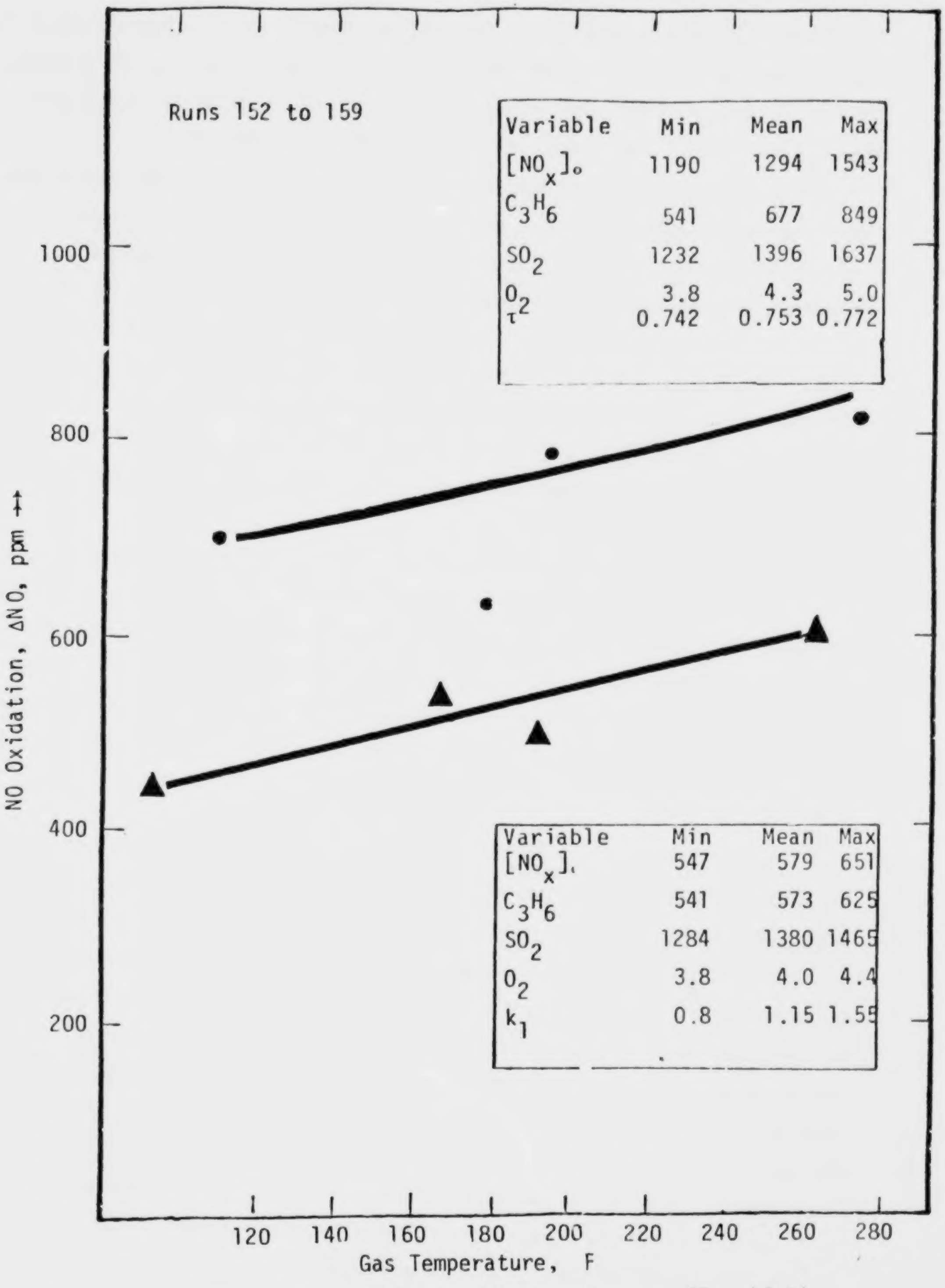

Variable	Min	Mean	Max
$[NO_x]_o$	1190	1294	1543
C_3H_6	541	677	849
SO_2	1232	1396	1637
O_2	3.8	4.3	5.0
τ^2	0.742	0.753	0.772

Variable	Min	Mean	Max
$[NO_x]_i$	547	579	651
C_3H_6	541	573	625
SO_2	1284	1380	1465
O_2	3.8	4.0	4.4
k_1	0.8	1.15	1.55

Figure 38. Influence of temperature on NO oxidation

particularly unfortunate since the collection of most scrubbers used in FGD systems are at a minimum in the 0.2 to 0.7 microns. A net increase in the levels of POM's and other potentially toxic organic compounds would also reduce the appeal of a photochemical approach.

The generation of secondary reaction products has been evaluated by performing nitrogen, sulfur, and carbon material balance calculations around the quartz CSTR and determining the fraction unaccountable. This represented the maximum quantity of material which could be in the form of toxic secondary products. Millipore filter samples were analyzed with x-ray fluorescence and ion chromotography to evaluate the fraction of missing sulfur and nitrogen which were in the form of sulfate and nitrate aerosols. The sulfate and nitrate content of wash waters of the reactor and effluent gas lines was also added to complete the material balances of sulfur and nitrogen.

For selected runs, samples of the reactor effluent were taken in 40-liter Teflon bags and were analyzed at the UNC Pittsboro research site where it was possible to convert the formaldehyde to CO for analysis in the gas chromotography. For the same set of runs, gas samples were taken in Tenax columns for GC-mass spectrometry. The purpose of these runs was to identify possible toxic organic products present at low concentrations.

Nitrogen Balances

The fraction of the nitrogen compounds measurable with the chemiluminescent analyzer are reported in Table 10. Low light and/or low propylene conditions provide only limited photochemical activity; therefore, most of the initial nitrogen can be accounted for as NO or measurable NO_x compounds. As reactivity increases, it is apparent that the portion of unaccountable nitrogen increases to 10 to 20% of the initial NO_x concentration. One possible reason for this is that the system has the capability to proceed beyond the peak where some of the NO_x has been converted to gaseous or aerosol forms which cannot be measured by the TECO instrument. This unaccountable nitrogen amounts to a maximum of 120 ppm.

To determine the fraction of the nitrogen present as aerosol, some of the Millipore filters (see Chapter 4, Figure 22) were analyzed using ion chromotography. The oxygen test series (runs 127 to 136) which

TABLE 10a. NITROGEN MATERIAL BALANCE, $[NO_x]_o \sim 600$ PPM

Relative Light Level	Hydrocarbon Target Concentration, PPM (v/v)					Runs
	0	250	500	1000	1500	
0	1.00	1.00	1.00	1.00	1.00	69 to 73
1/4	1.00	1.06	0.95	0.94	0.97	74 to 78
1/2	1.00	0.96	0.97	0.93	0.93	79 to 83
3/4	0.99	0.92	0.92	0.98	0.86	84 to 88
1	1.00	0.94	0.87	0.82	0.87	89 to 93

TABLE 10b. NITROGEN MATERIAL BALANCES, $[NO_x]_o \approx 1200$ PPM (v/v)

Relative Light Level	Hydrocarbon Target Concentration, PPM (v/v)					Runs
	0	250	500	1000	1500	
0	1.00	1.00	1.00	1.00	1.00	94 to 98
1/4	1.00	0.99	1.00	0.97	0.99	99 to 103
1/2	1.02	0.98	0.95	0.95	0.94	104 to 108
3/4	1.00	0.95	0.97	0.96	0.95	109 to 113
1	1.01	0.99	0.97	0.90	0.90	114 to 118

exhibited substantial variability in NO conversion were used to identify the possible range in quantities of nitrate aerosol. It should be noted that the gas temperature at the filter point had generally cooled to ambient levels; therefore, it is likely that most of the nitrate had condensed prior to collection. Observed nitrate levels expressed in terms of ppm of NO are in the range of 1 to 5, trivial when compared with the total NO unaccountable. The variability of the nitrate concentrations in Table 11 does not appear correlated with the extent of NO conversion.

At regular intervals, the reactor was flushed with distilled water to measure quantities of deposited material and to prevent major changes in the light transmission properties of the CSTR. Deposits were highly water soluble. Wet chemical analyses of the samples indicated very small quantities of nitrates as indicated on Figure 39. Considering that approximately 30 runs were performed between each washing, the quantities of nitrate represent less than 1% of the unaccountable fraction. Analysis of the line rinse water at the end of the experimental program also indicated that very little of the nitrates materials were deposited.

It is concluded that most of the unaccountable nitrogen is present as gaseous material which is not adequately reduced in the converter of the chemiluminescent analyzer. Possible compounds include, but are not limited to, nitric acid, nitrous acid, and organic nitrates. Since the chemical composition is uncertain and the concentrations may exceed 100 ppm, it must be concluded that some nitrogen compounds may represent toxic reaction products.

Sulfur Balances

Very little change in SO_2 concentrations was observed during the change from dark phase to light phase conditions in each of the runs. As indicated in Table 12, the maximum drop was 5% and the normal drop was in the range of 1 to 3%. These relatively small fractions represent the maximum amounts of potentially toxic sulfur compounds formed in the reactor. These quantities could be even smaller than suggested by the material balance since NO_2 formed during irradiation suppresses the SO_2 signal in the pulse fluorescent analyzer (refer to Chapter 4). Correcting the light phase SO_2 concentrations according to the steady state NO_2

Line Deposits (4-28-78)
Gram Moles NO_3^-

Line 1	
Sample 1	0
Sample 2	0
Line 2	
Sample 1	5.8×10^{-5}
Sample 2	1.1×10^{-5}
Line 3	
Sample	0

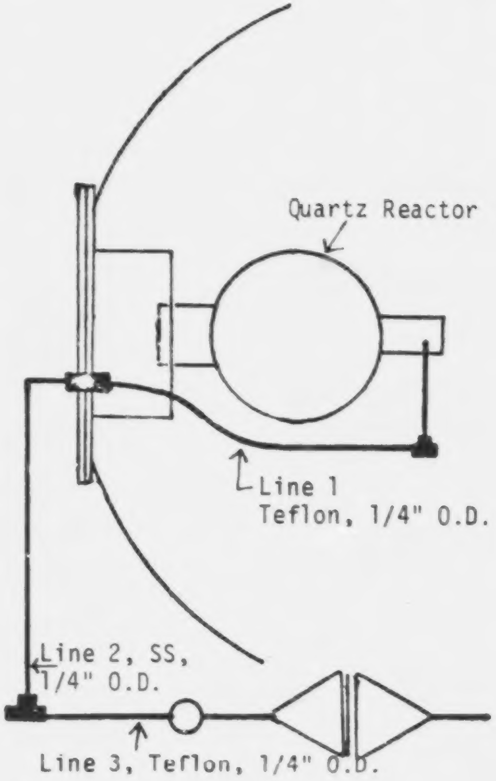
Quartz Reactor
Line 1
Teflon, 1/4" O.D.
Line 2, SS,
1/4" O.D.
Line 3, Teflon, 1/4" O.D.

Reactor Deposits
Gram Moles NO_3^-

Date of Wash	
3-15-78	2.9×10^{-5}
3-23-78	5.0×10^{-6}
4-5-78	7.0×10^{-5}
4-14-78	1.4×10^{-6}
4-27-78	3.0×10^{-6}

Figure 39. Nitrate deposits

TABLE 11. NITRATE AEROSOL QUANTITIES COMPARED WITH NO OXIDATION

Run	ΔNO_x as NO_3^-, ppm	ΔNO ppm	ΔNO %
127	2.39	404	37
128	3.00	990	95
129	2.12	493	98
130	1.42	626	61
131	2.15	392	69
132	1.87	558	95
133	1.96	126	12
134	1.98	120	24
135	2.52	559	96
136	2.50	781	69
90	3.05	285	44
91	4.78	464	76
114	2.91	27	3
115	2.08	247	25
116	1.44	339	34
117	1.78	517	51
118	2.22	594	60

TABLE 12. SULFUR MATERIAL BALANCE

	SULFUR MATERIAL BALANCE, CORRECTED AND UNCORRECTED					
	Hydrocarbon Target Concentration, PPM (v/v)					
Relative Light Level	0	250	500	1000	1500	Runs
0	N.D.	N.D.	N.D.	1.00	1.00	69 to 73
	N.D.	N.D.	N.D.	1.00	1.00	
1/4	1.00	0.99	0.98	0.99	1.00	74 to 78
	1.00	1.00	1.00	1.01	1.03	
1/2	0.98	0.98	0.99	0.97	0.98	79 to 83
	1.00	1.00	1.01	1.00	1.02	
3/4	0.97	0.97	0.99	0.95	1.00	84 to 88
	0.98	0.99	1.00	1.00	1.04	
1	0.97	0.97	0.95	0.97	0.98	89 to 93
	0.97	1.00	0.99	1.02	1.00	

levels and the relationship of Figure 18 accounts for most of the observed SO_2. These corrected sulfur material balances are reported as the second entry for each of the runs covered in Table 12. The amount of sulfur unaccountable is very small and approaches the inherent errors involved in reading the SO_2 analyzer analog scale.

X-ray fluorescent tests for sulfur have been performed for all of the runs of the experimental program. Results for runs 68 to 93 are presented in Table 13 in terms of the Δppm of SO_2. The very low quantities of sulfate aerosol confirm expectations of insignificant SO_2 conversion. This conclusion was checked further by performing ion chromatography analyses on a selected group of the Millipore filters. Results presented in Appendix B for each of the runs indicate that the sulfate levels are conceivably 50% lower than those suggested by x-ray fluorescence. No attempt was made to determine the most accurate analytical approach due to the small quantities of sulfur in the aerosol form.

There was an order of magnitude more sulfate material than nitrate material present in the reactor deposits and in the effluent handling lines. The measured quantities have been expressed in terms of gram moles of sulfate in Figure 40. These quantities are equivalent to approximately 3% of the sulfur unaccountable over the combined set of experimental runs. It is concluded that sulfate aerosol or toxic sulfur compounds are not formed in significant quantities in the photochemical system.

Carbon Material Balances

The extent of propylene consumption was a strong function of the light intensity and the initial propylene concentration. With reactive conditions 25 to 50% of the propylene reacted to form one or more degradation products. The fraction accountable as propylene for runs 68 to 118 is presented in Table 14. This set of runs was chosen since the quality of the Varian GC data was considered the best.

Possible reaction products accounting for the missing carbon include, but are not limited to, formaldehyde, acetaldehyde, carbon dioxide, carbon monoxide, and organic aerosols. The Varian gas chromotograph results (a sample run output is shown in Figure 41) suggests that only one or two major reaction products were formed. The large peak following

Line Deposits (4-28-78)

	Gram Moles $SO_4^{=}$
Line 1	
Wash 1	2.0×10^{-3}
Wash 2	7.2×10^{-5}
Line 2	
Wash 1	4.1×10^{-3}
Wash 2	1.0×10^{-4}
Line 3	
Wash 1	1.8×10^{-4}

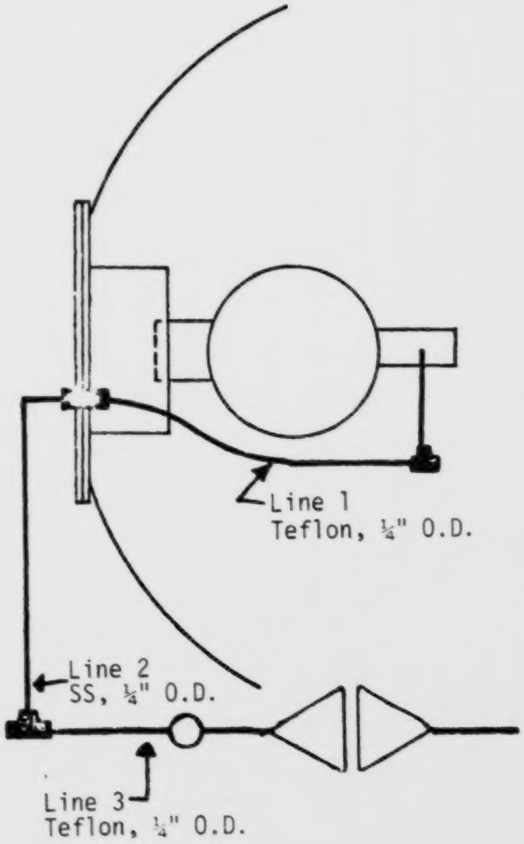
Line 1
Teflon, ¼" O.D.
Line 2
SS, ¼" O.D.
Line 3
Teflon, ¼" O.D.

Reactor Deposits

Date of Wash	Gram Moles $SO_4^{=}$
3-15	4×10^{-4}
3-23	2.7×10^{-5}
4-5	3.3×10^{-5}
4-14	4.4×10^{-5}
4-27	1.7×10^{-5}

Figure 40. Sulfate deposits

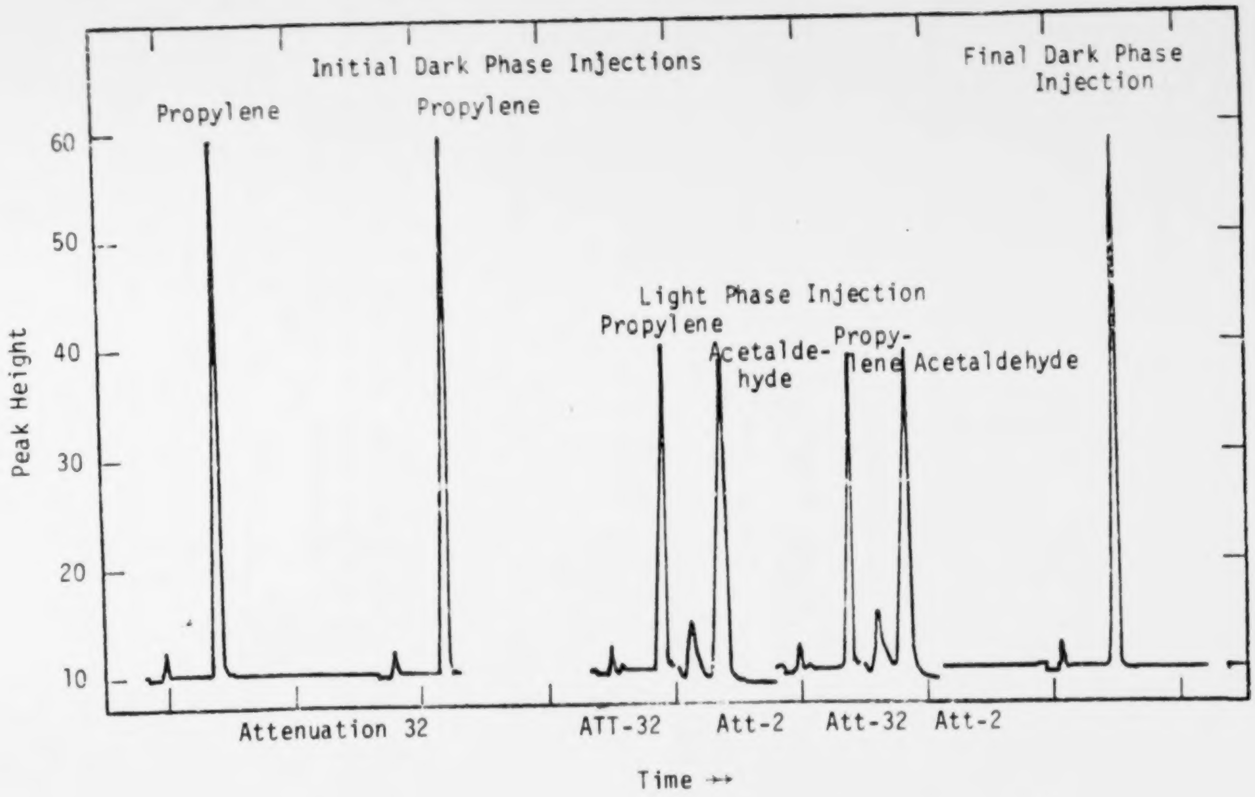

Figure 41. Typical gas chromatograph output

TABLE 13. X-RAY FLUORESCENT SULFUR MEASUREMENT EXPRESSED AS ΔPPM SO_2

Relative Light Level	Hydrocarbon Target Concentrations, PPM (v/v)					Runs
	0	250	500	1000	1500	
0	0.80	0.33	0.11	N.D.	N.D.	69 to 73
1/4	N.D.	0.45	0.10	0.18	0.13	74 to 78
1/2	0.21	1.53	0.09	0.12	0.73	79 to 83
3/4	0.25	1.59	0.22	0.37	0.25	84 to 88
1	0.40	1.48	1.03	0.80	0.97	89 to 93

TABLE 14a. CARBON MATERIAL BALANCES, $[NO_x]_\circ \sim 600$ PPM (v/v)

Relative Light Level	Hydrocarbon Target Concentration, PPM (v/v)					Runs
	0	250	500	1000	1500	
0	N/A	1.00	1.00	1.00	1.00	69 to 73
1/4	N/A	0.83	0.85	0.91	0.91	74 to 78
1/2	N/A	0.73	0.83	0.85	0.85	79 to 83
3/4	N/A	0.68	0.76	0.73	0.78	84 to 88
1	N/A	0.51	0.50	0.58	0.76	89 to 93

TABLE 14b. CARBON MATERIAL BALANCES, $[NO_x]_\circ \sim 1200$ PPM (v/v)

Relative Light Level	Hydrocarbon Target Concentration, PPM (v/v)					Runs
	0	250	500	1000	1500	
0	N/A	N.D.	1.00	0.99	1.00	94 to 98
1/4	N/A	0.85	0.90	0.89	0.93	99 to 103
1/2	N/A	0.80	N.D.	0.86	0.89	104 to 108
3/4	N/A	0.70	0.76	0.76	0.82	109 to 113
1	N/A	0.58	0.56	0.60	0.65	114 to 118

the propylene was identified as acetaldehyde and the very small peak directly proceeding it was presumed to be formaldehyde. Due to the limited ability of the Varian to detect formaldehyde, bag samples were taken for a limited group of runs so that the effluent could be analyzed at the UNC Pittsboro research site. The formaldehyde was converted to carbon monoxide and the treated effluent was analyzed on a Carle II gas chromato graph. The result of the special GC tests are presented in Table 15. The total aldehyde concentration (formaldehyde and acetaldehyde) accounted for 20 to 50% of the missing carbon. The major product was the formaldehyde which was generally present at concentrations of 1 to 3 times the levels of the acetaldehyde. The observed aldehyde concentrations displayed a strong correlation with the extent of NO conversion indicating that these are principal reaction products in propylene degradation and that the subsequent reaction of the aldehydes is incomplete. This is consistent with the observations in previous sections that aldehydes would compete only weakly for hydroxy radicals and would not photolyze rapidly under light limited conditions.

It is possible that the actual aldehyde concentrations are somewhat higher than indicated in Table 15. The observed propylene concentrations were approximately 50% lower than the corresponding values measured during the run using the Varian GC. Part of this difference could be due to decay by further reaction of the gas mixture during transport to the Pittsboro site. Elapsed times of 2 to 4 hours occurred between the time of sample acquisition and analysis due to the 18 mile distance between the labs and the difficulty in coordinating the runs with the transportation. The importance of this delay was evaluated by taking repeated readings on a bag sample which was not transported. The rate of propylene and acetaldehyde decay are apparent in Figure 42. Both compounds exhibit a first order rate of decay of 5% which is represented by the dotted line. If this is characteristic of the other bag samples, the aldehyde concentrations reported in Table 15 could be 10 to 15% higher.

While decay of the samples accounts for some of the difference in observed propylene concentrations there remains some difference between the two sets of GC data. The Varian data is considered more reliable

TABLE 15. CARBON BALANCE CORRECTIONS FOR ALDEHYDES

Run	102	107	112	115	116	117	118
%C Unaccounted for as C_3H_6	10.9	13.6	24.4	42.1	44.4	40.5	35.0
ΔPPM C as C_3H_6	600	540	1035	372	840	1602	1941
Measured $[C_3H_6]_{ss}$ vs. Actual $[C_3H_6]_{ss_1}$, %	54	46	62	100	51	N.D.	N.D.
Measured HCHO, ppmC	250	N.D.	325	195	186	315	348
Measured CH_3CHO, ppmC	58	32	114	60	104	42	212
Total RCHO, ppmC	308	32	439	255	290	357	610
%C Unaccounted for as RCHO	51	6	42	69	35	22	31
%C Unaccounted, Corrected for RCHO	5.4	12.8	14.1	13.2	29	32	24

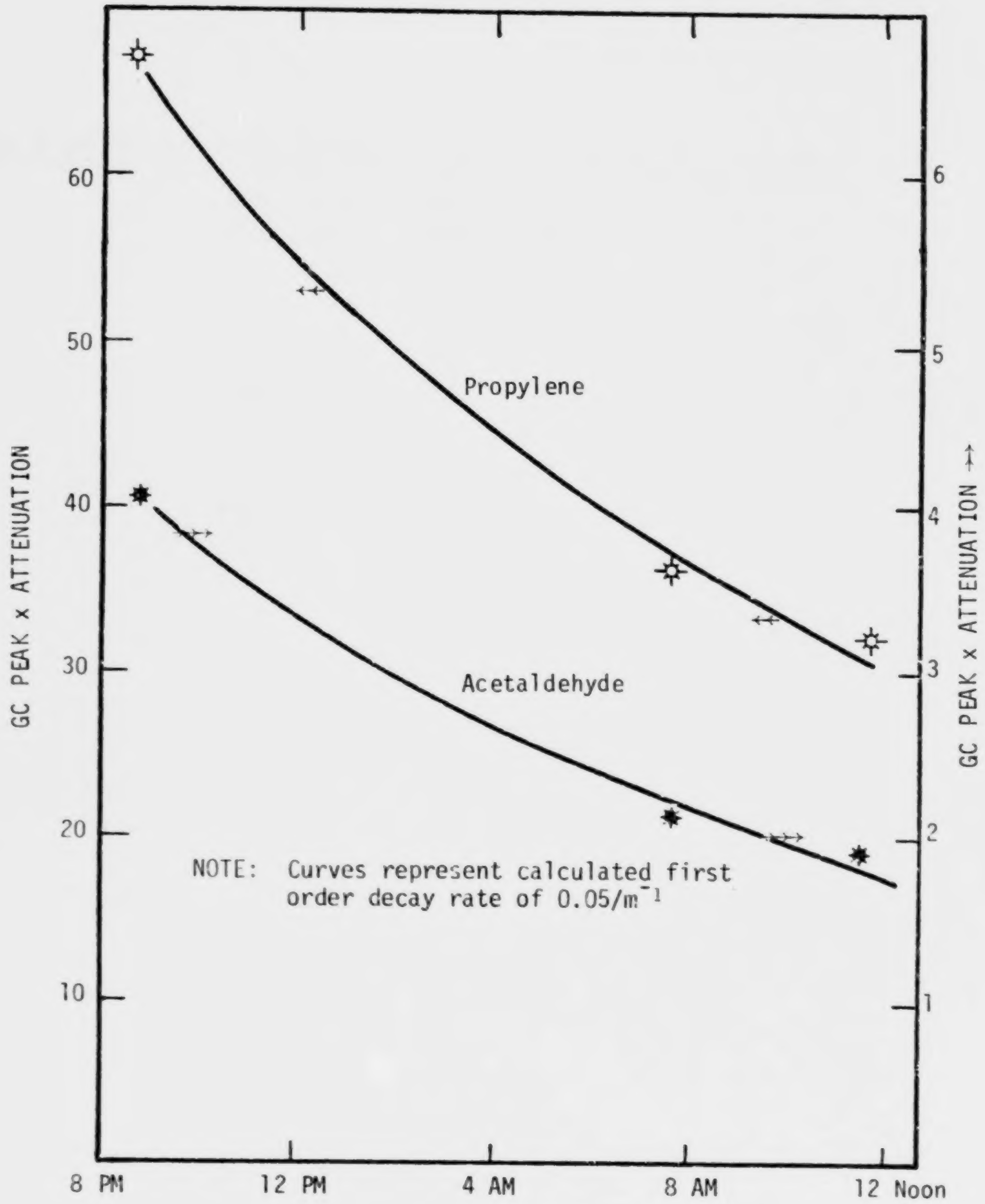

Figure 42. Aldehyde/propylene decay in sampling bags

TABLE 16. RELATIONSHIP BETWEEN ALDEHYDE FORMATION AND NO OXIDATION

Run	HCHO ppm	CH_3CHO ppm	ΔNO ppm
102	250	58	156
107	N.D.	32	219
112	325	114	334
115	195	60	247
116	186	315	339
117	315	42	517
118	398	212	594

since the absolute values agree within 10% of the propylene tank concentration and the observed gas stream flow rates.

Following inclusion of the aldehydes, the carbon material balances approach 80 to 95%. It is conceivable that the remaining fraction is partially composed of polycyclic organic matter and/or other potentially toxic organic compounds. To evaluate this possibility, a selected series of runs were performed with Tenax sampling columns. These were analyzed using a GC mass spectrometer at the Research Triangle Institute. The principal compounds identified in the 10 test samples are reported in Table 1[illegible]. In all of these tests, acetaldehyde and acetic acid were present in small but nevertheless significant quantities. The other compounds were present on an irregular basis and generally in much smaller quantities.

It is very unlikely that some of the observed compounds actually originated in the photochemical system. For example, methylene chloride is used in the extractionstep of the Tenax column treatment. Also, there are not halogenated precursors which could explain the presence of hexafluorobenzene and trichloroethylene. It must be assumed that these compounds and possibly some of the others in the upper group actually entered by way of the dilution air stream (refer to Figure 22) or were contaminants in the GC mass spectrometry laboratory.

The main conclusion drawn from the mass spectrometer results is that a large number of organic compounds are formed; however, the total concentration of such compounds measurable by the GC mass spectrometer is very small.

COST ESTIMATES

Photochemical system capital and annualized cost estimates have been prepared based on the experimental results discussed earlier. The basis of these calculations is the model system presented in Chapter 4. The cost estimates are indicative only of a propylene system as studied in this project. A more reactive hydrocarbon could conceivably allow a more economical system without the problem of unreacted hydrocarbon emissions. Development of improved ultraviolet lamps and reflectors could also have a major impact on the capital and annualized costs. For these reasons, the propylene system costs are considered a maximum cost for a photo-

TABLE 17. MAJOR ORGANIC COMPOUNDS DETERMINED IN GC/MS TESTS, PPM (v/v)

					RUN			
	117	115	118	117[a]	107	107	101	116
acetonitrite								
acetaldehyde	3.1	1.4	4.8	1.2	4.7	4.8		2.4
C_2H_6O isomer	1.1	0.5	2.3	0.7				1.6
propylene oxide		0						
nitromethane	1.3	0.44	2.1					
4-methyl-1,3-dioxolane								
acetic acid	24.8	13.2	1.6	1.6	3.2	2.8	3.6	2.3
acetone		1.1			1.1		1.0	
methyl formate			2.0					
methyl nitrate			1.1					
butyl formate				0.4				
ethylene								
propenal+methylether								
toluene							1.7	
xylene isomer							1.8	
alkyl dioxolane								
acetophenone								
methylene chloride								
hexafluorobenzene								
m-hexane		0.18						
trichloroethylene								

[a] >3000 A filter in place.

chemical system for NO oxidation.

Model Plant Characteristics

The cost estimates have been prepared for a 500-megawatt base loaded coal-fired boiler. It is assumed that no combustion modifications have been made to suppress NO_x formation and that the average inlet concentration is 600 ppm (v/v). Cost estimates were not prepared for the 1200 ppm (v/v) case since the results indicated maximum NO oxidation efficiencies of only 50%.

Irradiation of the effluent gas stream is accomplished in a set of cylindrical reactors (stainless steel) with medium pressure mercury arc lamps mounted on vertical supports along the centerline of the reactor. Baffles are included to improve mixing of the gas stream. The reactors are connected in parallel directly following the electrostatic precipitator so that flyash abrasion of the optical surfaces is minimized. A system of propylene distribution pipes is located in the breeching leading to the reactor. Liquified propylene is stored in spherical tanks (stainless steel). Sufficient supply for 2 months continuous operation is kept on site.

Absorption of the NO_2 formed in the photochemical reactor would be accomplished in conventional flue gas desulfurization system. It is assumed that absorption occurs according to reactions 49 and 50. Unlike nitric acid absorption towers, there does not appear to be any NO regeneration.

$$2NO_{2(g)} + 3SO_{2(l)}^{-2} \xrightarrow{H_2O} 2NO_{2(l)}^{-2} + 2HSO_{3(l)}^{-1} + SO_{4(l)}^{-2} + 2H^{+} \qquad (49)$$

$$4SO_{3(l)}^{-2} + 2NO_{2(l)} \longrightarrow N_{2(g)} + 4SO_{4(l)}^{-2} \qquad (50)$$

Approximately 10 to 50% of the absorbed NO_2 is ultimately corrected to NO_3^- salts (Faucett et al., 1977). Presumably, the remainder is absorbed according to reaction 50. Laboratory scale work done by Chappel (1973) indicates that sulfite scrubbing liquors such as used in some FGD systems provide high efficiency NO_2 removal. Based on this work complete NO_2 absorption will be assumed. No credit will be taken for possible NO absorption which in some cases appears to reach 10 to 20% (Chappel, 1973). Due to the very high solubilities of nitrites and nitrates, it is unlikely that any scaling will occur in the FGD system as a result of the photochemical system. Disposal of the nitrites and nitrates will be done at the same time that the calcium sulfite and calcium sulfate sludges are treated.

The system costs are limited to only those items needed in addition to the conventional FGD system. These include the propylene storage and distribution system, the photochemical reactor and lamps, and the electrical costs.

Model Plant Costs

The dominant cost components are the propylene cost and the electrical power costs. The latter were calculated from the k_1 level using equation 1 developed in Section 5. Based on the spectral effects runs (numbers 1 to 8), it was apparent that the $\Phi_{NO_2 calc}/\Phi_{NO_2}$ factor is in the range of 3 to 5. A value of 3 was used in conjunction with Figure 9, which relates the product quantum yield with the required electrical power. This biases the results high with respect to electrical costs.

Results of the propylene test series (runs 19 to 118) indicate that the desired NO reduction could be achieved at various combinations of propylene and UV light intensities. The possible operating conditions are indicated as isopleths on Figures 28 to 31. For several levels of NO control, the optimum operating point with respect to combined energy and propylene cost was determined by trial and error methods. The optimal operating conditions are the high UV light/low propylene regions of Figures 27 to 30. This is desirable in another sense since unreacted hydrocarbon emissions are also minimized in these regions. For these reasons, operating points shown in Table 18 have been selected for the cost evaluations.

The cost of propylene is based on reports in the Chemical Marketing Reporter (1979). The quoted price has been stable for over a year. An excess supply is forecast for at least the next 2 years (Ponder, 1978); therefore, it is unlikely that substantial price increases will occur. The quantities for the model plant represent 0.00075 of the national production rate.

Electrical costs have been assumed to be 30 mills per kWh. This is equivalent to the purchase of power for some utilities. The relatively high costs have been used to account for use of gas turbines to supplement generating capacity during peak periods.

The installed capital costs of the reactors and the storage tanks have bee based on the costs reported in Peters and Timmerhaus (1968). These have been updated to January 1979 using the CE factors as reported in Chemical Engineering (1979). The lamp and power supply costs are based on Canrad Hanovia lamp HST. These costs have also been updated

The calculated costs have been reported in Tables 18 and 19. Each of these includes four separate columns for various levels of NO oxidation. It is assumed that in most cases it would be desirable to reduce the NO by 500 PPM in order to achieve the stated EPA objectives. The other columns are presented to indicate the sensitivity of cost to NO control level and to facilitate comparisons with cost estimates of other systems most of which are applicable to 300 ppm NO oxidation. The capital cost estimates range from 37 to $50 per KW, depending on the number of UV lamps required. This is approximately 1/2 the cost for a limestone based flue gas desulfurization system (PEDCo., 1975). The annualized costs range from 3.8 to 5.6 mills per kWh. This is higher than originally anticipated due partially to poor propylene reactivity. A comparison of the reported costs for various flue gas treatment processes is presented in Table 20. The photochemical system is obviously much less costly than the various NO oxidation-NO_2 absorption processes. The reason that photochemistry is more attractive than the latter is the high cost of the ozone generating facility ($40/kW and 2.7 mills/kWh). The NH_3 injection technique is considerably more attractive based on the present cost estimates. These two systems, however, are subject to serious operational problems which have been discussed in earlier sections.

Based on the photochemical system cost estimates, it appears that a system based on propylene is only marginally competitive. Commercial utilization of the process would be unlikely unless there were serious operational problems in the selective noncatalytic and selective catalytic reduction techniques. Several improvements in the photochemical system could substantially improve the marketability of the technique. For

TABLE 18. CAPITAL COST ESTIMATES

Cost Component	COST, $			
	ΔPPM NO			
	500	400	300	200
Direct Costs				
Lamp and Power Supplies	5,300,000	4,321,540	3,261,540	1,793,846
Propylene Distribution	1,000,000	1,000,000	1,000,000	1,000,000
Subtotal Direct	6,300,000	5,321,540	4,261,540	2,793,846
Indirect Costs (42% Direct Cost)	2,646,000	2,235,046	1,789,847	1,173,415
Subtotal Direct and Indirect Costs	8,946,000	7,556,586	6,051,387	3,967,261
Contingency and Fees (25% Direct and Indirect Costs)	2,236,500	1,889,146	1,512,846	991,815
Subtotal (lamps and distribution system)	11,182,500	9,445,733	7,564,234	4,959,076
Subtotal (reactors)	12,380,000	12,380,000	12,380,000	12,380,000
Subtotal (propylene stage)	1,343,283	1,343,283	1,343,283	1,343,283
TOTAL	24,905,783	23,169,017	21,287,518	18,682,359
$/kW	50	46	43	37

TABLE 19. ANNUALIZED COSTS

ΔNO, ppm	Δ500[a]	Δ400	Δ300[a]	Δ200[a]
A. Raw Materials		1,800,000		
B. Utilities	5,031,000	4,102,200	3,096,000	1,548,000
C. Operating Labor				
Direct		175,200		
Supervision		26,280		
Subtotal		201,480		
D. Maintenance				
Labor and Materials		1,389,900		
Supplies		208,489		
Subtotal		1,598,389		
E. Overhead				
Plant		900,000		
Payroll		40,300		
Subtotal		940,300		
F. Fixed	5,058,205	4,705,627	4,323,495	3,794,387
TOTAL	14,579,370	13,347,966	11,914,630	9,832,387
MILLS/kWh	5.65	5.15	4.62	3.81

[a] Detailed cost components not shown. These can be calculated as a ratio of Δ400 values.

TABLE 20. COMPARISON OF COSTS FOR FLUE GAS TREATMENT PROCESSES

Technique	Δ ppm NO	Capital Cost $/kW	Annualized Cost Mills/kWh
Photochemical System	500	50	5.65
	400	46	5.15
	300	43	4.62
	200	37	3.81
Selective Non-Catalytic Reduction	200	N.D.	0.75-1.60
Selective Catalytic Reduction	200-300	10-36	0.20-1.80
Radiation Oxidation	200-300	100-1000	N.D.
NO Oxidation/NO_2 Absorption	200-300	84-134	6.7-8.9
NO Absorption, liquid phase condition	125	65-130	4.8-7.4

N.D. - NO Data Available

example, development of more efficient lamps or lamps with effective reflectors could allow installation of the lamps in the electrostatic precipitators, thereby allowing elimination of the very expensive reactors. This would have a secondary benefit since the reaction products would serve to reduce resistivity. Use of a more reactive hydrocarbon would reduce hydrocarbon demand and possible reduce the light energy requirements. A photochemical system based on hexene or acetone could conceivably operate at capital and annualized costs less than 1/2 those presented here for the propylene system.

REFERENCES

1. Acurex Corporation (1977). EPA Stationary Source Combustion Control Technology Program - FY1976. EPA Publication EPA-600/7-77-077, July 1977.

2. Acurex Corporation (1978). Control Techniques for Nitrogen Oxides Emissions from Stationary Sources - Second Edition. EPA Publication EPA-650/2-76-001, January 1978.

3. Armento, W. J. (1975). Effects of Design and Operating Variables on NO_x from Coal-Fired Furnaces - Phase II. EPA Publication EPA-650/2-74-002b, February 1975.

4. Browne, W. R. and Stone, E. E. (1965). Sulfur Dioxide Conversion Under Corona Discharge Catalysis. Final Report, U. S. Public Health Service Contract No. PH 86-67-2, March 1965.

5. Batayko, R. (1979). Personal Communication, March 1979.

6. Calvert, J. G., Su, F., Bottenheim, J. W., and Strauss, O. P. (1977). Mechanism of the Homogeneous Oxidation of Sulfur Dioxide in the Troposphere. Atmospheric Environment, Volume 12, Pages 197-226, February 1977.

7. Canrad Hanovia (1973). Publications B0238 and L0238, November 1973.

8. Chappell, G. A. (1973). Development of Aqueous Processes for Removing NO_x from Flue Gases. EPA Publication EPA-R2-73-051, June 1973.

9. Anonymous (1979). Economic Indicators. Chemical Engineering, Volume 86, No. 2, Page 7, January 15, 1979.

10. Anonymous (1979). Current Prices. Chemical Marketing Reporter, Volume 215, No. 4, Page 45, January 22, 1979.

11. Christian, S. D. and Grundnes, J. (1967). Charge Transfer Complex Between Sulfur Dioxide and Trimethylamine in the Gas Phase and in Heptane. Nature, Volume 214, Pages 1111-1112. 1967.

12. Corbett, W. E. Jones, G. D., Micheletti, W. C., Wells, R. M., and Wilkens, G. F. (1978). Assessment of the Need for NO_x Flue Gas Treatment Technology. EPA Publication EPA-600/7-78-215, November, 1978.

13. Crawford, A. R., Manny, E. H., and Bartok, W. (1977). "Application of Combustion Modifications to Power Generating Combustion Sources" in Proceedings of the Second Stationary Source Combustion Symposium; Volume II, Utility and Large Industrial Boilers. EPA Publication EPA-600/7-77-073b, Pages 3-40, July 1977.

14. Ctvrtnicek, T. E., and Rusek, S. N. (1977). "Cyclone Boilers - Their Emissions and Population" in Proceedings of the Second Stationary Source Combustion Symposium; Volume II, Utility and Large Boilers. EPA Publication EPA_600/7-77-073b, Pages 123-142, July 1977.

15. Demerjian, K. L., Kerr, J. A., and Calvert, J. G. (1975). "The Mechanism of Photochemical Smog Formation" in Advances in Environmental Sciences and Technology, Volume 4, Pages 1-213, 1975.

16. Dols, M. J. and Boknoven, C. (1974). Process for the Photochemical Oxidation of NO to NO_2. U. S. Patent 3,120,479, Issued February 4. 1979.

17. Dykema, O. W. (1978). Combustion Modification Effects on NO_x Emissions from Gas-, Oil-, and Coal-Fired Utility Boilers. EPA Publication EPA-600/2-78-217, December 1978.

18. Faucett, H. L., Maxwell, J. D., and Burnett, T. A. (1977). Technical Assessment of NO_x Removal Processes for Utility Applications. EPA Publication EPA-600/7-77-127, November 1977.

19. Hamm, J. R. (1965). Study of Physiochemical Techniques for Removal of SO_2 from Stack Gases. Final Report, U.S Department of Health, Education and Welfare Contract, November 1978.

20. Harrison, L. J. (1976). Technology and Economics of Flue Gas NO_x Oxidation by Ozone. Final Report, EPA Contract 68-02-1325, November 1976.

21. Heap, M. P., Tyson, T. J., Carver, G. P., Martin, G. B., and Lowes, T. M. (1976). "The Optimization of Burner Design Parameters to Control NO_x Formation in Pulverized Coal and Heavy Oil Flames" in Proceedings of the Stationary Source Combustion Symposium EPA Publication EPA-600/2-76-152b, June 1976.

22. Howe , J. P., and Noyes, W. A. Jr. (1936). Photochemical Studies XXIII, The Photochemical Decomposition of Acetone Vapor Near 1900 A. A Comparison with the Decomposition at Longer Wave Lengths. Journal of The American Chemical Society, Volume 58, Pages 1404-1412, 1936.

23. Jeffries , H.E. Photochemical Kinetic Simulation System, Version 2a. Unpublished Report. June 1977.

24. Kemp, V. E., and Dykema, O. W. (1977). "Inventory of Atmospheric Emissions from Stationary Point Sources" in Proceedings of the Second Stationary Source Combustion Symposium, Volume II, Utility and Large Boilers. EPA Publication EPA-600/7-77-073b, Pages 257- 278, July 1977.

25. Lachapelle, D. (1979). Personal Communication, May 1979.

26. Levenspeil, O. (1972). Chemical Reaction Engineering. John Wiley and Sons Publishing Co, New York, 1972.

27. Machi, S., Kawamura, K., Dawaakami, W., Aoki, S., Hashimoto,S., Yotamoto, K., and Sunaga, H. (1975). Process for the Photochemical Oxidation of NO to NO_2. U. S. Patent 3,869,362, Issued February 4, 1975.

28. Mason, H., Shimiza, A., Ferrell, J., Poe, G., Waterland, L., and Evans, R. (1977). Preliminary Environmental Assessment of Combustion Modification Techniques; Volume II, Technical Results. EPA Publication EPA-600/7-77-119b, October 1977.

29. McCutchen, G. P. (1977). NO_x Emission Trends and Federal Regulation. Chemical Engineering Progress, Page 38, August 1977.

30. Muzio, L. J., and Arand J. K. (1976). Homogeneous Gas Phase Decomposition of Oxides of Nitrogen. Electric Power Research Institute Publication FP-253, August 1976.

31. National Academy of Sciences, Subcommittee on Nitrogen Oxides (1977). Ozone and Other Photochemical Oxidants. EPA Publication EPA-600/ 1-77-013, February 1977.

32. PEDCo Environmental (1975). Flue Gas Desulfurization Process Cost Assessment. Final Report, Environmental Protection Agency Contract No. 68-01-3150, May 1975.

33. Peters M. S., and Timmerhaus, K. D. (1968). Plant Design and Economics for Chemical Engineers, Second Edition. McGraw Hill Book Company, 1968.

34. Ponder T. (1978). U. S. Propylene: Demand vs. Supply. Hydrocarbon Processing, Volume 57, Number 7, Pages 186-188, July 1978.

35. Ricci, L. J. (1977). Nixing NO_x Emissions. Chemical Engineering, Volume 84, Number 4, Pages 84-89, April 11, 1977.

36. Richards, J., Fox, D., and Reist, P. (1976). The Influence of Molecular Complexes on the Photooxidation of Sulfur Dioxide. Atmospheric Environment, Volume 10, Pages 211-217, 1976.

37. Salvesen, K. G., Wolfe K. J., Chu, E., and Herther, M. A. (1978). Emission Characterization of Stationary NO_x Sources; Volume I, Results. EPA Publication EPA-650/7-78-120a, June 1978.

38. Selker, A P. (1975). Program for Reduction of NO_x from Tangential Coal-Fired Boilers, Phase II. EPA Publication EPA-650/2-73-005a, June 1975.

39. Sickles, J. E. II, and Jeffries , H. E. (1975). Development and Operation of a Device for the Continuous Measurement of k_a for Nitrogen Dioxide. University of North Carolina at Chapel Hill, Department of Environmental Sciences and Engineering Publication ESE-396, June, 1976.

40. Thompson, R. E.,and McElroy, M. W. (1976). Effectiveness of Gas Recirculation and Staged Combustion in Reducing NO_x on a 560 MW Coal-Fired Boiler. Electric Power Research Institute Publication FP-257, September 1976.

41. Wolf, D., and Resnick, W. (1963). Residence Time Distribution in Real Systems. Chemcial Engineering Progress, Volume 2, Pages 283-293, 1963.

42. Yeager, K E., and Teixeira, D. P. (1977). "The EPRI Program on NO_x Control Using Combustion Modification Techniques" in Proceedings of the Second Stationary Source Combustion Symposium; Volume II, Utility and Large Boilers. EPA Publication EPA-600/7-77-073b, July 1977.

APPENDIX A

Reactor Flow Characterization

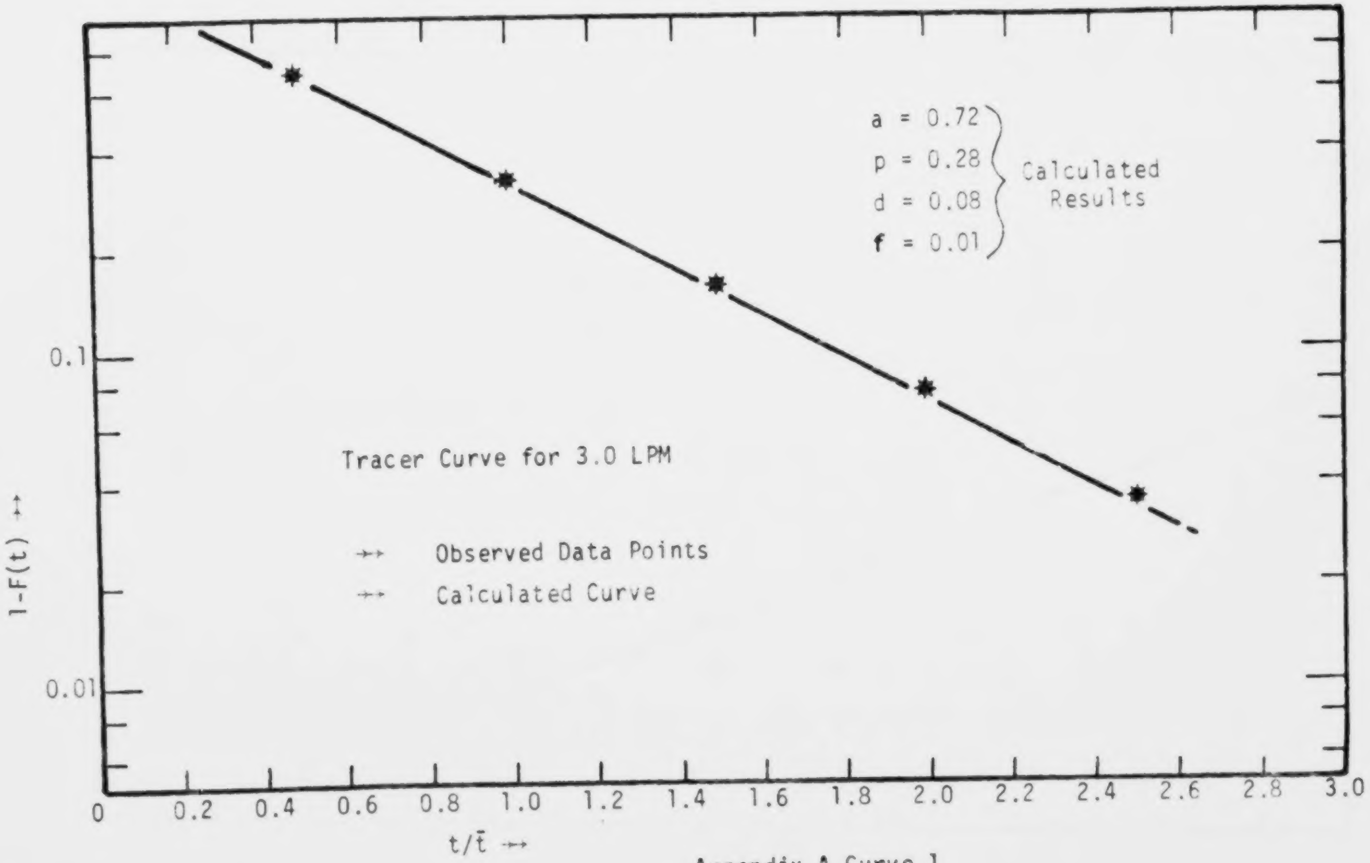

Appendix A Curve 1

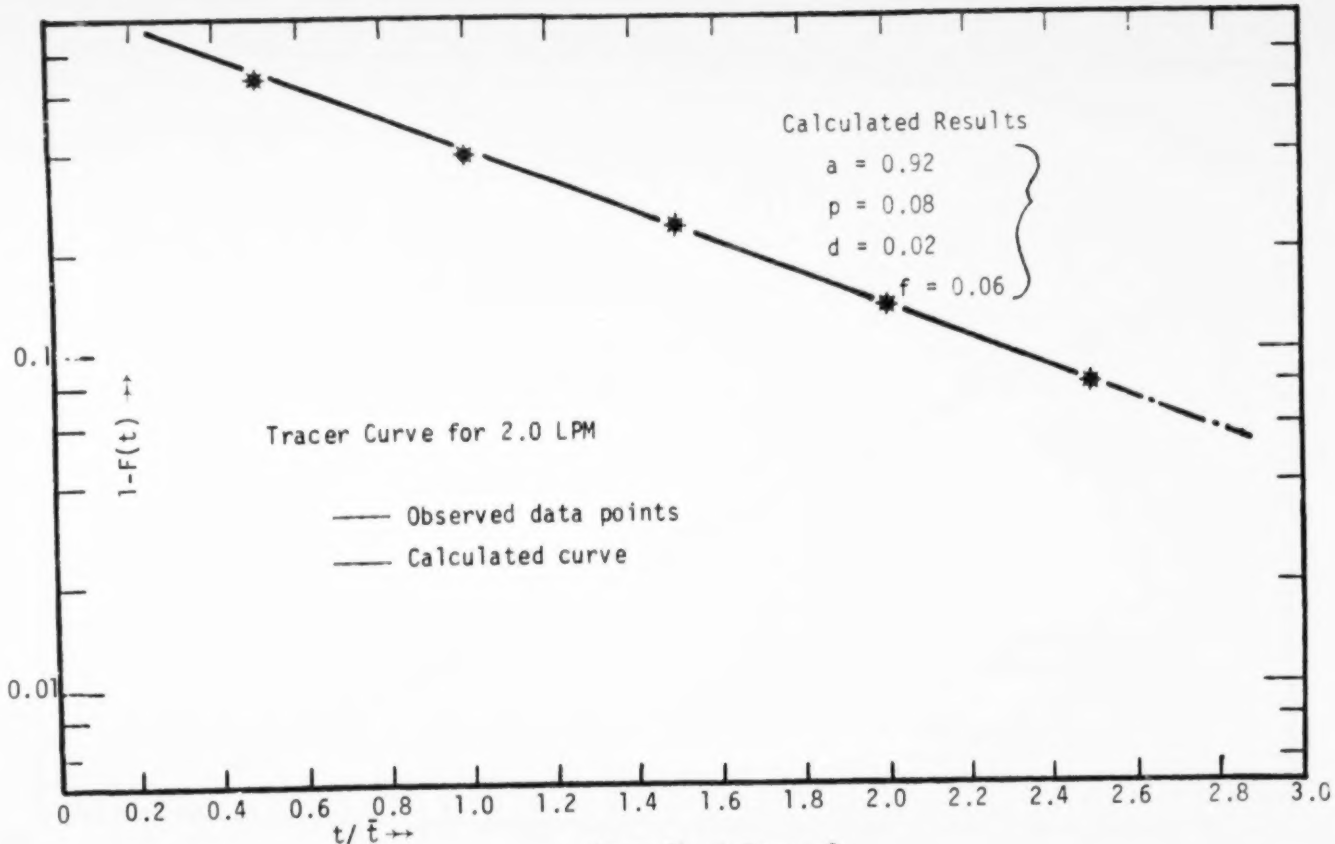

Appendix A Curve 2

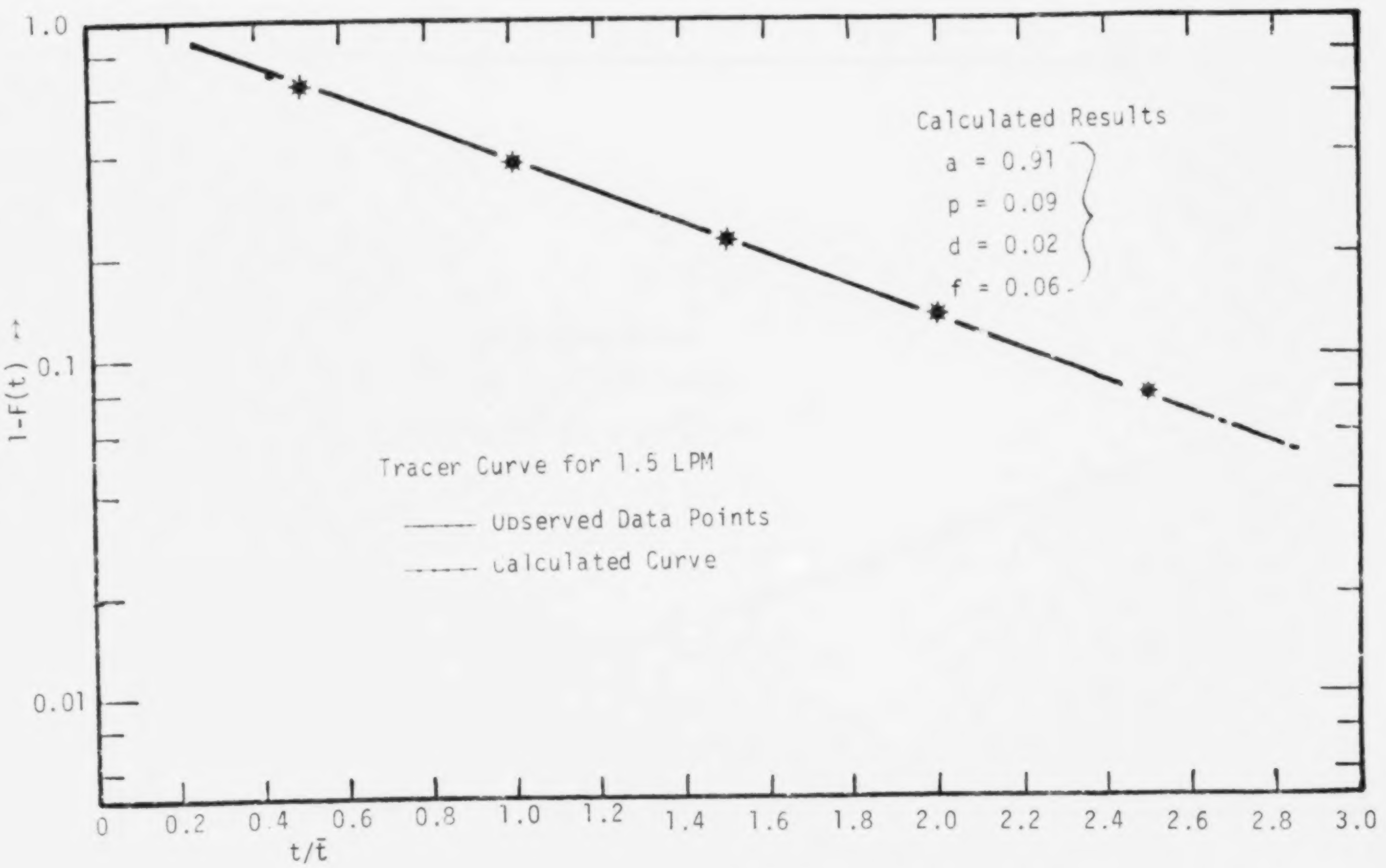

Appendix A Curve 3

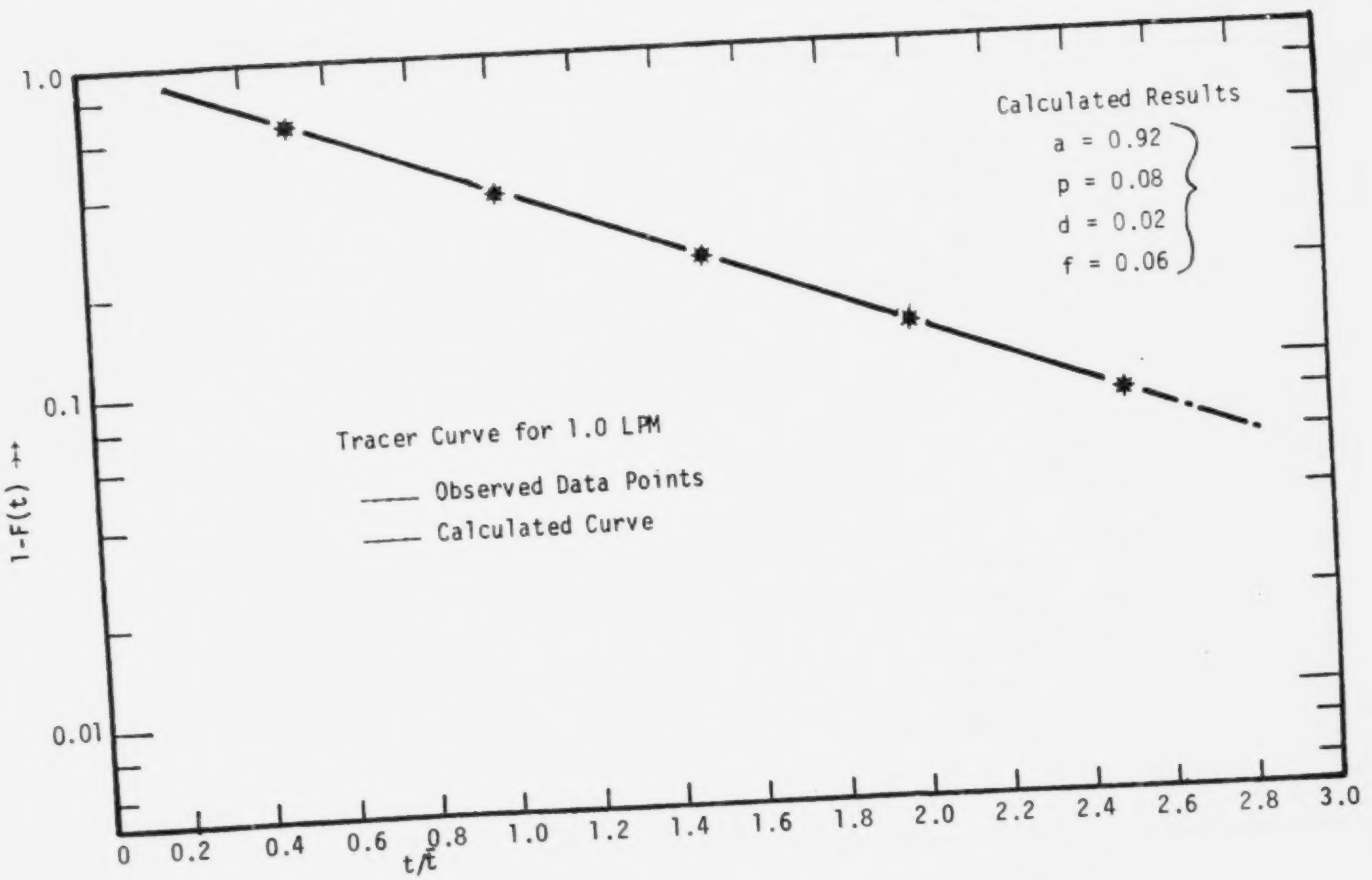

Appendix A Curve 4

APPENDIX B

Experimental Results

TABLE B-1. EXPERIMENTAL DATA, INFLUENCE OF MIDDLE UV FILTER ON NO OXIDATION.

Run Number	1	2	3	4
Chronological No.	81	84	79	77
Conditions				
$[NO]_{\circ}$, ppm	596	665	626	637
$[C_3H_6]_{\circ}$, ppm	N.D.	1441	1355	1390
$[SO_2]_{\circ}$, ppm	1500	1478	1339	1485
$[O_2]$, %	4.5	4.7	4.5	4.0
k_1, min^{-1}	0.124	0.248	0.34	1.20
τ, min	0.783	0.758	0.760	0.755
Temp., °F	251	274	272	277
Filter	>1800, Å	>1800 Å	>3000 Å	>1800 Å
Gas Analyses				
ΔNO, ppm	223	367	108	599
NO Oxid., %	37.5	55.2	17.3	95.6
$[NO_2]$, ppm	202	283	92	535
$[NO_x]/[NO_x]_{\circ}$	0.929	0.929	0.957	0.88
ΔC_3H_6, ppm	N.D.	168	194	256
$\Delta NO/\Delta C_3H_6$	N.D.	2.18	0.56	2.34
ΔSO_2, ppm	64	37	27	86
SO_2 Oxid., %	4.3	2.5	2.0	5.8
Filter Analysis				
XRF, ppm SO_2	0.01	0.01	0.01	0.07

TABLE B-1 (continued)

Run Number Chronological No.	5 82	6 83	7 80	8 78
Conditions				
$[NO]_{\circ}$, ppm	608	655	610	616
$[C_3H_6]_{\circ}$, ppm	N.D.	1302	1415	1360
$[SO_2]$, ppm	1457	1460	1393	1312
$[O_2]$, %	4.5	4.7	4.4	3.8
k_1, min^{-1}	0.08	0.158	0.68	0.60
τ, min	0.764	0.760	0.758	0.737
Temp., °F	269	272	274	295
Filter	>3000 Å	>3000 Å	>1800 Å	>3000 Å
Gas Analyses				
ΔNO, ppm	16	36	567	448
NO Oxid., %	2.6	5.5	93.0	72.7
$[NO_2]$, ppm	31	41	481	394
$[NO_x]/[NO_{x\circ}]$	1.00	0.982	0.832	0.895
ΔC_3H_6, ppm	N.D.	77	281	161
$\Delta NO/\Delta C_3H_6$	N.D.	0.47	2.02	2.78
ΔSO_2, ppm	16	26	108	59
SO_2 Oxid., %	1.1	1.8	7.8	4.5
Filter Analyses				
XRF, ppm SO_2	N.D.	N.D.	0.04	0.03

TABLE B-2. EXPERIMENTAL DATA, INFLUENCE OF SULFUR DIOXIDE ON NO OXIDATION.

Run Number Chronological No.	9 49	10 50	11 51	12 52
Conditions				
$[NO_x]_\circ$, ppm	1068	558	550	577
$[C_3H_6]_\circ$, ppm	837	990	819	790
$[SO_2]_\circ$, ppm	510	540	1066	0
$[O_2]$, %	4.3	4.4	4.3	4.2
k_1, min^{-1}	4.1	4.52	4.52	4.52
, min	0.768	0.758	0.753	0.753
Temp., °F	266	274	279	279
Gas Analyses				
NO, ppm	902	541	526	555
NO Oxid., %	88.8	99.2	98.8	98.4
$[NO_2]$, ppm	807	462	464	493
$[NO_x]_\circ/[NO_x]_\circ$	0.861	0.836	0.855	0.869
C_3H_6, ppm	300	376	N.D.	N.D.
NO/ C_3H_6	3.0	1.44	N.D.	N.D.
SO_2, ppm	48	92	44	0
SO_2 Oxid., %	9.4	16.9	4.2	0
Filter Analyses				
XRF, ppm SO_2	0.08	0.08	0.07	N.D.

(continued)

TABLE B-2 (continued)

Run Number Chronological No.	13 53	14 54	15 55	16 56
Conditions				
$[NO_x]_o$, ppm	1203	1248	506	528
$[C_3H_6]_o$, ppm	790	818	877	819
$[SO_2]_o$, ppm	1119	3241	1332	3197
$[O_2]$, %	4.5	4.0	4.3	4.3
k_1, min^{-1}	4.52	4.51	4.52	4.63
τ, min	0.753	0.750	0.767	0.767
Temp., °F	279	282	266	266
Gas Analyses				
ΔNO, ppm	928	857	479	497
NO Oxid., %	77.4	69.2	98.2	97.4
$[NO_2]$, ppm	804	675	426	448
$[NO_x]/[NO_x]_o$	0.893	0.847	0.860	0.874
ΔC_3H_6, ppm	359	321	189	N.D.
$\Delta NO/\Delta C_3H_6$	2.58	2.67	2.54	N.D.
ΔSO_2, ppm	62	133	67	133
SO_2 Oxid., %	5.6	4.1	5.0	4.2
Filter Analyses				
XRF, ppm SO_2	0.15	0.04	0.08	N.D.

(continued)

TABLE B-2 (continued)

Run Number	17	18
Chronological No.	57	58
Conditions		
$[NO_x]_o$, ppm	1199	1106
$[C_3H_6]_o$, ppm	643	702
$[SO_2]_o$, ppm	1368	0
$[O_2]$, %	4.7	4.2
k_1, min^{-1}	4.52	4.52
, min	0.758	0.764
Temp., °F	274	269
Gas Analyses		
NO, ppm	972	941
NO Oxid., %	87.6	86.9
$[NO_2]$, ppm	861	826
$[NO_x]_o/[NO_x]_o$	0.889	0.276
C_3H_6, ppm	N.D.	219
NO/ C_3H_6	N.D.	4.30
SO_2, ppm	71	0
SO_2 Oxid., %	5.2	0
Filter Analyses		
XRF, ppm SO_2	N.D.	0.02

TABLE B-3. EXPERIMENTAL DATA, INFLUENCE OF PROPYLENE CONCENTRATION AND UV LIGHT INTENSITY ON ON OXIDATION.

Run Number Chronological No.	19 39	20 47	21 28	22 18
Conditions				
$[NO_x]_o$ ppm	592	569	548	N.D.
$[C_3H_6]_o$ ppm	0	331	475	N.D.
$[SO_2]_o$	1492	1374	1772	N.D.
$[O_2]$ %	4.3	4.5	4.6	N.D.
k_1, min^{-1}	0	0	0	N.D.
τ, min	0.794	0.786	0.788	N.D.
Temp., °F	241	248	246	N.D.
Gas Analyses				
ΔNO, ppm	0	0	0	N.D.
NO Oxid., %	0	0	0	N.D.
$[NO_2]$, ppm	14	9	14	N.D.
$[NO_x]/[NO_x]_o$	1.00	1.00	1.02	N.D.
ΔC_3H_6, ppm	0	16	N.D.	N.D.
$\Delta NO/\Delta C_3H_6$	-	0	N.D.	N.D.
ΔSO_2, ppm	N.D.	N.D.	0	N.D.
SO_2 Oxid., %	N.D.	N.D.	0	N.D.
Filter Analyses				
XRF, ppm SO_2	0.01	N.D.	N.D.	N.D.

TABLE B-3 (Continued)

Run Number Chronological No.	23 34	24 40	25 7	26 23
Conditions				
$[NO_x]_\circ$ ppm	557	597	542	512
$[C_3H_6]_\circ$ ppm	1856	0	246	394
$[SO_2]_\circ$	1446	1492	1487	1386
$[O_2]$ %	4.5	4.6	4.2	4.3
k_1, min^{-1}	0	0.10	0.10	0.38
τ, min	0.813	0.781	0.750	0.758
Temp., °F	225	253	282	274
Gas Analyses				
ΔNO, ppm	0	23	155	155
NO Oxid., %	0	3.8	0.289	31.4
$[NO_2]$, ppm	14	27	115	155
$[NO_x]/[NO_x]_\circ$	1.00	0.992	0.918	0.967
ΔC_3H_6, ppm	N.D.	0	0	N.D.
$\Delta NO/\Delta C_3H_6$	N.D.	-	-	N.D.
ΔSO_2, ppm	N.D.	9	44	0
SO_2 Oxid., %	N.D.	0.6	3.0	0
Filter Analyses				
XRF, ppm SO_2	0.04	0.02	N.D.	0.01

(continued)

TABLE B-3 (Continued)

Run Number Chronological No.	27 17	28 6	29 25	30 27
Conditions				
$[NO_x]_o$, ppm	497	529	529	566
$[C_3H_6]_o$, ppm	905	1788	0	247
$[SO_2]_o$, ppm	1439	1615	1431	1558
$[O_2]$, %	4.5	4.8	4.3	4.2
k_1, min^{-1}	0.38	0.38	0.96	0.96
τ, min	0.794	0.764	0.758	0.767
Temp., °F	241	269	274	266
Gas Analyses				
ΔNO, min	244	356	37	183
NO Oxid., %	50.5	67.2	7.0	33.1
$[NO_2]$, ppm	222	300	32	159
$[NO_x]/[NO_x]_o$	0.929	0.942	0.982	0.933
ΔC_3H_6, ppm	0	80	0	N.D.
$\Delta NO/\Delta C_3H_6$	-	4.45	-	N.D.
ΔSO_2, ppm	44	94	37	5
SO_2, %	3.0	5.8	2.6	0.3
Filter Analyses				
XRF, ppm SO_2	0.02	0.02	N.D.	0.03

(continued)

TABLE B-3 (Continued)

Run Number Chronological No.	31 7	32 36	33 44	34 45
Conditions				
$[NO_x]_o$, ppm	566	561	565	565
$[C_3H_6]_o$, ppm	519	979	1850	0
$[SO_2]_o$, ppm	1700	1333	1275	1425
$[O_2]$, %	4.0	4.3	4.3	4.2
k_1, min^{-1}	0.72	0.33	0.47	0.41
τ, min	0.764	0.767	0.774	0.764
Temp., °F	269	266	259	269
Gas Analyses				
ΔNO, min	269	363	454	39
NO Oxid., %	47.5	66.4	81.5	6.9
$[NO_2]$, ppm	222	331	398	34
$[NO_x]/[NO_x]_o$	0.958	0.918	0.886	0.977
ΔC_3H_6, ppm	74	280	162	0
$\Delta NO/\Delta C_3H_6$	3.61	1.30	2.81	-
ΔSO_2, ppm	71	68	34	47
SO_2, %	4.2	5.1	2.7	3.3
Filter Analyses				
XRF, ppm SO_2	0.02	0.03	N.D.	N.D.

(continued)

TABLE B-3 (Continued)

Run Number Chronological No.	35 41	36 33	37 46	38 15
Conditions				
$[NO_x]_\circ$, ppm	555	524	586	606
$[C_3H_6]_\circ$, ppm	331	475	475	2108
$[SO_2]_\circ$, ppm	1381	1550	1395	1761
$[O_2]$, %	4.5	4.6	4.5	5.3
k_1, min^{-1}	1.37	1.83	1.11	1.37
τ, min	0.768	0.758	0.760	0.783
Temp., °F	264	274	272	251
Gas Analyses				
ΔNO, ppm	262	317	471	585
NO Oxid., %	48.0	61.6	81.5	98.4
$[NO_2]$, ppm	226	262	411	528
$[NO_x]/[NO_x]_\circ$	0.920	0.877	0.883	0.889
ΔC_3H_6, ppm	126	N.D.	153	0
$\Delta NO/\Delta C_3H_6$	2.08	N.D.	3.07	-
ΔSO_2, ppm	4	46	51	71
SO_2 Oxid., %	0.3	3.0	3.7	4.1
Filter Analyses				
XRF, ppm SO_2	0.05	0.03	N.D.	0.16

(continued)

TABLE B-3 (Continued)

Run Number Chronological No.	39 31	40 38	41 35	42 22
Conditions				
$[NO_x]_o$, ppm	538	505	524	502
$[C_3H_6]_o$, ppm	475	344	475	979
$[SO_2]_o$, ppm	1498	1465	1460	1442
$[O_2]$, %	4.9	4.6	4.5	4.2
k_I, min^{-1}	3.68	3.21	2.40	3.21
τ, min	0.750	0.745	0.764	0.774
Temp., °F	282	287	269	259
Gas Analyses				
ΔNO, ppm	61	342	389	481
NO Oxid., %	11.5	57.9	75.4	98.3
$[NO_2]$, ppm	61	275	344	418
$[NO_x]/[NO_x]_o$	0.983	0.880	0.897	0.850
ΔC_3H_6, ppm	N.D.	200	283	N.D.
$\Delta NO/\Delta C_3H_6$	N.D.	1.70	1.38	N.D.
ΔSO_2, ppm	37	71	18	64
SO_2 Oxid., %	2.5	4.8	1.2	4.3
Filter Analyses				
XRF, ppm SO_2	0.44	0.07	0.02	N.D.

(continued)

TABLE B-3 (Continued)

Run Number Chronological No.	43 12	44 32	45 30	46[a]
Conditions				
$[NO_x]_\circ$, ppm	534	1150	955	
$[C_3H_6]_\circ$, ppm	1738	0	265	
$[SO_2]_\circ$, ppm	1685	1481	1488	
$[O_2]$, %	4.0	4.5	4.6	
k_1, min^{-1}	3.21	0	0	
τ, min	0.772	0.788	0.797	
Gas Analyses				
ΔNO, ppm	505	0	0	
NO Oxid., %	0.973	0	0	
$[NO_2]$, ppm	440	9	14	
$[NO_x]/[NO_x]_\circ$	0.851	1.00	N.D.	
ΔC_3H_6, ppm	217	N.D.	N.D.	
$\Delta NO/\Delta C_3H_6$	2.33	N.D.	N.D.	
ΔSO_2, ppm	47	0	N.D.	
SO_2 Oxid., %	2.8	0	N.D.	
Filter Analyses				
XRF, ppm SO_2	0.11	0.04	N.D.	

[a] Data missing

(continued)

TABLE B-3 (Continued)

Run Number	47	48	49	50
Chronological No.	42	48	3	13
Conditions				
$[NO_x]_\circ$, ppm	1055	1327	1217	1030
$[C_3H_6]_\circ$, ppm	1072	2066	0	243
$[SO_2]_\circ$, ppm	1386	1340	1615	1615
$[O_2]$, %	4.3	4.7	4.3	4.8
$k_1 min^{-1}$	0	0	0.32	0.18
τ, min	0.810	0.792	0.758	0.768
Temp., °F			274	264
Gas Analyses				
ΔNO, ppm	9	9	0	103
NO Oxid., %	0.8	0.6	0	10.1
$[NO_2]$, ppm	17	21	23	103
$[NO_x]/[NO_x]_\circ$	1.00	1.00	1.00	0.990
ΔC_3H_6, ppm	0	N.D.	0	0
$\Delta NO/\Delta C_3H_6$	0	N.D.	0	-
ΔSO_2, ppm	N.D.	N.D.	19	23
SO_2 Oxid., %	N.D.	N.D.	1.2	1.4
Filter Analyses				
XRF, ppm SO_2	N.D.	N.D.	0.01	0.01

(continued)

TABLE B-3 (Continued)

Run Number Chronological No.	51 14	52 21	53 16	54 5
Conditions				
$[NO_x]_o$, ppm	1095	1018	1028	1123
$[C_3H_6]_o$, ppm	562	937	1917	1886
$[SO_2]_o$, ppm	1714	1576	1547	1451
$[O_2]$, %	4.8	4.5	4.3	4.8
k_1, min^{-1}	0.18	0.25	0.38	0.72
τ, min.	0.794	0.783	0.768	0.764
Temp., °F	241	251	264	269
Gas Analyses				
ΔNO, ppm	138	158	271	460
NO Oxid., %	12.8	16.6	26.8	41.0
$[NO_2]$, ppm	133	200	262	398
$[NO_x]/[NO_x]_o$	0.983	0.975	0.977	0.917
ΔC_3H_6, ppm	0	0	0	98
$\Delta NO/\Delta C_3H_6$	-	-	-	4.69
ΔSO_2, ppm	0	64	24	70
SO_2 Oxid., %	0	4.1	1.5	4.8
Filter Analyses				
XRF, ppm SO_2	0.01	0.02	0.02	0.05

(continued)

TABLE B-3 (Continued)

Run Number Chronological No.	55 20	56 29	57 9	58
Conditions				
$[NO_x]_\circ$, ppm	980	1025	1040	
$[C_3H_6]_\circ$, ppm	265	475	1016	
$[SO_2]_\circ$, ppm	1555	1460	1627	
$[O_2]$, %	4.5	4.6	4.6	
k_1, min^{-1}	0.72	0.96	1.14	
τ, min	0.768	0.781	0.760	
Temp., °F	264	253	272	
Gas Analyses				
ΔNO, min	145	187	312	
NO Oxid., %	15.4	18.5	30	
$[NO_2]$, ppm	153	178	249	
$[NO_x]/[NO_x]_\circ$	0.970	0.977	0.972	
ΔC_3H_6, ppm	0	N.D.	157	
$\Delta NO/\Delta C_3H_6$		N.D.	1.99	
ΔSO_2, ppm	21	42	45	
SO_2, %	1.4	2.9	2.8	
Filter Analyses				
XRF, ppm SO_2	0.03	0.02	0.03	

(continued)

TABLE B-3 (Continued)

Run Number Chronological No.	59 24	60[a]	61 19	62 2
Conditions				
$[NO_x]_\circ$, ppm	949		963	1035
$[C_3H_6]_\circ$, ppm	0		380	740
$[SO_2]_\circ$, ppm	1344		1541	1541
$[O_2]$, %	4.5		4.2	4.3
k_1, min^{-1}	1.83		1.37	1.85
τ, min	0.755		0.764	0.745
Temp., °F	277		269	287
Gas Analyses				
ΔNO, ppm	29		201	391
NO Oxid., %	3.3		21.7	37.8
$[NO_2]$, ppm	67		214	345
$[NO_x]/[NO_x]_\circ$	0.991		0.978	0.933
ΔC_3H_6, ppm	0		0	73
$\Delta NO/\Delta C_3H_6$	-		-	5.36
ΔSO_2, ppm	34		43	69
SO_2 Oxid., %	2.5		2.8	4.5
Filter Analyses				
XRF, ppm SO_2	0.02		0.05	0.06

[a] Data missing

(continued)

TABLE B-3 (Continued)

Run Number Chronological No.	63 1	64 26	65 43	66 4
Conditions				
$[NO_x]_\circ$, ppm	1150	1063	976	1147
$[C_3H_6]_\circ$, ppm	1587	0	255	543
$[SO_2]_\circ$, ppm	1472	1509	1361	1755
$[O_2]$, %	4.6	4.5	4.3	4.7
k_1, min^{-1}	2.34	3.21	3.21	3.21
τ, min	0.767	0.747	0.760	0.750
Temp., °F	272	285	272	282
Gas Analyses				
ΔNO, ppm	552	41	295	445
NO Oxid., %	48.0	4.0	30.8	38.8
$[NO_2]$, ppm	460	60	218	328
$[NO_x]/[NO_x]_\circ$	0.920	0.996	0.904	0.878
ΔC_3H_6, ppm	253	0	142	136
$\Delta NO/\Delta C_3H_6$	2.18	-	2.08	3.28
ΔSO_2, ppm	46	28	86	140
SO_2 Oxid., %	3.1	1.8	6.3	8.0
Filter Analyses				
XRF, ppm SO_2	0.33	0.08	4.13	0.33

(continued)

TABLE B-3 (Continued)

Run Number Chronological No.	67 37	68 10	69 121	70 157
Conditions				
$[NO_x]_\circ$, ppm	1175	977	658	460
$[C_3H_6]_\circ$, ppm	979	1856	0	480
$[SO_2]_\circ$, ppm	1424	1554	1984	1770
$[O_2]$, %	4.3	4.5	4.64	4.17
k_1, min^{-1}	2.80	5.00	0	0
τ, min	0.750	0.740	0.772	0.774
Temp., °F	282	292	261	259
Gas Analyses				
ΔNO, ppm	601	932	0	0
NO Oxid., %	53.2	96.7	0	0
$[NO_2]$, ppm	511	755	16	5
$[NO_x]/[NO_x]_\circ$	0.885	0.805	1.00	N.D.
ΔC_3H_6, ppm	519	257	0	0
$\Delta NO/\Delta C_3H_6$	1.16	3.62	N.A.	N.A.
ΔSO_2, ppm	86	111	0	N.D.
SO_2 Oxid., %	6.0	7.1	0	N.D.
Filter Analyses				
XRF, ppm SO_2	0.06	0.40	0.08	N.D.

(continued)

TABLE B-3 (Continued)

Run Number Chronological No.	71 156	72 144	73 128	74 120
Conditions				
$[NO]_\circ$, ppm	443	612	625	614
$[C_3H_6]_\circ$, ppm	540	1415	1970	0
$[SO_2]_\circ$, ppm	1701	1835	1792	1934
$[O_2]$, %	4.64	4.64	4.64	4.56
k_1, min^{-1}	0	0	0	0.27
τ, min	0.774	0.774	0.774	0.752
Temp., °F	259	259	259	280
Gas Analyses				
ΔNO, ppm	0	0	0	11
NO Oxid., %	0	0	0	1.78
$[NO_2]$, ppm	5	11	11	27.4
$[NO_x]/[NO_x]_\circ$	N.D.	0.994	1.00	1.00
ΔC_3H_6, ppm	0	0	0	0
$\Delta NO/\Delta C_3H_6$	-	-	-	N.A.
ΔSO_2, ppm	N.D.	10	0	0
SO_2 Oxid., %	N.D.	0.5	0	0
Filter Analyses				
XRF, ppm SO_2	N.D.	0.18	0.11	N.D.

(continued)

TABLE B-3 (Continued)

Run Number	75	76	77	78
Chronological No.	114	132	155	140
Conditions				
$[NO_x]_\circ$, ppm	652	626	537	589
$[C_3H_6]_\circ$, ppm	240	630	2080	1940
$[SO_2]_\circ$, ppm	1908	1836	1743	1808
$[O_2]$, %	4.64	4.64	4.64	4.47
k_1, min^{-1}	0.23	0.24	0.25	0.26
τ, min	0.753	0.770	0.760	0.769
Temp., °F	279	263	272	264
Gas Analyses				
ΔNO, min	49	205	186	286
NO Oxid., %	7.6	32.8	34.7	48.6
$[NO_2]$, ppm	104	173	153	265
$[NO_x]/[NO_x]_\circ$	0.991	0.981	0.920	1.00
ΔC_3H_6, ppm	40	97	193	180
$\Delta NO/\Delta C_3H_6$	1.23	-	0.69	-
ΔSO_2, ppm	16	32	16	0
SO_2, %	0.8	1.8	0.9	0
Filter Analyses				
XRF, ppm SO_2	0.16	0.23	0.54	0.59

(continued)

TABLE B-3 (Continued)

Run Number	79	80	81	82
Chronological No.	133	108	124	139
Conditions				
$[NO]_o$, ppm	570	626	652	583
$[C_3H_6]_o$, ppm	0	303	620	1300
$[SO_2]_o$, ppm	1907	2035	1912	1825
$[O_2]$, %	4.48	4.70	4.64	4.47
k_1, min^{-1}	0.49	0.48	0.47	0.47
τ, min	0.777	0.76	0.764	0.760
Temp., °F	256	269	269	272
Gas Analyses				
ΔNO, ppm	44	192	252	367
NO Oxid., %	7.7	30.9	38.6	63.0
$[NO_2]$, ppm	44	184	225	324
$([NO] + [NO_2]/[NO]_o)$	0.983	0.980	0.991	0.973
ΔC_3H_6, ppm	0	81	106	196
$\Delta NO/\Delta C_3H_6$	N.A.	2.39	1.80	2.04
ΔSO_2, ppm	33	38	16	9
SO_2 Oxid., %	1.7	1.8	0.9	2.7
Filter Analyses			(Both sides)	
XRF, ppm SO_2	0.27	1.08	0.15/0.19	N.D.

(continued)

TABLE B-3 (Continued)

Run Number Chronological No.	83 113	84 135	85 145	86 116
Conditions				
$[NO_x]_o$, ppm	619	616	617	641
$[C_3H_6]_o$, ppm	2005	0	370	630
$[SO_2]_o$, ppm	1911	1809	1863	1902
$[O_2]$, %	4.56	4.47	4.64	4.64
k_1, min^{-1}	0.48	0.58	0.63	0.91
τ, min	0.745	0.760	0.769	0.755
Temp., °F	287	272	264	277
Gas Analyses				
ΔNO, ppm	416	54	183	323
NO Oxid., %	67.3	8.8	29.7	50.4
$[NO_2]$, ppm	384	49	133	285
$[NO_x]/[NO_x]_o$	0.977	0.970	0.902	0.940
ΔC_3H_6, ppm	305	0	120	161
$\Delta NO/\Delta C_3H_6$	1.36	N.A.	1.31	2.48
ΔSO_2, ppm	44	54	44	22
SO_2 Oxid., %	2.3	3.0	2.4	1.15
Filter Analyses				
XRF, SO_2 ppm	3.80	0.82	1.15	0.35

(continued)

TABLE B-3 (Continued)

Run Number Chronological No.	87 118	88 148	89 154	90 126
Conditions				
$[NO]_\circ$, ppm	614	548	592	647
$[C_3H_6]_\circ$, ppm	1270	2040	0	350
$[SO_2]_\circ$, ppm	1896	1836	1808	1819
$[O_2]$, %	4.56	4.56	4.46	4.64
k_1, min^{-1}	0.63	0.63	1.55	1.55
τ, min	0.755	0.750	0.747	0.760
Temp., °F	277	282	285	272
Gas Analyses				
ΔNO, ppm	449	482	38	285
NO Oxid., %	73.1	88.0	6.5	44.0
$[NO_2]$, ppm	449	405	38	247
$[NO_x]/[NO_x]_\circ$	0.954	0.845	0.982	0.910
ΔC_3H_6, ppm	343	452	0	170
$\Delta NO/\Delta C_3H_6$	1.04	0.89	N.A.	1.67
ΔSO_2, ppm	87	0	54	55
SO_2 Oxid., %	4.6	0	3.0	3.0
Filter Analyses				
XRF, SO_2 ppm	0.25	0.81	0.28	2.19

(continued)

TABLE B-3 (Continued)

Run Number Chronological No.	91 136	92 112	93 109	94 127
Conditions				
$[NO]_\circ$, ppm	610	635	606	992
$[C_3H_6]_\circ$, ppm	680	1320	2120	0
$[SO_2]_\circ$, ppm	1809	1880	1995	2000
$[O_2]$, %	4.47	4.64	4.64	4.64
k_1, min^{-1}	1.55	1.59	1.59	0
τ, min	0.758	0.75	0.75	0.777
Temp., °F	274	279	282	256
Gas Analyses				
ΔNO, ppm	464	603	596	0
NO Oxid., %	76.0	94.9	98.3	0
$[NO_2]$, ppm	383	504	532	16
$[NO_x]/[NO_x]_\circ$	0.949	0.976	0.894	N.D.
ΔC_3H_6, ppm	342	550	N.D.	N.D.
$\Delta NO/\Delta C_3H_6$	1.29	1.10	N.D.	N.A.
ΔSO_2, ppm	92	60	37	N.D.
SO_2 Oxid., %	5.1	3.2	1.8	N.D.
Filter Analyses				
XRF, ppm SO_2	5.67	N.D.	1.07	0.70

(continued)

TABLE B-3 (Continued)

Run Number Chronological No.	95 129	96 125	97 115	98 111
Conditions				
$[NO_x]_\circ$, ppm	943	1008	1162	1090
$[C_3H_6]_\circ$, ppm	320	670	1320	1927
$[SO_2]_\circ$, ppm	1748	1852	1857	1852
$[O_2]$, %	4.64	4.64	4.64	4.64
k_1, min^{-1}	0	0	0	0
τ, min	0.781	0.788	0.771	0.77
Temp., °F	253	246	262	259
Gas Analyses				
ΔNO, ppm	0	0	0	6
NO Oxid., %	0	0	0	0.55
$[NO_2]$, ppm	16	22	22	29
$[NO_x]/[NO_x]_\circ$	1.00	0.991	1.00	1.00
ΔC_3H_6, ppm	0	0	17	0
$\Delta NO/\Delta C_3H_6$	-	-	0	-
ΔSO_2, ppm	0	16	0	0
SO_2 Oxid., %	0	0.9	0	0
Filter Analyses				
XRF, ppm SO_2	0.41	0.75	N.D.	N.D.

(continued)

TABLE B-3 (Continued)

Run Number Chronological No.	99 117	100 131	101 157	102 143
Conditions				
$[NO]_\circ$, ppm	1178	992	1014	1006
$[C_3H_6]_\circ$, ppm	0	310	720	1415
$[SO_2]_\circ$, ppm	1956	1765	1874	1835
$[O_2]$, %	4.56	4.48	4.64	4.64
k_1, min^{-1}	0.27	0.31	0.20	0.18
τ, min	0.769	0.764	0.753	0.769
Temp., °F	264	269	279	264
Gas Analyses				
ΔNO, ppm	6	93	82	156
NO Oxid., %	0.51	9.4	8.1	15.5
$[NO_2]$, ppm	33	88	88	128
$[NO_x]/[NO_x]_\circ$	0.994	0.991	0.984	0.957
ΔC_3H_6, ppm	0	45	72	200
$\Delta NO/\Delta C_3H_6$	N.A.	2.1	1.0	0.78
ΔSO_2, ppm	11	16	22	11
SO_2 Oxid., %	0.6	0.9	1.2	0.6
Filter Analyses				
XRF, SO_2 ppm	N.D.	0.95	0.25	0.59

(continued)

TABLE B-3 (Continued)

Run Number Chronological No.	103 149	104 134	105 130	106 110
Conditions				
$[NO]_o$, ppm	1014	1026	937	1138
$[C_3H_6]_o$, ppm	2040	0	320	~670
$[SO_2]_o$, ppm	1863	1874	1754	1942
$[O_2]$, %	4.56	4.47	4.48	4.64
k_1, min^{-1}	0.18	0.47	0.47	0.48
τ, min	0.755	0.764	0.767	0.75
Temp., °F	277	269	266	282
Gas Analyses				
ΔNO, ppm	170	19	148	250
NO Oxid., %	16.7	1.8	15.8	22.0
$[NO_2]$, ppm	137	38	121	218
ΔC_3H_6, ppm	147	0	64	N.D.
$\Delta NO/\Delta C_3H_6$	0.74	N.A.		N.D.
ΔSO_2, ppm	33	22	11	48
SO_2 Oxid., %	1.8	1.2	0.6	2.5
Filter Analyses				
XRF, SO_2 ppm	0.31	0.42	3.20	0.25

(continued)

TABLE B-3 (Continued)

Run Number Chronological No.	107 152	108 138	109 142	110 137
Conditions				
$[NO]_\circ$, ppm	1008	1010	1006	1021
$[C_3H_6]_\circ$, ppm	1320	2030	0	370
$[SO_2]_\circ$, ppm	1841	1809	1846	1793
$[O_2]$, %	4.64	4.47	4.64	4.47
k_1, min^{-1}	0.33	0.47		0.88
τ, min	0.772	0.758	0.764	0.755
Temp., °F	261	274	269	277
Gas Analyses				
ΔNO, ppm	219	367	39	200
NO Oxid., %	21.7	36.3	3.9	19.6
$[NO_2]$, ppm	164	308	39	146
$[NO_x]/[NO_x]_\circ$			0.984	0.927
ΔC_3H_6, ppm	180	235	0	110
$\Delta NO/\Delta C_3H_6$	1.22	0.94	N.A.	1.54
ΔSO_2, ppm	71	54	0	32
SO_2 Oxid., %	3.9	3.0	0	1.8
Filter Analyses				
XRF, SO_2 ppm	0.83	1.78	0.42	2.65

(continued)

TABLE B-3 (Continued)

Run Number Chronological No.	111 150	112 141	113 119	114 153
Conditions				
$[NO]_\circ$, ppm	1014	1001	1222	948
$[C_3H_6]_\circ$, ppm	720	1415	2035	0
$[SO_2]_\circ$, ppm	1874	1910	1869	1814
$[O_2]$, %	4.64	4.64	4.56	4.46
k_1, min^{-1}	0.63	0.63	0.88	1.30
τ, min	0.750	0.786	0.747	0.747
Temp., °F	282	248	285	285
Gas Analyses				
ΔNO, ppm	197	334	477	27
NO Oxid., %	19.5	33.3	39.0	2.9
$[NO_2]$, ppm	164	295	444	33
$[NO_x]/[NO_x]_\circ$	0.942	0.930	0.962	0.988
ΔC_3H_6, ppm	170	345	363	0
$\Delta NO/\Delta C_3H_6$	1.0	0.97	0.94	N.A
ΔSO_2, ppm	38	73	71	60
SO_2 Oxid., %	2.0	3.8	3.8	3.3
Filter Analyses				
XRF, SO_2 ppm	0.76	1.00	0.54	0.53

TABLE B-3 (Continued)

Run Number	115	116	117	118
Chronological No.	123	122	146	147
Conditions				
$[NO_x]_\circ$, ppm	1200	1174	1012	983
$[C_3H_6]_\circ$, ppm	270	630	1320	1848
$[SO_2]_\circ$, ppm	1923	1918	1812	1728
$[O_2]$, %	4.56	4.64	4.64	4.56
k_1, min^{-1}	0.47	1.55	1.10	1.75
τ, min	0.750	0.758	0.755	0.747
Temp., °F	282	274	277	285
Gas Analyses				
ΔNO, ppm	236	378	517	594
NO Oxid., %	19.6	32.2	51.0	60.4
$[NO_2]$, ppm	219	340	417	497
$[NO_x]/[NO_x]_\circ$	0.980	0.977	0.882	0.886
ΔC_3H_6, ppm	124	280	534	647
$\Delta NO/\Delta C_3H_6$	1.82	1.35	0.89	2.59
ΔSO_2, ppm	38	60	78	76
SO_2 Oxid., %	2.0	3.1	4.3	4.4
Filter Analyses				
XRF, ppm SO_2	0.57	1.43	2.94	2.91

(continued)

TABLE B-4 EXPERIMENTAL DATA, COMPARISON OF ETHYLENE AND PROPYLENE

Run Number Chronological No.	119 92	120 90	121 86	122 87
Conditions				
$[NO_x]_\circ$, ppm	913	960	917	901
$[Olefin]_\circ$, ppm	1326	759	1048	1886
$[SO_2]_\circ$, ppm	1600	1553	1582	1651
k_1, min^{-1}	1.8	1.8	1.8	1.8
τ, min	0.764	0.769	0.769	0.767
Temp., °F	269	264	264	266
Olefin	C_3H_6	C_2H_4	C_2H_4	C_2H_4
Gas Analyses				
ΔNO, ppm	593	243	330	744
NO Oxid., %	65.0	25.3	36.0	82.6
$[NO_2]$, ppm	511	206	262	561
ΔOlefin, ppm	516	242	335	581
ΔNO/Δ Olefin	1.15	0.76	0.68	1.09
ΔSO_2, ppm	46	83	131	162
SO_2 Oxid., %	2.9	5.3	8.3	9.8
Filter Analyses				
XRF, SO_2 ppm	0.23	0.08	0.12	0.11

(continued)

TABLE B-4 (Continued)

Run Number Chronological No.	123 91	124 85	125 89	126 88
Conditions				
$[NO_x]_o$, ppm	898	865	954	927
[Olefin], ppm	1393	482	980	1624
$[SO_2]_o$, ppm	1610	1609	1598	1614
$[O_2]_o$, ppm		4.6	4.5	4.7
k_1, min^{-1}	1.8	1.8	1.8	1.8
τ, min	0.764	0.774	0.767	0.769
Temp., °F	269	259	266	264
Olefin	C_2H_4	C_3H_6	C_3H_6	C_3H_6
Gas Analyses				
ΔNO, ppm	521	314	487	686
NO Oxid., %	48.0	36.3	51.1	74.1
$[NO_2]$, ppm	439	241	409	561
$[NO_x]/[NO_x]_o$		0.958	0.961	0.916
ΔOlefin, ppm	412	194	371	566
$\Delta NO/\Delta$Olefin	1.26	1.62	1.31	1.21
ΔSO_2, ppm	88	68	62	136
SO_2 Oxid., %	5.4	4.2	3.9	8.4
Filter Analyses				
XRF, SO_2 ppm	0.06	0.26	0.06	0.27

TABLE B-5 EXPERIMENTAL DATA, INFLUENCE OF OXYGEN CONTENT ON NO OXIDATION.

Run Number Chronological No.	127 66	128 63	129 64	130 61
Conditions				
$[NO_x]_\circ$, ppm	515	580	597	519
$[C_3H_6]_\circ$, ppm	569	569	569	702
$[SO_2]_\circ$, ppm	1371	1260	1317	1328
$[O_2]$, %	0	0.81	2.45	4.43
k_1, min^{-1}	4.5	4.5	4.5	4.5
τ, min	0.738	0.768	0.758	0.772
Temp., °F	295	264	274	261
Gas Analyses				
ΔNO, ppm	120	392	558	493
NO Oxid., %	23.5	68.5	94.8	98.2
$[NO_2]$, ppm	44	300	462	444
$[NO_x]/[NO_x]_\circ$	0.845	0.827	0.825	0.872
ΔC_3H_6, ppm	26	117	190	157
$\Delta NO/\Delta C_3H_6$	4.64	3.34	2.94	3.14
ΔSO_2, ppm	9	52	118	40
SO_2 Oxid., %	0.6	4.1	8.9	3.0
Filter Analyses				
XRF, SO_2 ppm	0.06	0.05	0.13	0.12

TABLE B-5 (Continued)

Run Number	131	132	133	134
Chronological No.	67	65	59	62
Conditions				
$[NO_x]_\circ$, ppm	604	1020	1101	1043
$[C_3H_6]_\circ$, ppm	695	569	637	702
$[SO_2]_\circ$, ppm	1465	1347	1314	1296
$[O_2]$, %	7.42	0	0.86	2.54
k_1, min^{-1}	4.5	4.5	4.5	4.5
τ, min	0.767	0.738	0.764	0.784
Temp., °F	266	295	269	256
Gas Analyses				
ΔNO, ppm	559	126	404	626
NO Oxid., %	95.5	12.4	37.1	61.3
$[NO_2]$, ppm	506	44	280	484
$[NO_x]/[NO_x]_\circ$	0.882	0.914	0.875	0.842
ΔC_3H_6, ppm	N.D.	102	109	231
$\Delta NO/\Delta C_3H_6$	N.D.	1.23	3.70	2.71
ΔSO_2, ppm	49	9	49	N.D.
SO_2 Oxid., %	3.3	0.6	3.7	N.D.
Filter Analyses				
XRF, SO_2 ppm	0.09	0.08	0.06	0.08

TABLE B-6 EXPERIMENTAL DATA, INFLUENCE OF CO ON NO OXIDATION.

Run Number Chronological No.	137 106	138 105	139 107	140 104
Conditions				
$[NO_x]_\circ$, ppm	875	848	842	896
$[C_3H_6]_\circ$, ppm	1137	1180	1137	1180
$[SO_2]_\circ$, ppm	0	0	0	0
$[O_2]$, %	4.5	4.7	4.5	4.7
k_1, min^{-1}	1.55	1.45	1.65	1.95
τ, min	0.764	0.764	0.767	0.764
Temp., °F	269	269	266	269
[CO], ppm	0	1124	1985	3000
Gas Analyses				
ΔNO, ppm	680	718	783	832
NO Oxid., %	81.3	86.4	95.4	96.2
$[NO_2]$, ppm	653	621	707	718
$[NO_x]/[NO_x]_\circ$	0.926	0.866	0.885	0.837
ΔC_3H_6, ppm	N.A.	N.A.	N.A.	N.A.
$\Delta NO/\Delta C_3H_6$	N.A.	N.A.	N.A.	N.A.
ΔSO_2, ppm	N.A.	N.A.	N.A.	N.A.
SO_2 Oxid., %	N.A.	N.A.	N.A.	N.A.
Filter Analyses				
XRF, SO_2 ppm	N.D.	N.D.	N.D.	N.D.

TABLE B-7 EXPERIMENTAL DATA, INFLUENCE OF INITIAL NO_x CONCENTRATION ON NO OXIDATION.

Run Number Chronological No.	141 97	142 98	143 100	144 102
Conditions				
$[NO_x]_\circ$, ppm	445	770	1231	1001
$[C_3H_6]$, ppm	1183	917	917	904
$[SO_2]_\circ$, ppm	1582	2086	1614	1719
$[O_2]$, %	4.5	4.5	4.5	4.7
k_1, min^{-1}	N.D.	N.D.	N.D.	N.D.
τ, min	0.771	0.764	0.758	0.764
Temp., °F	261	269	274	269
Gas Analyses				
ΔNO, ppm	430	519	445	482
NO Oxid., %	100.0	68.8	37.0	49.5
$[NO_2]$, ppm	372	445	377	419
$[NO_x]/[NO_x]_\circ$	0.835	0.884	0.923	0.911
ΔC_3H_6, ppm	N.D.	N.D.	N.D.	N.D.
$\Delta NO/\Delta C_3H_6$	N.D.	N.D.	N.D.	N.D.
ΔSO_2, ppm	73	73	63	37
SO_2 Oxid., %	4.6	3.5	3.9	2.1
Filter Analyses				
XRF, SO_2 ppm	N.D.	N.D.	N.D.	N.D.

TABLE B-7 (Continued)

Run Number Chronological No.	145 103	146 101	147 99
Conditions			
$[NO_x]_o$, ppm	1467	1886	2017
$[C_3H_6]_o$, ppm	904	872	1019
$[SO_2]_o$, ppm	1729	1651	1582
$[O_2]$, %	4.7	4.5	4.5
k_1, min^{-1}	N.D.	N.D.	N.D.
τ, min	0.764	0.767	0.760
Temp., °F	269	266	272
Gas Analyses			
ΔNO, ppm	445	367	367
NO Oxid., %	30.9	20.0	18.7
$[NO_2]$, ppm	367	341	341
$[NO_x]/[NO_x]_o$	0.929	0.958	0.961
ΔC_3H_6, ppm	N.D	N.D.	N.D.
$\Delta NO/\Delta C_3H_6$	N.D.	N.D.	N.D.
ΔSO_2, ppm	47	52	37
SO_2, Oxid., %	2.7	3.2	2.3
Filter Analyses			
XRF, SO_2 ppm	N.D.	N.D.	N.D.

TABLE B-8 EXPERIMENTAL DATA, INFLUENCE OF CO_2 CONCENTRATION ON NO OXIDATION.

Run Number	148	149	150	151
Chronological No.	94	93	96	95
Conditions				
$[NO_x]_\circ$, ppm	862	859	898	846
$[C_3H_6]_\circ$, ppm	1018	966	1000	855
$[SO_2]_\circ$, ppm	0	0	0	0
$[O_2]$, %	4.2	4.4	4.5	4.2
k_1, min^{-1}	1.55	1.55	1.55	1.55
τ, min	0.768	0.771	0.771	0.768
Temp., °F	264	261	261	264
$[CO_2]_\circ$, %	0	6.3	12.6	18.5
Gas Analyses				
ΔNO, ppm	501	477	506	470
NO Oxid., %	59.1	57.2	58.0	56.9
$[NO_2]$, ppm	428	409	439	413
$[NO_x]/[NO_x]_\circ$	0.898	0.890	0.897	0.908
ΔC_3H_6, ppm	N.D.	N.D.	N.D.	N.D.
$\Delta NO/\Delta C_3H_6$	N.D.	N.D.	N.D.	N.D.
ΔSO_2, ppm	N.A.	N.A.	N.A.	N.A.
SO_2 Oxid., %	N.A.	N.A.	N.A.	N.A.
Filter Analyses				
XRF, SO_2 ppm				

TABLE B-9 EXPERIMENTAL DATA, INFLUENCE OF GAS TEMPERATURE ON NO OXIDATION.

Run Number Chronological No.	152 73	153 74	154 71	155 76
Conditions				
$[NO_x]_\circ$, ppm	547	572	547	651
$[C_3H_6]_\circ$, ppm	548	541	625	579
$[SO_2]_\circ$, ppm	1387	1385	1465	1284
$[O_2]$, %	3.7	4.2	4.4	4.2
k_1, min^{-1}	1.55	1.45	0.8	1.45
τ, min	0.772	0.760	0.747	0.753
Temp., °F	115	187	214	285
Gas Analyses				
ΔNO, ppm	453	542	498	600
NO Oxid., %	84.9	97.3	93.2	94.7
$[NO_x]/[NO_x]_\circ$	0.844	0.845	0.851	0.829
ΔC_3H_6, ppm	199	90	74	77
$\Delta NO/\Delta C_3H_6$	2.28	6.09	6.75	7.80
ΔSO_2, ppm	100	44	63	N.D.
SO_2 Oxid., %	7.2	3.2	4.3	N.D.
Filter Analyses				
XRF, SO_2 ppm	0.33	0.53	N.D.	0.16

TABLE B-9 (Continued)

Run Number Chronological No.	156 70	157 75	158 69	159 72
Conditions				
$[NO_x]_\circ$, ppm	1543	1203	1190	1238
$[C_3H_6]_\circ$, ppm	849	584	734	541
$[SO_2]_\circ$, ppm	1359	1232	1357	1637
$[O_2]$, %	5.0	3.8	4.3	4.0
k_1, min^{-1}	1.45	1.55	1.45	1.23
τ, min	0.742	0.763	0.753	0.753
Temp., °F	132	198	214	295
Gas Analyses				
ΔNO, ppm	703	631	790	823
NO Oxid., %	46.8	53.5	68.0	67.8
$[NO_x]/[NO_x]_\circ$	0.911	0.881	0.912	0.885
ΔC_3H_6, ppm	100	N.D.	145	127
$\Delta NO/\Delta C_3H_6$	7.04	N.D.	5.34	6.70
ΔSO_2, ppm	98	59	143	100
SO_2 Oxid., %	7.2	4.8	10.5	6.1
Filter Analyses				
XRF, SO_2 ppm	0.25	0.08	0.17	0.15

APPENDIX C - KINETIC MODELING

A preliminary attempt was made to adapt a propylene/NO_x kinetic mechanism developed by Jeffries (1977) for use in analyzing experimental results with the Photochemical Kinetics Simulation System (PKSS) also developed by Jeffries. This kinetic mechanism had successfully been used to simulate smog chamber results at the UNC research facility. Since these tests were conducted in a batch reactor and at ambient conditions, some mechanism modifications were necessary.

One change was to operate the program so as to simulate a CSTR using dilution and continuous mass input. By balancing these two factors it was possible to simulate the CSTR conditions at an average reactor residence time of 0.75 minutes. Model runs under dark phase conditions confirmed that the concentrations of NO, SO_2, and C_3H_6 remained constant.

Initial simulation runs indicated that certain reactions were too rapid for the time scale chosen. Rescaling of the variables was necessary to simulate the short time scale events; the units used in the rescaling were one-thousandth of a minute. These units required no change in the second order rate constants. It was necessary to divide the first order rate constants (including k_1) by a factor of 1000 and multiply the third order rate constants by a factor of 1000. The resulting mechanism is shown in the attached sample computer printout. The basic PKSS program was not changed, therefore, the units continued to be printed in units of "minutes" while the actual time was "minutes x 10^{-3}".

There are several obvious deficiencies in this mechanism: (1) ozone -propylene reactions were inadvertently omitted, (2) no attempt was made to adjust photolysis rates of aldehydes due to middle UV light, and (3) photolysis rates were not adjusted to reflect absorbance changes as a function of temperature.

The NO conversion estimates of the sample run are approximately 15% of the actual results based on runs 44 to 68. The primary reason for the

Preceding page blank

difference is probably the first error identified above. Other possible contributing factors are listed below:

(1) Aldehyde photolysis in the middle UV

(2) Photolysis of species other than aldehydes in the middle UV

(3) Improper selection of composite reactions due to high gas temperature and/or low oxygen concentration.

(4) Improper selection of photolysis rates due to temperature effects and/or middle UV light.

(5) Improper use of kinetic model

(6) Improper mechanism for high concentration, high temperature system

Although, initial attempts at modeling the experimental results with PKSS were not successful, there is no apparent reason why this mechanism can not be improved so that PKSS could be used to simulate a system such as that used in the project. It is recommended that modeling efforts be emphasized in future work.

Reproduced from best available copy.

```
                    P H O T O C H E M I C A L   K I N E T I C S   S I M U L A T I O N   S Y S T E M
                          VERSION 003A        CREATED 07/12/77
                          DATE:22/07/78       TIME:13:11:29,453

 . . . . . . . . . . . . . . . . . . . . . . .  U S E R   D O C U M E N T A T I O N . . . . . . . . . . . . . . . . . . . . . . . .
                    THIS IS A TEST RUN
                    USING A NEW MECHANISM BASED ON RECENT FINDINGS INCLUDING:
                        1) NEW RATES FOR HO2,OH WITH NO & NO2 GIVING HNO2, HNO3, &
                         PNA(HO2NO2) WHICH HAS HIGH TEMP DEPEND.
                        2) NEW O3 & OLEFIN CHEM: CREGIEE MECH, STABLE BIRADICALS, HOT
                         ACETIC ACID.
                        3) NEW PAN CHEM: EITHER HENDRY'S RATES OR COX'S RATES.
                    MECHANISM HAS UNDERGONE SUCESSIVE REVISION AS COMPARISON PROCEED
                        ,    ADDED RO2+NO->KETONE+HNO2 TO PROPY CHEM

                        VERSION 6B

 THE MAXIMUM NUMBER OF:

      SPECIES IS  40:

      REACTIONS IS  75:

      TABLE VALUES IS  15:

      ITEMS TO BE SAVED IS ZERO-NO SELECTIVE PUNCHING OF OUTPUTS

 DILUTION RATE PROFILE FROM:CONSTANT DILUTION OF 1.5E-3 USED TO SIMULATE TAU OF 0.75 MIN

 INITIAL CONCENTRATION OF NO    =1.0

 INITIAL CONCENTRATION OF NO2   =0.1

 INITIAL CONCENTRATION OF PROPYL=1.0

 INITIAL CONCENTRATION OF O3    =0.05

 INITIAL CONCENTRATION OF SO2   =2.5

 INITIAL CONCENTRATION OF HCHO  =0.1

 INITIAL CONCENTRATION OF O2    =40.

 INITIAL CONCENTRATION OF N2O5  =1.0E-5

 INITIAL CONCENTRATION OF NO3   =1.0E-5

 INITIAL CONCENTRATION OF HNO2  =1.0E-4

 INITIAL CONCENTRATION OF CCHO  =0.5

 INITIAL CONCENTRATION OF COO   =1.0E-7

 INITIAL CONCENTRATION OF CCO3  =1.0E-7

 INITIAL CONCENTRATION OF O1D   =1.0E-8

 INITIAL CONCENTRATION OF OH    =1.0E-10
```

```
INITIAL CONCENTRATION OF HO2    =1.0E-6
INITIAL CONCENTRATION OF O      =1.0E-10
INITIAL CONCENTRATION OF PAN    =1.0E-3
OPTIONS SELECTED:

 CNSTOIL                0.0015
 TMAX                   4000.
 CNSTCAT                1.
 CNSTTE                 400.
 CNSTH2                 10.
 CNSTLI                 0.0017
 CMPTFI
 HMAX                   20.
 PRTSTEP     50
 PLTSTEP     50
 END
THIS RUN USES CONSTANT LIGHT INTENSITY EQUAL TO 1.70000E-03
THIS RUN USES CONSTANT TEMPERATURE EQUAL TO 4.00000E+02
THIS RUN USES CONSTANT WATER CONC EQUAL TO 1.00000E+01
THIS RUN USES CONSTANT CATALYSIS CONC EQUAL TO 1.00000E+00
THIS RUN USES CONSTANT DILUTION RATE EQUAL TO 1.50000E-03
```

```
* * * * * * * * * * * * * * * * * * * * * * * * * * * M E C H A N I S M * * * * * * * * * * * * * * * * * * * * * * * * * *
                THIS IS A TEST RUN
  1)              NO2    --HV--> 1.00 NO      + 1.00 O                         1.000E+00                   < 4.800E-01>
  2)              O3     --HV--> 1.00 O1D                                      1.000E+00                   < 4.800E-01>
  3)              O      ------> 1.00 O3                                       ..00E+02*EXP( 5.10E+02/T)< 8.859E+02>
  4)      O3    + NO     ------> 1.00 NO2                                      1.350E+03*EXP(-1.20E+03/T)< 2.371E+01>
  5)      NO    + O      ------> 1.00 NO2                                      4.400E+03                   < 3.500E+03>
  6)      NO2   + O      ------> 1.00 NO                                       1.380E+04                   < 1.380E+04>
  7)      NO2   + O      ------> 1.00 NO3                                      3.640E+03                   < 3.640E+03>
  8)      O3    + NO2    ------> 1.00 NO3                                      1.774E+02*EXP(-2.45E+03/T)< 4.768E-02>
  9)      NO3   + NO     ------> 2.00 NO2                                      2.808E+04                   < 2.808E+04>
 10)      NO3   + NO2    ------> 1.00 N2O5                                     2.187E+02*EXP( 8.61E+02/T)< 3.933E+03>
 11)              N2O5   ------> 1.00 NO3     + 1.00 NO2                       7.440E+15*EXP(-1.03E+04/T)< 6.854E+00>
 12)              N2O5   ------> 2.00 WHNO3                      (H2O)*        8.000E-07                   < 8.000E-03>
 13)              O3     --HV--> 0.11 O1D     + 0.89 O                   (C)*  5.380E-02                   < 2.582E-02>
 14)              O1D    ------> 1.00 O                                        8.540E-01                   < 8.540E-01>
 15)              O1D    ------> 2.00 OH                         (H2C)*        5.140E-06                   < 5.140E-02>
 16)      O3    +        ------>                                               4.620E-07                   < 4.620E-07>
 17)      O3    + OH     ------> 1.00 HO2                                      2.217E+03*EXP(-1.00E+03/T)< 7.734E+01>
 18)      OH    + NO     ------> 1.00 HNO2                                     3.859E+02*EXP( 1.11E+03/T)< 1.600E+04>
 19)              HNO2   --HV--> 1.00 NO      + 1.00 OH                        5.000E-01                   < 2.400E-01>
 20)      OH    + NO2    ------> 1.00 HNO3                                     1.400E+04                   < 1.400E+04>
 21)      OH    + HNO3   ------> 1.00 NO3                                      8.868E+02*EXP(-4.00E+02/T)< 2.317E+02>
 22)      O3    + HO2    ------> 1.00 OH                                       1.079E+02*EXP(-1.28E+03/T)< 1.496E+00>
 23)      HO2   + NO     ------> 1.00 NO2     + 1.00 OH                        1.182E+04                   < 1.182E+04>
 24)      HO2   + NO2    ------> 1.00 HO2NO2                                   9.000E+03                   < 9.000E+03>
 25)              HO2NO2 ------> 1.00 NO2     + 1.00 HO2                       4.500E+14*EXP(-1.17E+04/T)< 4.206E-03>
 26)      HO2   + NO3    ------> 1.00 HNO3                                     2.500E+03                   < 2.500E+03>
 27)      HO2   + HO2    ------> 1.00 H2O2                                     4.894E+04*EXP(-5.41E+02/T)< 7.980E+03>
 28)              H2O2   --HV--> 2.00 OH                                       1.000E-01                   < 4.800E-02>
 29)      NO    + NO     ------> 2.00 NO2                                      2.520E-05*EXP( 5.30E+02/T)< 1.492E-04>
```

```
30)   NO     + NO2    ------> 2.00 HNO2                                   (H2O)*   2.200E-09                        < 2.200E-05>
31)   HNO2   + HNO2   ------> 1.00 NO     + 1.00 NO2                               1.300E-03                        < 1.300E-03>
32)   OH     + CO     ------> 1.00 HO2                                             4.000E+02                        < 4.000E+02>
33)            HCHO   --HV--> 1.00 CO     + 0.58 HO2                         (C)*  2.000E-02                        < 9.600E-03>
34)   OH     + HCHO   ------> 1.00 HO2    + 1.00 CO                                1.400E+04                        < 1.400E+04>
35)            CCHO   --HV--> 1.00 CO     + 1.00 HO2    + 0.99 COO           (C)*  4.000E-02                        < 1.920E-02>
36)   OH     + CCHO   ------> 1.00 CCO3                                            2.400E+04                        < 2.400E+04>
37)   CCO3   + NO     ------> 1.00 NO2    + 1.00 COO                               4.600E+03                        < 4.600E+03>
38)   CCO3   + NO2    ------> 1.00 PAN                                             1.560E+03                        < 1.560E+03>
39)                   ------> 1.00 PROPYL                                          1.500E-03                        < 1.500E-03>
40)                   ------> 1.00 O2                                              6.000E-02                        < 6.000E-02>
41)                   ------> 1.00 NO                                              1.500E-03                        < 1.500E-03>
42)                   ------> 1.00 NO2                                             1.500E-05                        < 1.500E-05>
43)                   ------> 1.00 SO2                                             3.700E-03                        < 3.700E-03>
44)   NO3    + PROPYL ------> 1.00 NO2                                             7.820E+00                        < 7.820E+00>
45)   O3     + PROPYL ------> 1.00 HCHO   + 0.20 CCHO2  + 0.80 HOCHO*              4.510E+00*EXP(-1.90E+03/T)< 7.677E-03>
46)   O3     + PROPYL ------> 1.00 CCHO   + 0.20 HO2    + 0.70 CO                  4.510E+00*EXP(-1.90E+03/T)< 7.677E-03>
47)   C3OHO2 + HO2    ------>                                                      8.000E+03                        < 8.000E+03>
48)   C3OHO2 + C3OHO2 ------> 2.00 CCHO   + 2.00 HCHO   + 2.00 HO2                 5.000E+02                        < 5.000E+02>
49)   MO     + NO2    ------> 1.00 MONO2                                           1.500E+04                        < 1.500E+04>
50)   MO     + NO2    ------> 1.00 HCHO   + 1.00 HNO2                              4.400E+03                        < 4.400E+03>
51)   OH     + PROPYL ------> 1.00 C3OHO2                                          3.740E+04                        < 3.740E+04>
52)   C3OHO2 + NO     ------> 1.00 NO2    + 2.00 HCHO   + 2.00 HO2                 6.000E+03                        < 6.000E+03>
53)   C3OHO2 + NO     ------> 1.00 NO2    + 2.00 CCHO                              6.000E+03                        < 6.000E+03>
54)   CCO3   + HO2    ------>                                                      8.000E+03                        < 8.000E+03>
55)   COO    + NO     ------> 1.00 NO2    + 1.00 MO                                9.600E+03                        < 9.600E+03>
56)   COO    + NO     ------> 1.00 HCHO   + 1.00 HNO2                              2.400E+03                        < 2.400E+03>
57)   COO    + HO2    ------>                                                      8.000E+03                        < 8.000E+03>
58)   COO    + COO    ------> 1.50 MO                                              8.000E+03                        < 8.000E+03>
59)   O2     + MO     ------> 1.00 HCHO   + 1.00 HO2                               1.000E+00                        < 1.000E+00>
```

```
60)               PAN   ------> 1.00 NO2    + 1.00 CCO3                 1.190E+18*EXP(-1.35E+04/T)< 2.224E-02>
61)       SO2   + OH    ------> 1.30 SO3                                1.656E+03                 < 1.656E+03>
62)       SO2   + NO3   ------> 1.00 SO3    + 1.00 NO2                  2.500E-03                 < 2.500E-03>
63)       SO2   + HO2   ------> 1.00 OH     + 1.00 SO3                  1.330E+00                 < 1.330E+00>
64)       COO   + SO2   ------> 1.00 SO3    + 1.00 HO                   7.500E-01                 < 7.500E-01>
```

```
 . . . . . . . . . . . . . . . . . . . . . . . . . C O N C E N T R A T I O N S . . . . . . . . . . . . . . . . . . . . . . . . . .
                   THIS IS A TEST
  NUMBER       TIME         STPSIZ       NXTSTP       ORDER        LIGHT        TEMP         WATER        CAT          DILRAT
  NO2          NO           O            O3           O1D          NO3          N2O5         WHNO3        OH           HO2
  HNO2         HNO3         HO2NO2       H2O2         CO           HCHO         CCHO         COO          CCO3         PAN
  PROPYL       O2           SO2          CCHO2        HOCHO*       C3OHO2       MO           MONO2        SO3

 -----------------------------------------------------------------------------------------------------------------------
       0        0.000        0.0000       0.0001         0    0   1.70000E-03  4.00000E+02  1.00000E+01  1.00000E+00  1.50000E-03
  1.00000E-01  1.00000E+00  1.00000E-10  5.00000E-02  1.00000E-08  1.00000E-05  1.00000E-05  0.00000E+00  1.00000E-10  1.00000E-06
  1.00000E-04  0.00000E+00  0.00000E+00  0.00000E+00  0.00000E+00  1.00000E-01  5.00000E-01  1.00000E-07  1.00000E-07  1.00000E-03
  1.00000E+00  4.00000E+01  2.50000E+00  0.00000E+00  0.00000E+00  0.00000E+00  0.00000E+00  0.00000E+00  0.00000E+00
 -----------------------------------------------------------------------------------------------------------------------
      50        0.011        0.0006       0.0104         2   33   1.70000E-03  4.00000E+02  1.00000E+01  1.00000E+00  1.50000E-03
  1.27762E-01  9.72265E-01  3.55747E-08  2.43508E-02  6.77618E-07  4.48834E-08  2.30967E-10  3.51386E-15  1.34940E-08  7.35383E-08
  4.86109E-04  1.14743E-06  1.85507E-06  4.57896E-11  1.21844E-05  1.00437E-01  5.00026E-01  1.70035E-08  3.66698E-08  3.10720E-09
  9.99941E-01  4.00000E+01  2.50000E+00  3.06261E-06  1.22504E-05  4.34527E-08  6.50702E-08  6.12530E-04  4.20037E-06
 -----------------------------------------------------------------------------------------------------------------------
     100        2.283        0.3125      20.0000         1   56   1.70000E-03  4.00000E+02  1.00000E+01  1.00000E+00  1.50000E-03
  1.52017E-01  9.47550E-01  3.95441E-08  3.60070E-07  2.32189E-07  8.22935E-10  5.03468E-12  3.75387E-15  1.53124E-09  8.55064E-09
  5.50602E-04  8.92239E-06  1.26399E-07  4.84161E-11  1.12419E-04  1.00282E-01  4.98356E-01  4.56043E-09  4.20176E-09  4.17361E-10
  9.99774E-01  4.00000E+01  2.49987E+00  6.03096E-06  2.41239E-05  5.03536E-09  1.38812E-08  6.83863E-04  2.40436E-05
 -----------------------------------------------------------------------------------------------------------------------
     150      510.095       20.0000      20.0000         2   79   1.70000E-03  4.00000E+02  1.00000E+01  1.00000E+00  1.50000E-03
  1.31520E-01  9.05774E-01  3.70387E-08  3.52832E-07  7.05486E-10  6.97675E-10  3.69283E-12  2.61033E-14  1.34928E-09  6.41839E-09
  6.34504E-03  1.02072E-03  8.20868E-08  2.57343E-10  9.73990E-03  6.91460E-02  2.39634E-01  2.19775E-09  1.86244E-09  1.60053E-10
  9.80791E-01  3.99999E+01  2.48004E+00  3.80037E-06  1.52015E-05  4.55353E-09  7.37588E-09  7.77312E-03  2.78961E-03
 -----------------------------------------------------------------------------------------------------------------------
     200     1510.095       20.0000      20.0000         2   89   1.70000E-03  4.00000E+02  1.00000E+01  1.00000E+00  1.50000E-03
  1.03232E-01  9.06466E-01  3.16458E-08  3.01285E-07  6.02440E-10  4.67518E-10  1.94234E-12  2.64100E-14  5.64628E-10  2.78304E-09
  3.81926E-03  9.85127E-07  2.79375E-08  1.50780E-10  7.25937E-03  3.37309E-02  6.54388E-02  5.00867E-10  2.50332E-10  1.68856E-11
  9.78371E-01  3.99999E+01  2.46770E+00  2.11432E-06  8.45728E-06  2.23574E-09  2.13420E-09  4.96339E-03  3.15295E-03
 -----------------------------------------------------------------------------------------------------------------------
     250     2510.095       20.0000      20.0000         2   90   1.70000E-03  4.00000E+02  1.00000E+01  1.00000E+00  1.50000E-03
  8.95270E-02  9.18674E-01  2.84516E-08  2.67302E-07  5.34446E-10  3.59675E-10  1.29592E-12  1.82258E-14  2.61177E-10  1.05226E-09
  1.50417E-03  4.86792E-04  9.16077E-09  4.46937E-11  3.23465E-03  1.50240E-02  2.06480E-02  1.37807E-10  3.06261E-11  1.79154E-12
  9.87762E-01  4.00000E+01  2.46607E+00  1.57861E-06  6.31444E-06  8.75219E-10  6.84149E-10  1.91918E-03  1.77458E-03
 -----------------------------------------------------------------------------------------------------------------------
     300     3510.095       20.0000      20.0000         2   90   1.70000E-03  4.00000E+02  1.00000E+01  1.00000E+00  1.50000E-03
  8.38715E-02  9.25172E-01  2.70379E-08  2.52246E-07  5.04314E-10  3.17958E-10  1.07325E-12  1.35103E-14  9.69348E-11  3.86050E-10
  5.53315E-04  2.00285E-04  3.14855E-09  1.06579E-11  1.28149E-03  6.17314E-03  7.02446E-03  4.40589E-11  3.83944E-12  2.10405E-13
  9.94434E-01  4.00000E+01  2.46622E+00  1.38243E-06  5.52972E-06  3.24731E-10  2.34778E-10  6.73531E-04  8.01165E-04
 -----------------------------------------------------------------------------------------------------------------------
     325     4010.095       20.0000      20.0000         2   90   1.70000E-03  4.00000E+02  1.00000E+01  1.00000E+00  1.50000E-03
  8.25356E-02  9.26832E-01  2.66958E-08  2.48610E-07  4.97037E-10  3.08381E-10  1.02434E-12  1.22556E-14  5.87560E-11  2.33495E-10
  3.34004E-04  1.24861E-04  1.87402E-09  4.99967E-12  7.93374E-04  3.87917E-03  4.15947E-03  2.56997E-11  1.37545E-12  7.41741E-14
  9.96395E-01  4.00000E+01  2.46635E+00  1.33641E-06  5.34564E-06  1.96867E-10  1.39359E-10  3.95753E-04  5.16852E-04
 -----------------------------------------------------------------------------------------------------------------------
```

```
FINAL INTEGRATED REACTION RATES
  52*            4010.10
  1:  6.995E-01   2:  3.321E-06   3:  7.141E-02   4:  1.213E-01   5:  3.994E-01   6:  1.809E-01   7:  4.772E-02   8:  8.634E-05   9
 :  4.781E-02  10:  3.828E-04
 11:  3.927E-04  12:  6.715E-14  13:  1.797E-07  14:  3.402E-06  15:  2.047E-10  16:  9.026E-10  17:  6.561E-09  18:  1.349E-02  19
 :  9.663E-03  20:  3.968E-03
 21:  6.424E-07  22:  8.584E-10  23:  1.175E-01  24:  1.181E-02  25:  1.181E-02  26:  1.845E-11  27:  7.298E-10  28:  7.362E-11  29
 :  3.187E-01  30:  8.282E-06
 31:  6.418E-08  32:  6.731E-06  33:  4.352E-03  34:  1.782E-03  35:  2.488E-02  36:  1.030E-02  37:  1.144E-02  38:  5.476E-04  39
 :  6.015E+00  40:  2.406E+02
 41:  6.015E+00  42:  6.015E-02  43:  1.484E+01  44:  1.434E-05  45:  7.556E-05  46:  7.556E-05  47:  3.197E-10  48:  1.403E-11  49
 :  2.190E-02  50:  6.425E-03
 51:  8.784E-02  52:  4.392E-02  53:  4.392E-02  54:  2.093E-09  55:  2.886E-02  56:  7.215E-03  57:  9.626E-10  58:  4.656E-08  59
 :  4.659E-04  60:  1.650E-03
 61:  9.796E-03  62:  1.151E-08  63:  3.587E-05  64:  6.098E-06
 ---------------------------------------------------------------------------------------------------------------------
```

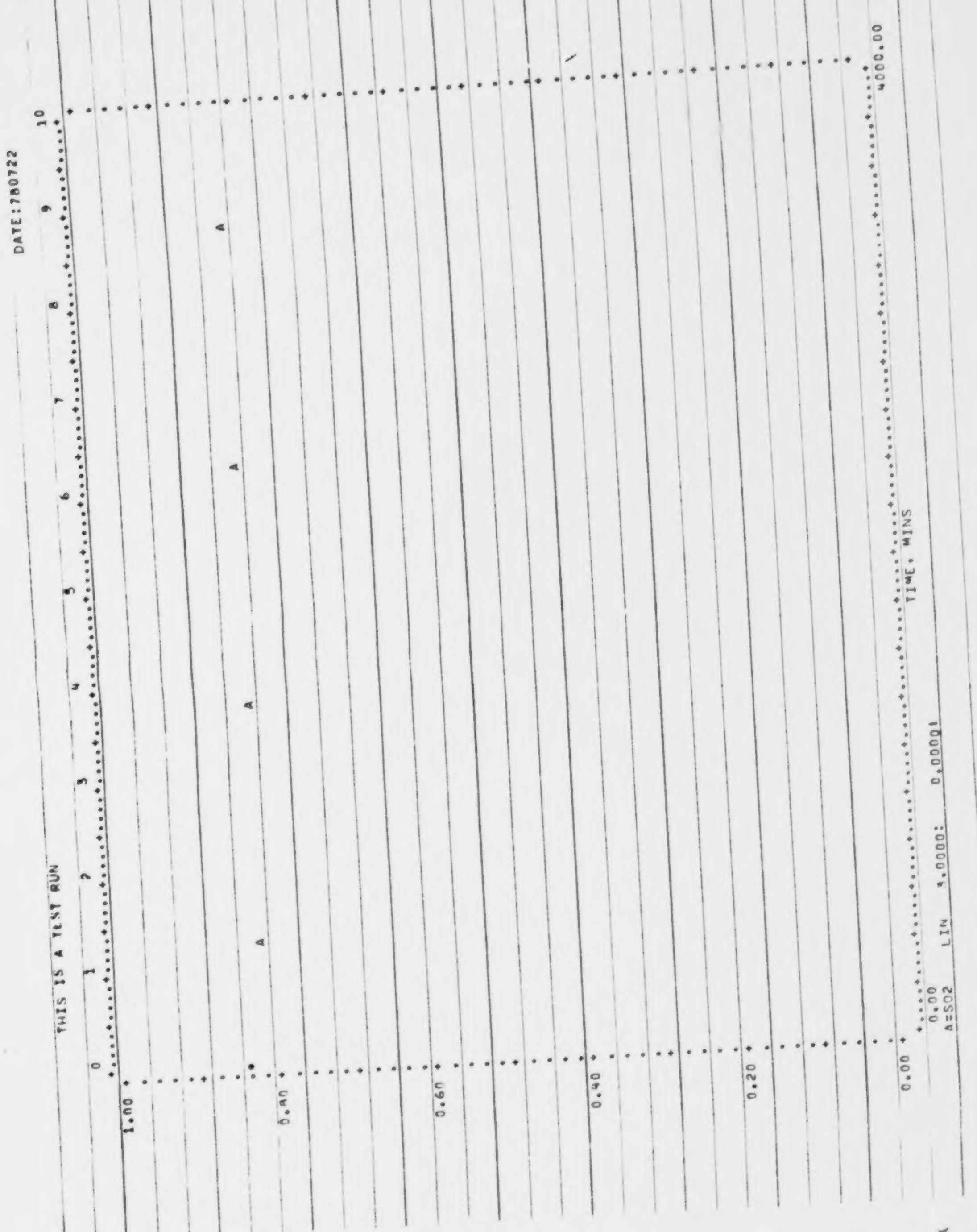
THIS IS A TEST RUN
DATE:780722
0
1
2
3
4
5
6
7
8
9
10
1.00
0.80
0.60
0.40
0.20
0.00
0.00
4000.00
A=SO2 LIN 1.0000: 0.00001
TIME, MINS
A

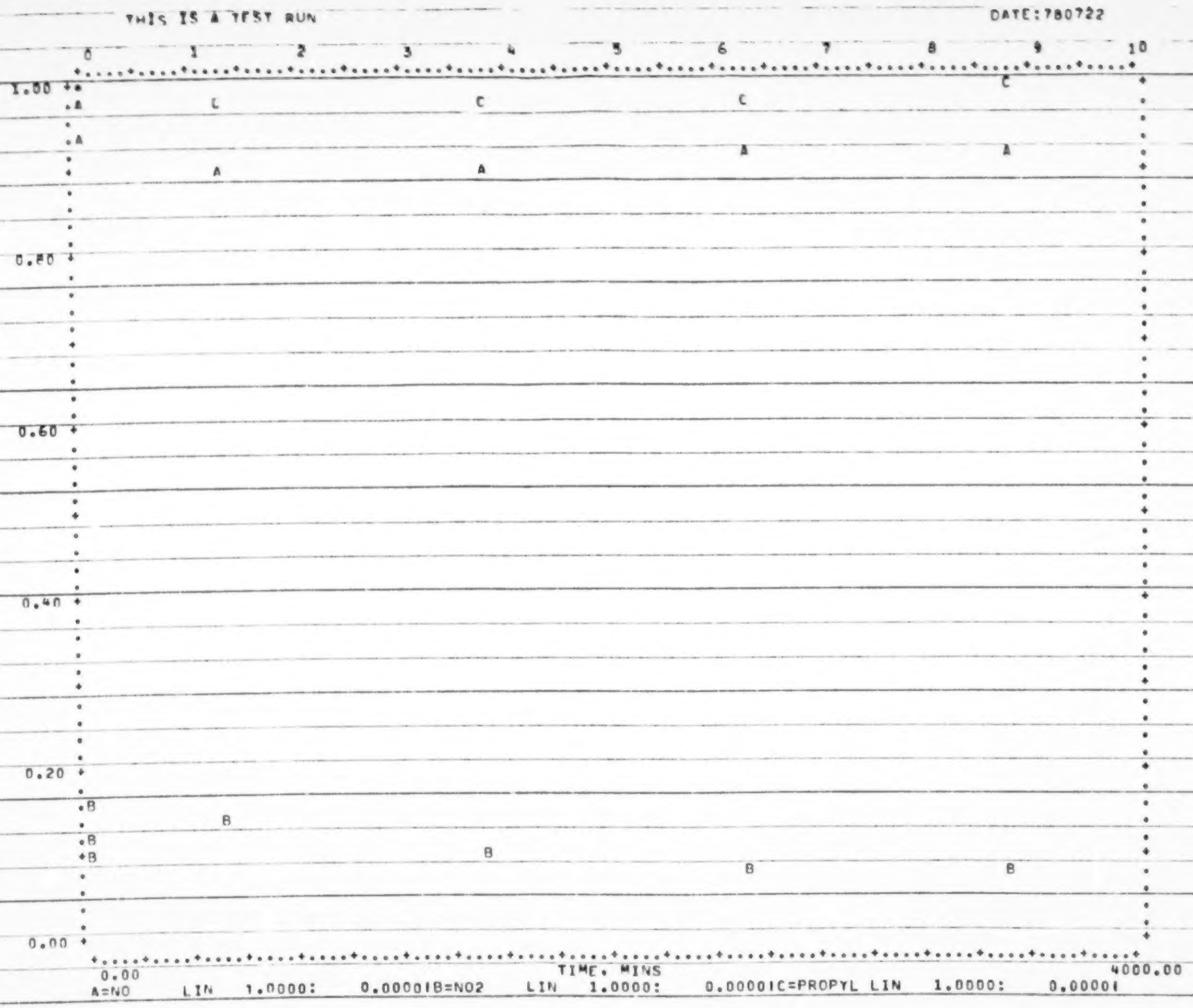
THIS IS A TEST RUN
DATE:780722
0
1
2
3
4
5
6
7
8
9
10
1.00
0.80
0.60
0.40
0.20
0.00
0.00
TIME, MINS
4000.00
A=NO LIN 1.0000: 0.0000|B=NO2 LIN 1.0000: 0.0000|C=PROPYL LIN 1.0000: 0.0000|
A
B
C

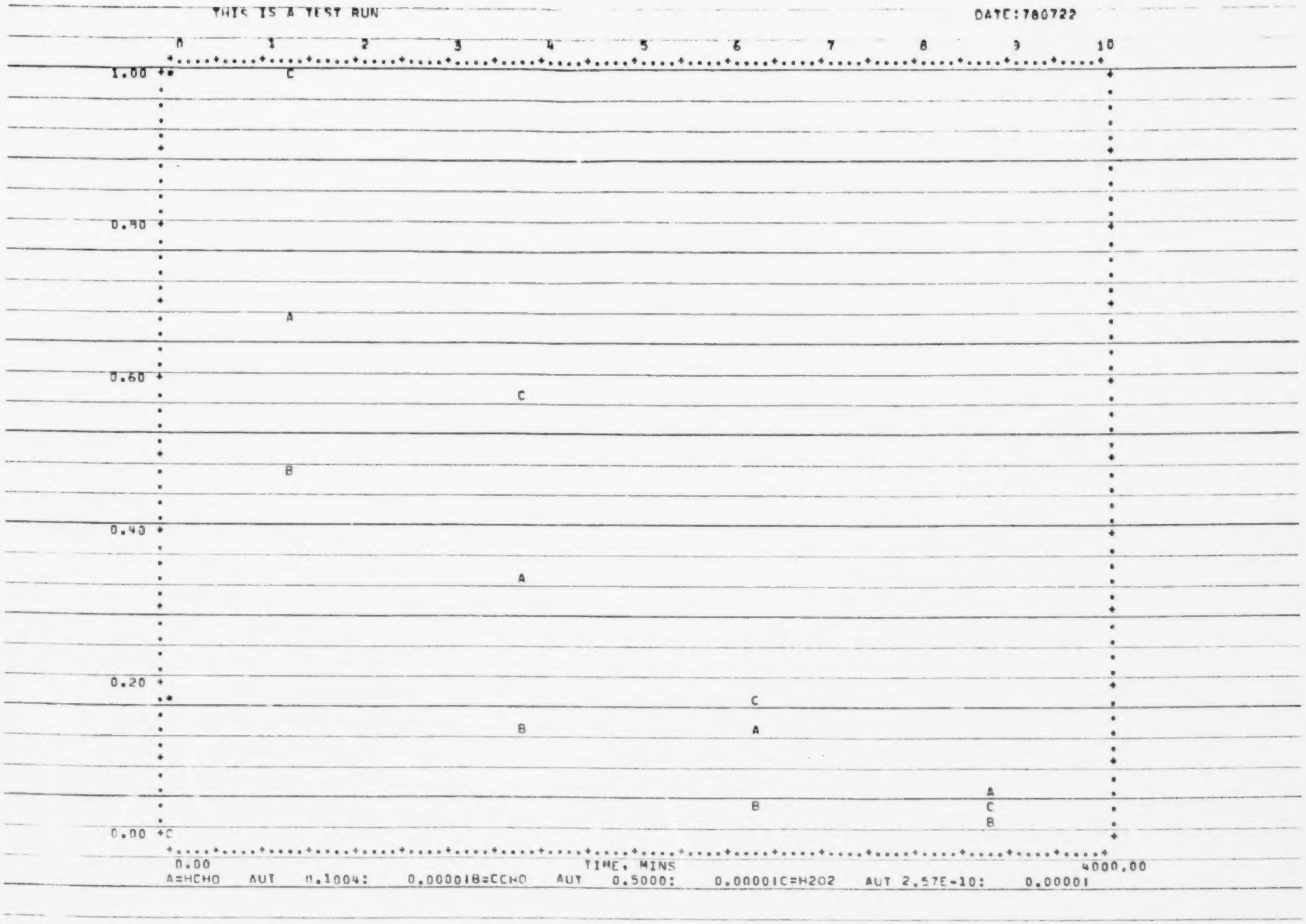
THIS IS A TEST RUN
DATE:780722
0
1
2
3
4
5
6
7
8
9
10
1.00
0.80
0.60
0.40
0.20
0.00
A
B
C
0.00
TIME, MINS
4000.00
A=HCHO AUT 0.1004: 0.00001B=CCHO AUT 0.5000: 0.00001C=H2O2 AUT 2.57E-10: 0.00001